2013-06-17

Investigating Cancer Molecular Genetics using Genome-wide RNA Interference Screens: A Dissertation

Ryan W. Serra
University of Massachusetts Medical School

Investigating Cancer Molecular Genetics using Genome-wide RNA Interference Screens

A Dissertation Presented

By

RYAN WILLIAM SERRA

Submitted to the Faculty of the

University of Massachusetts Graduate School of Biomedical Sciences, Worcester

in partial fulfillment of the requirements for the degree of

DOCTOR OF PHILOSOPHY

June, 17th 2013

CANCER MOLECULAR GENETICS

Investigating Cancer Molecular Genetics using
Genome-wide RNA Interference Screens

A Dissertation Presented

By

RYAN WILLIAM SERRA

The signatures of the Dissertation Committee signify
completion and approval as to the style and content of the Dissertation

Michael R. Green, M.D./Ph.D., Thesis Advisor

William Theurkauf, Ph.D., Member of Committee

Sharon Cantor, Ph.D., Member of Committee

Oliver Rando, M.D./Ph.D., Member of Committee

Christopher Lengner, Ph.D., External Member of Committee

The signature of the Chair of the Committee signifies that the written dissertation meets the requirements of the Dissertation Committee

Roger Davis, Ph.D., Chair of Committee

The signature of the Dean of the Graduate School of Biomedical Sciences signifies that the student has met all graduation requirements of the school.

Anthony Carruthers, Ph.D.,

Dean of the Graduate School of Biomedical Sciences

Cancer Biology Program

June 17th, 2013

DEDICATION

This thesis dissertation is dedicated to all my family and friends who have supported me throughout this journey. I could not have thought of completing this work all on my own. All the good times in the company of grateful people recharged my soul for the long road ahead. A special thanks goes out to my wife, Kerry, who has unflinchingly stood beside me throughout all the difficult times over the past eight years. Without her, I would be lost and this work would have been forsaken long ago. She has been the wind at my back this whole time. Finally, my newborn daughter, Hazel, has given me a renewed purpose and motivation for completing this work. She has offered clarity and focus in the face of this immense body of research and the task of compiling it into this thesis.

ACKNOWLEDGEMENTS

John Donne said “No man is an island” and this is the unequivocal truth for every scientist. Not only do we stand on the shoulders of the great men and women who came before us, but we also rely on those that stand beside us. This work was launched with the help of three principle scientists. First, Michael Green, has provided me with ample opportunities and resources to explore the biology of cancer as I saw fit. His lab has been an incubator for my own inquisitive nature and the proving grounds for skills I have developed over the years. Without Michael, none of this work would have been possible. Secondly, when I joined the lab in 2005, there was a flurry of excitement as the shRNA libraries were brought online and we were breaking new ground in cancer biology [and other fields too]. Claude Gazin, Narendra Wajapeyee and myself threw our shoulders to the wheel with facing the technical challenges of pioneering the use of the libraries as well as diving head first into some of the most interesting emerging concepts in cancer biology. Claude and Narendra were my role models, mentors, critics and ultimately peers throughout much of this work. Their insights and constructive criticisms enlightened me but also pushed me to be a better scientist.

The members of the Green lab have also proven to be instrumental in this research. Our lab meetings have yielded innumerable insights into the work performed. Our lab community, I believe, is one of the toughest around in terms

of critiques. This constructive criticism strengthens our work, ourselves and ultimately our lab as a whole. Without this “trial by fire” I wouldn’t have the presentation skills, critical thinking skills and fortitude that I have today. Furthermore, the many casual talks with co-workers over the years have provided a plethora of good advice. The geniality of my co-workers has made it possible to discuss issues and in turn receive insight and help when needed. While not a formal contribution to this work, in a sense, this community dialogue is the glue that holds it all together.

There have been many members of the lab that have contributed to this work. Narendra Wajapeyee was the leader and architect of the IGFBP7 story and a tremendous colleague. Julie Zhu performed countless recombinant IGFBP7 preps for our studies. Our collaborator, Meera Mahingliham, with her eagerness and expertise in dermatopathology were critical to the success of the IGFBP7 story in melanoma. Claude Gazin generated the reporter construct backbone used in the $p14^{ARF}$ screen. Minggang Fang has proven a great resource in investigating the role of ZNF304 in CIMP. Sungmi Park and her technical *in vitro* skills proved invaluable to studying the specificity of PRKD1 phosphorylation. Finally, collaborators Shuji Ogino and Xiaoyun Liao from the Dana-Farber Cancer Center in Boston, MA were instrumental in acquiring and analyzing colon cancer samples for the ZNF304 story.

Finally, a very special thanks goes out to Sara Deibler, our scientific writer and editor. She has painstakingly gone through my work, both writing and data, over the last eight years. Her comments have been invaluable to my success and in turn have instructed me to be a much better author and scientist. She has selflessly dedicated herself to the work of this lab and we owe her a debt of gratitude.

ABSTRACT

The development of RNAi based technologies has given researchers the tools to interrogate processes as diverse as cancer biology, metabolism and organ development. Here I employ genome-wide shRNA screens to discover the genes involved in two different processes in carcinogenesis, oncogene-induced senescence [OIS] and epigenetic silencing of tumor suppressor genes [TSGs].

OIS is a poorly studied yet significant tumor suppressing mechanism in normal cells where they enter cell cycle arrest [senescence] or programmed cell death [apoptosis] in the presence of an activated oncogene. Here I employ a genome-wide shRNA screen and identify a secreted protein, IGFBP7, that induces senescence and apoptosis in melanocytes upon introduction of the oncogene $BRAF^{V600E}$. Expression of $BRAF^{V600E}$ in primary cells leads to synthesis and secretion of IGFBP7, which acts through autocrine/paracrine pathways to inhibit BRAF-MEK-ERK signaling and induce senescence and apoptosis. Apoptosis results from IGFBP7-mediated upregulation of BNIP3L, a proapoptotic BCL2 family protein. Recombinant IGFBP7 has potent pro-apoptotic and anti-tumor activity in mouse xenograft models using $BRAF^{V600E}$-postive melanoma cell lines. Finally, IGFBP7 is epigenetically silenced in human melanoma samples suggesting IGFBP7 expression is a key barrier to melanoma formation.

Next I investigated the factors involved in epigenetic silencing in cancer. The TSG $p14^{ARF}$ is inactivated in a wide range of cancers by promoter

hypermethylation through unknown mechanisms. To discover *p14*^{ARF} epigenetic silencing factors, I performed a genome-wide shRNA screen and identified ZNF304, a zinc finger transcription factor that contains a Krüppel-associated box [KRAB] repressor domain. I show that ZNF304 binds to the *p14*^{ARF} promoter and recruits a KRAB co-repressor complex containing KAP1, SETDB1 and DNMT1 for silencing. We find oncogenic RAS signaling to promote the silencing of *p14*^{ARF} by USP28-mediated stabilization of ZNF304. In addition I find ZNF304 to be overexpressed in human colorectal cancers and responsible for hypermethylation of over 50 TSGs known as Group 2 CIMP marker genes. My findings establish ZNF304 as a novel oncogene that directs epigenetic silencing and facilitates tumorigenicity in colorectal cancer.

TABLE OF CONTENTS

LIST OF TABLES

LIST OF FIGURES

LIST OF SYMBOLS, ABBREVIATIONS OR NOMENCLATURE

OIS	Oncogene-Induced Senescence
TSG	Tumor Suppressor Gene
CIMP	CpG Island Methylator Phenotype
DNA	DeoxyriboNucleic Acid
RB	RetinoBlastoma [gene/protein]
RSV	Rous Sarcoma Virus
ALV	Avian Leukemia Virus
RTK	Receptor Tyrosine Kinase
MAPK	Mitogen Activated Protein Kinase
REF	Rat Embryonic Fibroblast
ARF	Alternative Reading Frame [gene/protein]
CDK	Cyclin-Dependent Kinase
TSS	Transcription Start Site
CpG	Cytosine-phospho-Guanine
RNA	RiboNucleic Acid
PTGS	Post-Translational Gene Silencing
mRNA	messenger RNA
miRNA	micro RNA
siRNA	short interfering RNA
dsRNA	double stranded RNA
shRNA	short hairpin RNA
RISC	RNA Induced Silencing Complex
SA-βGal	Senescence Associated Beta Galactosidase
qRT-PCR	quantitative Reverse Transcribed Polymerase Chain Reaction
ChIP	Chromatin ImmunoPrecipitation
KD	KnockDown
rIGFBP7	recombinant IGFBP7
DDR	DNA Damage Response

BrdU	BromodeoxyUridine
NS	Non-Silencing
H&E	Hematoxylin and Eosin
NaB	Sodium Bisulfite
gDNA	genomic DNA
IHC	ImmunoHistoChemistry
WT	WildType
ATP	Adenosine TriPhosphate
GTP	Guanosine TriPhosphate
GTPase	Guanosine TriPhosphatase
GDP	Guanosine DiPhosphate
RAF	Rapidly Accelerated Fibrosarcoma
PI_3K	PhosphoInositide 3-Kinase
kDa	kilo Dalton
SDS-PAGE	Sodium DodecylSulfate PolyAcrylamide Gel Electrophoresis
ChIP	Chromatin ImmunoPrecipitation
Co-IP	co-ImmunoPrecipitation
PAT-ChIP	PATient Chromatin ImmunoPrecipitation
MEF	Mouse Embryonic Fibroblast
KO	Knock Out
hESC	human Embryonic Stem Cells
CM	Conditioned Medium
TUNEL	Terminal deoxynucleotidyl transferase dUTP Nick End Labeling
IL-8	InterLeukin-8
IL-6	Interleukin-6
CRC	ColoRectal Cancer

CHAPTER I: INTRODUCTION

The latter half of the 20th century saw a revolution in understanding of biological processes that continues till this day. From the 1962 Nobel Prize winning work of James Watson and Francis Crick's discovery of deoxyribonucleic acid's [DNA's] double-helical structure and its base-paired nucleotide encoded information, to the sequencing of the entire human genome, we have been forced to rethink how biological systems function and are related to one another. One field that has experienced a dramatic paradigm shift is the biology of cancer. Once a mysterious scourge of man is now revealed to be a complex disease with environmental, genetic and epigenetic components [Watson and Crick, 1953].

Cancer is not new to the human race and there is evidence that it existed in ancient Egypt and Greece. For instance, cancer has been found in the form of growths in the bones of Egyptian mummies that are typical of osteosarcoma [History of Cancer, ACS, page 1]. Furthermore, the very word *carcinoma* originates in Greece from the "Father of Medicine," Hippocrates, and evokes the crab-like appearance of the growths [History of Cancer, ACS, page 1]. Furthermore, environmental contributors to the disease were very obvious in certain instances. The link between chimney soot and scrotal cancer provides a clear example, where the soot collected in the folds of skin on the scrotum in chimney sweeps [History of Cancer, ACS, page 4]. There were also clear examples of genetic components early on as well. Families that exhibited an

increased frequency of particular malignancies that were passed down from one generation to another were the first clue that cancer can be a genetic disease. Indeed, one of the first tumor suppressor genes [TSG], RetinoBlastoma [RB] was discovered through familial linkage analysis [Weinberg, 2007, pgs. 214-216].

Cancer is largely a disease of age, meaning that the incidence increases among the older segment of the population. This suggests that cancer is a complex disease that requires a significant amount of time to acquire the right combination of components for progression. Another way to think about this paradigm, in light of the genomic revolution, is that cancer is a multi-gene disease that requires a certain combination of genetic alterations in order to progress. The average mutation rate of the human genome is rather constant and it takes time for mutations to accumulate. Hence the disease is more likely in an older individual who has had more time to acquire mutations. This dependence on increased mutations in the genome explains how certain compounds that mutate the DNA or affects its ability to repair itself are carcinogenic. A carcinogen increases the abundance of mutations and thus increases the likelihood that a detrimental or cancer-causing combination will occur [Weinberg, 2007, pgs. 400-402].

Cancer is a disease that manifests as uncontrolled growth of a cell population. Unregulated proliferation is a key phenotype for several reasons. This proliferation increases the size of the aberrant *population* and increases the

likelihood that a member of the population will acquire further changes that will allow progression to the more aggressive phenotypes. Increased proliferation also essentially increases the likelihood that a *single cell* will acquire more mutations. So there is a distinct Darwinian process that takes place in cancer; one manifested at the *population* level and another at the *individual* level.

As the tumor population grows, there is a greater chance that it will advance to further stages of the disease. This tumor progression is ultimately dependent on a sub-population that gives rise to other members within the tumor. Cancer cells often display immortalization or a bypass of the finite number of cell divisions a cell can undergo. This is a critical phenotype that frees the pre-cancerous cell population from the limits of hereditary evolution.

Normal cells can duplicate themselves a certain number of times before they stop growing. This is called the “Hayflick Limit” after Leonard Hayflick who described this process definitively in 1961. At the time, researchers believed that cells transplanted into cell culture conditions would be immortal and never stop replicating. However while preparing for an experiment, Hayflick noticed his cultures would stop growing in cell culture after a while. Hayflick believed there to be some sort of counting mechanism inherently in cells to tell how old they were. Therefore, with cytologist Paul Moorhead, Hayflick performed an experiment where he took “old” male fibroblast cells and cultured them in equal

numbers with a “young” population of female fibroblasts. Subsequent analysis revealed that there were only the “young” female fibroblasts after a certain amount of time. Therefore the male cells somehow knew they were old and stopped growing irrespective of the cell culture conditions [Weinberg, 2007, pgs. 358-360].

The Hayflick limit describes a widely observed phenomenon and has now been explained using modern molecular biological approaches. The 2009 Nobel Prize winning work of Elizabeth Blackburn, Carol Greider and Jack Szostak revealed that at the end of the chromosomes in the genome, there are specialized DNA sequences that create a protective structure called telomeres. These regions are unable to be completely replicated when DNA is synthesized during cell division. With each cell division, the telomeres shorten a defined length. Therefore the length of the telomere region correlates with the age of the cell; longer telomeres are in a young cell, shorter telomeres are in an older cell. Once a telomere is eroded, the cell undergoes programmed cell death, called apoptosis. This counting mechanism, detection of telomere erosion and apoptosis ultimately remove older and more mutated members from the population of cells. Hence this acts as a tumor suppressive system and must be disrupted in a tumor cell population [Weinberg, 2007, pgs. 368-370].

As described before, a normal population of fibroblasts can be put into culture and one will eventually see a significant drop in growth rate. This drop in growth rate is due to two related phenomenon, “apoptosis” and “senescence”. Apoptosis is programmed cell death or suicide whereas senescence is irreversible growth arrest. A senescent cell exits the cell cycle but lingers afterwards and displays a distinct morphology. Given the shear number of cells that can be analyzed in cell culture experiments [on the order of millions], there can be exceptions to this apoptosis and senescence induction. After the massive drop in growth rate, termed “crisis”, one can continue to culture the plates [Weinberg, 2007, pgs. 369-372]. Eventually there will be cell populations that regrow and take over the plate again. These cells are “immortalized” and can now be cultured indefinitely [Weinberg, 2007, pgs. 361-362]. These cells are no longer constrained by telomere shortening. Either they have subverted the short telomere detection system or they have repaired their telomeres through an enzyme called telomerase that rebuilds the eroded ends of chromosomes [Weinberg, 2007, pgs. 376-380].

Immortalization is a very early step in carcinogenesis since it allows these cells to expand their population and in the process acquire additional mutations. Hence, immortalization is the key criterion that allows the *population* and *individual* to undergo Darwinian evolution to the more advanced stages of cancer. Since a cell never dies, it [and its progeny] is now capable of evolving. If their sequence

of acquired mutations is advantageous to cancer progression, then they will begin to represent more and more of the total population. In the process the tumor, a bulk population of cancer cells, itself has evolved to be more adapted to its new environment and displays a more aggressive and advanced phenotype.

Due to the requirement for certain mutational events to take place, cancer possesses another characteristic property in that their global DNA integrity is compromised. Cancer cells often display an increased mutation frequency compared to normal cells but they can also be unstable at the chromosomal level [Weinberg, 2007, pgs. 423-424]. Many cancer cells are aneuploid, meaning they have abnormal numbers of chromosomes. There can significant numbers of extra chromosomes or conversely there can be missing chromosomes [Weinberg, 2007, pgs. 11-13]. To complicate things further, the chromosomes can break and refuse incorrectly thereby generating translocations. These translocations are prevalent in cancer since they often times fuse two different genes [Weinberg, 2007, pgs. 109-115]. This aberrant genome integrity ultimately contributes to the genetic alterations required for cancer and drives the disease forward to more advanced phenotypes.

A more advanced stage of cancer is characterized by several phenotypes such as defective cell death, self-sufficient pro-growth signaling, defective anti-growth signaling, angiogenesis [*de novo* growth of new blood vessels] and finally,

invasion into nearby and distant sites within the body [Hannahan and Weinberg, 2011] A typical tumor progression involves the growth of the primary tumor at a site within the body. Here the tumor mass increases and it evolves many of the cancer phenotypes previously mentioned. As nutrients and oxygen become depleted, angiogenesis must take place and new blood vessels must be grown. This process is very disordered and the blood vessels are often times leaky and irregular, sometimes described as having a “tortuous” appearance [Weinberg, 2007, pgs. 559-563].

As the tumor itself grows, it is increasingly putting pressure on the surrounding tissue and membranes. Eventually, the tumor breaks through these constraints and starts to invade local regions. This is a critical stage since the tumor can now disseminate to other parts of the body and start new tumors. This invasion often results in tumor cells being shed and ultimately entering both the *de novo* blood vessels formed during angiogenesis as well as the normal blood and lymphatic vessels that reside nearby. Once in the vascular or lymphatic system, tumors cells can travel to distant parts of the body. Here they can enter new tissue and reside, sometimes for many years, until they evolve or acquire the ability to grow in this new environment [Weinberg, 2007, pgs. 26-28, 594-597].

This entire invasion process is termed “metastasis” and presents itself as one of the greatest hurdles in treating cancer. Surgery is very effective at removing the

primary tumor and eradicating this founding population. However, once a cancer has spread, it is difficult or impossible to remove every cell that has left the primary site.

So how does a normal cell become a cancer cell and acquire all these abnormal traits and abilities? An early clue that cancer is a genetic disease and DNA, and with its encoded genes, are involved came from a rather crude but unequivocally significant experiment by Manuel Perucho [Perucho et al., 1981]. The DNA from transformed cells was isolated and subsequently transfected into normal mouse fibroblasts using the calcium phosphate co-precipitation method. Unexpectedly, the normal fibroblasts began to display cancer cell phenotypes such as increased proliferation and the ability to form a tumor when explanted into mice. Therefore the ability to become a cancer cell was an inherent property of the DNA. Thus one can conclude that cancer is a disease with genetic contributing factors.

Since cancer involves so many complex phenotypes and cellular processes, there must be a tremendous number of genes involved. Through the work of countless individuals, it has emerged that there are two major kinds of cancer genes, those that promote cancer phenotypes and those that prevent cancer phenotypes. Cancer promoting genes are termed “oncogenes” and they derive from normal cellular genes termed “proto-oncogenes.” Proto-oncogenes are altered by DNA mutation or viral genomes and acquire the ability to function as

an oncogene. An oncogene induces cancer and has the ability to transform normal cells into cancer cells [Weinberg, 2007, pgs. 77-79]. Conversely the genes responsible for cancer prevention are known as “tumor suppressor genes” [TSGs]. These genes restrain cell growth and maintain the integrity of the genome [Weinberg, 2007, pgs. 209-210]. Oncogenes have their activity increased while TSGs have their activity decreased in cancer. There are numerous ways in which a cell can have gene activity increased and decreased and all can be found in diverse examples of cancer.

Oncogenes can be hyper-activated by a number of events such as point mutation to mimic an activated state, point mutation or deletion of an inactivation domain, translocation to a new promoter or enhancer, translocation with an oligermerization domain of another protein [where oligermerization enhances activity], genomic amplification, epigenetic derepression, and viral delivery of a proto-oncogene [Weinberg, 2007, pgs. 103-115]. Analogous to the tumor DNA transfection experiment mentioned earlier, viral delivery of exogenous DNA resulted in the discovery of many proto-oncogenes such as SRC, ABL, KIT, H-RAS, K-RAS and MYC [Weinberg, 2007, pgs. 57-58, 81].

Francis Peyton Rous’s 1966 Nobel Prize winning discovery, resulted from studies with a chicken sarcoma. Rous observed that preparations from the sarcoma tissue could then be used to generate a new sarcoma in a disease-free Plymouth

Rock chicken. These preparations were then prepared to be devoid of live sarcoma cells by grinding them up with sand and filtering the solution. This cell-free solution could also cause sarcomas when injected into chickens. This cancer-causing property of the lysate was the first defined biological preparation to study tumor formation [Weinberg, 2007, pgs. 58-61]. It was later revealed that the preparation contained a retrovirus, named Rous Sarcoma Virus [RSV] after its discoverer. The genetic elements of RSV were later determined and when compared to related viruses such as Avian Leukemia Virus [ALV], it was found to have an extra gene called SRC, named after the type of cancer it causes, sarcoma [Weinberg, 2007, pgs. 75-76].

Some time later, the 1989 Nobel Prize winning work of Harold Varmus and Michael Bishop discovered a cellular version of SRC, called c-SRC. The viral version, termed v-SRC, lacks a C-terminal phosphorylation domain found in c-SRC, which inactivates the protein. Therefore v-SRC is a constitutively active version of the proto-oncogene, c-SRC [Weinberg, 2007, pgs. 76-82]. Further studies revealed that c-SRC is a tyrosine kinase that is involved with cell movement and growth. Enhanced activity of c-SRC, through point mutation or v-SRC, causes cell transformation upon introduction.

Another mechanism to increase the activity of a gene is genomic amplification. In this instance, the DNA sequence encoding the gene is unaltered yet the

number of copies of the gene increases. There are several ways that this can occur but all require some compromise in the genomic integrity of the cell. Cells that display aneuploidy for instance might favor members of the population that harbor extra copies of oncogenes. MYC, a transcription factor, is one such oncogene and is overexpressed in various carcinomas such as pediatric neuroblastoma, Burkitt's lymphoma, ovarian cancer and lung cancer [Meyer and Penn, 2008]. Genomic analysis of copy number variations in neuroblastoma samples compared with normal tissue reveals an abundance of copy number gains in the region containing the MYC gene, therefore it is amplified at a genomic level. MYC is a powerful oncogene that regulates up to 10% of genes by some estimates [Meyer and Penn, 2008]. More recent evidence suggests that *total* transcription levels increase when MYC is upregulated [Meyer and Penn, 2008]. Given the plethora of transcriptional targets of MYC, the mechanistic details of its transforming ability are an area of intense research.

Alternatively and in contrast to solid tumors, MYC expression can be increased by genomic rearrangement. In Burkitt's lymphoma samples, it was revealed that MYC was frequently fused with the Immunoglobulin Heavy [IgH] Translocation of the MYC gene with the IgH chain promoter and enhancer causes dramatically escalated MYC expression and mimics MYC amplification [Weinberg, 2007, pgs. 109]. Mouse models of the MYC translocation develop clonal lymphoma in the B

cell compartment, thus mimicking the disease state it was originally identified within [Adams et al. 1985].

One of the most prevalent and widely studied forms of proto-oncogene activation is point mutation. Point mutations in various signaling molecules have been implicated in virtually every type of human cancer. Often times these single nucleotide mutations result in a protein that is constitutively active. In the case of kinases, their phosphorylation activity may be hundreds of times higher than their wildtype counterparts. Therefore a single mutation in one allele can have a dominant phenotype and be oncogenic.

Receptor tyrosine kinases [RTKs], which are responsible for growth factor signaling and downstream phosphorylation cascades are prime targets of point mutations [Weinberg, 2007, pgs. 129-140]. An activating mutation in an upstream RTK can cause a dramatic effect downstream due to the signal being propagated and amplified at every tier of the kinase cascade. Some signaling cascades are more frequently targeted due to their potent ability to accelerate cell growth. Alternatively the ease of causing a specific activating point mutation may account for its predominance in cancers. For instance, a valine to glutamic acid substitution in B-RAF at position 600 results from a single nucleotide substitution, thymine 1799 to adenine. Consequently, the enzymatic activity of the B-RAF increases significantly and results in constitutive signaling. B-RAF a

Rapidly Accelerated Fibrosarcoma [RAF] family serine/threonine kinase is a critical upstream regulator of the pro-growth mitogen-activated protein kinase [MAPK] pathway. The B-RAF^{V600E} oncogene is a major driver of several human cancers such as melanoma, colorectal cancer, papillary thyroid cancer and non-small cell lung cancer [Davies et al., 2002].

In a parallel fashion, the RAS subfamily of small guanosine triphosphatases [GTPases] is found to be point mutated frequently in human cancers [Karnoub, A.E. and Weinberg R.A., 2008]. First identified in rat sarcomas, hence the name RAS, their oncogenic potential was revealed via their viral homologs in two different rat sarcoma viruses [Weinberg, 2007, pg 99]. RAS GTPases are small single-subunit G proteins that have two conformational positions, a GDP-bound or GTP-bound state. The GTP-bound state results in downstream phosphorylation and signaling whereas the GDP-bound state is functionally inactive [Weinberg, 2007, pgs. 150-153]. Similar to the B-RAF^{V600E} mutation, a single nucleotide substitution from guanine to adenine at position 38 results in a glycine to aspartic acid change at residue 13 in the protein. Consequently RAS is now locked in a GTP-bound state and is constitutively active. One of RAS's target substrates is the RAF family kinases such as B-RAF. Therefore RAS activation also results in enhanced MAPK pathway signaling in addition to other kinase signaling cascades such as the phosphoinositide 3-kinase [PI_3K] pathway [Weinberg, 2007, pgs. 173-184].

Further upstream from RAS [and similar signaling factors] reside the growth factor receptors called RTKs. RTKs traverse the cellular membrane and require extracellular ligand binding in order for downstream signaling to occur. Extracellular ligand binding causes dimerization with other local RTKs and the close proximity of the two monomers allows *trans*-phosphorylation at tyrosine residues in partnered receptors. These newly phosphorylated residues serve as binding sites for additional proteins that facilitate signal transduction throughout the cytoplasm. Some binding partners include SRC, SOS [an activator of RAS] and PI_3K. These partners act as intracellular messengers of extracellular conditions via the RTKs [Weinberg, 2007, pgs. 166-173].

RTK signaling is increased numerous ways such as genomic amplification and point mutations. In contrast to B-RAF and RAS, there are numerous potential point mutants found for the RTK Epidermal Growth Factor Receptor [EGFR]. There are particular “hot spots” found in the protein that have a plethora of potential mutations and all are found within the tyrosine kinase domain. For instance the tyrosine kinase activation domain L858R mutation occurs about 43% of the time in EGFR mutant lung cancer but nucleotide-binding loop G719C/S/A mutations account for 5% of mutations as well. Furthermore these two sub-regions account for less than half of all EGFR mutations suggesting that there are multiple avenues to achieve enhanced kinase activity in EGFR [Pao, W. and Miller, V.A., 2005].

As mentioned previously, cancer is a complex multi-gene disease; *ipso facto* numerous genetic alterations must combine to achieve the transformed phenotype. However there must be certain combinations that cooperate better than others. In fact within human tumors we know that RAS and RAF mutations are mutually exclusive due to the fact that they are both activators of the same MAPK signaling pathway [Li W.Q. et al. 2006] A wide variety of cell culture and mouse models has found there to be an overarching theme among oncogenes and their cooperation. Intracellular signaling oncogenes, such as RAS, cooperate and give rise to a more aggressive cancer phenotype when combined with nuclear transcription factors that have oncogenic properties such as MYC. For example in rat embryonic fibroblast [REF] cell culture experiments, there is low transformation efficiency when activated RAS or MYC is added alone. However when both are introduced together, the REFs now form foci, a characteristic of proliferating cancerous cells [Weinberg, 2007, pgs. 427-429].

We will now shift focus to the other class of cancer genes, TSGs and their history, properties and how they interact with oncogenes. Early studies with heterokaryons, or fused cells, revealed a cell intrinsic tumor suppression activity. Normal mouse cells were mixed with a radio-labeled population of tumor cells. They were then induced to fuse using murine Sendai virus. The resulting cell fusion was no longer transformed and could not form tumors when explanted on naïve mice. Therefore there was some cellular component that was capable of

suppressing the tumor phenotype. The identity and nature of this component became an area of intense research because of its obvious role in stopping cancer [Weinberg, 2007, pgs. 210-213].

As mentioned previously, cancer is a disease of age where the older you get, the more likely you are to develop the right combination of genetic attributes that allow the disease to progress. However, this is not always the case. Unfortunately, there are early-onset syndromes where patients contract the disease in childhood or young adulthood. These individuals often times are not the only members of their family to experience this disease. Familial syndromes with a cancer predisposition have been invaluable to the study of the disease since they represent a human genetic model.

Retinoblastoma syndrome was the fertile ground that resulted in the discovery of one of the first TSG. Retinoblastoma is a cancer that forms within the retina of the eye usually resulting in blindness and in very rare cases, death. There are two forms of retinoblastoma, non-heritable or sporadic [no prevalence in the family history] and heritable where an immediate relative had the disease. Sporadic retinoblastoma presents the disease later in life and it is unilateral, or only in one eye. Heritable retinoblastoma presents early in life and can be screened for within the first months of life via an eye exam. Heritable retinoblastoma has a very high likelihood of presenting multiple tumors in both

eyes, known as bilateral retinoblastoma. Due to its early detection and low mortality, afflicted individuals can be cured and go on to live a normal reproductive life. However, their progeny now carry the risk of developing the disease as well [Weinberg, 2007, pgs. 214-216].

Analysis of disease presentation among numerous heritable retinoblastoma families gave rise to a seminal theory in cancer biology called “Knudson’s Two Hit Hypothesis”. In 1971 Alfred Knudson formulated a statistical analysis of disease presentation and age of onset. He noted that heritable retinoblastoma occurred earlier than the sporadic form of the disease and that the inherited form is almost always found in both eyes. When age of onset is plotted against percentage of disease-free population, the two groups of retinoblastoma patients differed significantly. The heritable retinoblastoma group formed a very linear relationship. In contrast, the sporadic retinoblastoma group had a later onset and a more gradual curve. Therefore Knudson hypothesized that cancer is a disease that requires multiple genetic alterations or “hits”. Children with heritable retinoblastoma were born with one “hit” already and were more likely to acquire the second “hit” than normal children [Weinberg, 2007, pg 216].

When applied to genes, this hypothesis suggests that one of two copies of a gene is disrupted in children with heritable retinoblastoma. They will acquire a second inactivating mutation at a rate concordant with the normal cellular

mutation rate, thus the linear relationship between time and frequency of disease, in other words, a quadratic kinetic relationship. However, an individual in the sporadic group started out with two normal copies of the gene. Therefore they will acquire a mutation in the gene at the same rate as the heritable group. However they will then need to acquire a second mutation in that same cell in order to cause retinoblastoma. This second hit has the same probability of occurring as the first but the overall rate is the normal rate multiplied against the normal rate. This results in a significantly lower rate in the sporadic group versus the heritable group, hence the later onset in the sporadic group and a polynomial kinetic relationship. For instance, if the average rate is one mutation in the gene of interest every 5 weeks, then the rate for the sporadic group is two mutations in the genes of interest every 25 weeks. The conclusion from this theory is that a single copy of a tumor-suppressing gene is sufficient for its function. In order to have the disease progress, both copies of the gene must be inactivated. The loss of the second copy is known as loss of heterozygosity [LOH] [Weinberg, 2007, pgs. 216-223]. It is interesting to note that the inheritance pattern among heritable retinoblastoma families suggests a dominant gene is being inherited. Yet it is the disease that is inherited dominantly, not the genes, which display a recessive mutation pattern.

Later through a technique called restriction fragment length polymorphism [RFLP], the gene responsible for preventing retinoblastoma was identified

[Weinberg, 2007, pgs. 222-223]. Called Rb, for retinoblastoma, it turned out to be a very important gene in cell cycle regulation. Rb is normally bound to the E2F transcription factor that is responsible for S phase transcription and progression through cell division. Rb binding prevents E2F-dependent transcription and the cells do not divide. However when Rb becomes hyperphosphorylated, it cannot bind E2F and S-phase progresses. Therefore individuals with absent or defective Rb genes have uncontrolled cell growth and a much higher propensity for cancer [Weinberg, 2007, pgs. 277-284].

In contrast to retinoblastoma, Li-Fraumeni syndrome presents individuals with many different types of cancer. Analysis of family trees revealed a dominant inheritance pattern with many afflicted individuals being immediately related [Weinberg, 2007, pg 333]. Due to the diversity of cancers presented in Li-Fraumeni syndrome patients we can infer that there is a critical, or more general, TSG being inactivated in this syndrome. Through numerous studies by Lionel Crawford, David Lane, Arnold Levine, Lloyd Old, Wafik El-Deiry and Bert Vogelstein, the identity of this tumor suppressor was determined to be a 44 kilo Dalton [kDa] protein called TP53, or tumor protein 53 because it ran at around 53 kDa on a sodium dodecyl sulfate polyacrylamide gel electrophoresis [SDS-PAGE] gel [see for example Linzer D.I.H and Levine A.J., 1979; Lane, D.P. and Crawford, L.V. 1979; De Leo A.B. et al. 1979; Crawford, L.V. et al., 1982; el-Deiry, W.S., et al. 1992 and Baker, S.J. et al., 1990]. When TP53 is deleted in a

mouse model, the mice develop mostly lymphomas but when a mouse harbors a mutation found in Li-Fraumeni syndrome they develop a wide spectrum of tumors analogous to Li-Fraumeni patients. Both mice model develop cancer with a greatly accelerated rate over normal or heterozygous mice. Therefore we can conclude that TP53 is a broadly used and critical tumor suppressor in the body [Olive, K.P. et al., 2004 and Donehower, L.A., et al. 1992].

TP53 has been an area of intense research given its generalizability and importance in cancer prevention and is arguably the most widely studied protein. It is now widely accepted that TP53 is a central hub of many intracellular signals and executes a critical role in deciding the major decisions of a cell. TP53 integrates signals from DNA damage, oxygen levels, nucleotide abundance and oncogene signaling. In return, TP53 tetramerizes with itself and turns transcription of genes on in a process otherwise known as transactivation. The result of this transcriptional regulation is upregulating processes such as DNA repair, cell cycle arrest, senescence, apoptosis and the inhibition of angiogenesis. For instance, if the cell is damaged, TP53 executes a transcriptional program to repair the cell or enter apoptosis. Thus, TP53 is the essential factor that oversees the integrity of cells and maintains the “normalcy” of a cell population [Zilfou, J.T. and Lowe, S.W. 2009]

Interestingly, TP53 was initially considered an oncogene not a tumor suppressor. It was originally cloned from a tumor cell, hence the name tumor protein 53. The tumor cell was capable of expressing this protein since it was mutated and did not properly function. This mutated form was capable of transforming normal cells and thusly acted as a dominant negative isoform with oncogenic properties [Weinberg, 2007, pgs. 310-314]. The nature of this ability to prevent the normal functioning TP53 in the fibroblasts is derived from the tetramerization requirement of protein. Hence the TP53 gene must tetramerize with three additional wildtype copies of TP53 in order to function. Otherwise the tetramer is "poisoned" and displays dysfunctional transcriptional activation of target genes.

When mouse fibroblasts are introduced with an activated RAS allele and possess a wildtype copy of TP53, the cells fail to create foci in cell culture. However if the fibroblasts lack TP53 due to genetic deletion in mouse model such as TP53 knock out [KO] mouse embryonic fibroblasts [MEFs], the introduction of RAS allows foci to form. Interestingly, the introduction of RAS to mouse fibroblasts that harbor a $TP53^{C135V}$ ultimately form many more foci than the TP53 deletion. This reinforces the previous theory that TP53 must tetramerize with three wildtype copies of itself to function. However the $TP53^{C135V}$ version actually displays a gain of function in terms of foci formation [Weinberg, 2007, pgs. 310-314]. This experiment also displays an important relationship between TSGs and oncogenes. A TSG must be inactivated prior to oncogene activation. Otherwise,

the TSG is able to detect the oncogene activation and in turn activate TP53 who in turn removes the oncogene-bearing cell from the proliferating population via apoptosis or senescence in a process known as OIS. Despite the firm grasp researchers have on this concept, there is a poor understanding as to how this detection and execution takes place.

This surveillance mechanism is critical for maintaining the integrity of the cell population. The genes that have been identified related to this function are all TSGs and among some of the most well studied genes of all time. One of the critical genes that detect oncogene signaling and up-regulates TP53 is $p14^{ARF}$ in humans and $p19^{ARF}$ in mouse. $p14^{ARF}$ responds to hyperactivated cell growth signaling such as the RAS/RAF/MEK/ERK pathway or aberrant E2F transcriptional activity and subsequently inactivates the protein responsible for TP53 degradation, HDM2 [Weinberg, 2007, pgs. 318-323]. HDM2 is an E3 ubiquitin ligase that targets TP53 for degradation by the proteasome. $p14^{ARF}$ antagonizes HDM2 function in two ways, first it inhibits the E3 ubiquitin ligase activity and secondly it blocks the nuclear localization of HDM2 and in turn sequesters it in the nucleolus. TP53, being a nuclear-localized transcription factor, is thusly protected from HDM2's activities and is allowed to accumulate [Weinberg, 2007, pgs. 318-323]. Upon accumulation TP53 goes on to transactivate target genes that halt cell cycle progression and ultimately initiate either senescence or apoptosis.

$p14^{ARF}$ resides within a unique genetic locus with two other important cell cycle regulators in chromosome 9, $p16^{INK4A}$ and $p15^{INK4B}$, and collectively they are known as the *INK4-ARF* locus. $p16^{INK4A}$ and $p15^{INK4B}$ are classical cyclin-dependent kinase [CDK] inhibitors that bind to CDKs and prevent their phosphorylation of Rb. Therefore $p16^{INK4A}$ and $p15^{INK4B}$ maintain Rb binding to E2F and inhibit S-phase progression. $p16^{INK4A}$ and $p14^{ARF}$ share exons two and three, yet have unique and distantly located first exons and promoters. Unexpectedly, $p14^{ARF}$'s exons two and three are read in an alternative reading frame from $p16^{INK4A}$, hence the name ARF [Sherr, C.J., 2006].

Mouse models that delete the endogenous copies of $p19^{ARF}$ display a marked increase in tumor frequency [Kamijo, T. et al. 1999]. Furthermore, $p14^{ARF}$ is absent in many different human cancers such as colorectal, bladder and breast cancer [Sherr, C.J., 2006]. It is interesting to note that the deletion of TP53 or $p14^{ARF}$ does not always cause cancer in cell lines or mouse models immediately. However, if an oncogene, such as RAS, is introduced subsequently, then there is a bypass of the OIS response and the transformed phenotype is much more readily obtained. Given their paramount importance in tumor suppression and close genomic proximity, it should come as no surprise that genetic alterations that inactivate all three *INK4-ARF* genes are prevalent in cancer [Sherr, C.J., 2006].

Two such methods of inactivating large portions of DNA are genomic deletion and epigenetic silencing. Genomic deletions result in losses of large segments of the chromosome. While the *INK4-ARF* locus is frequently deleted in many cancers, the three genes in the *INK4-ARF* locus are also among the top ten genes epigenetically silenced in all cancers [Esteller, M., 2002]. Epigenetic silencing is an emerging element in the progression of cancer. Epigenetics is defined as any heritable change in gene expression that does not result from a change in the DNA sequence.

Two major classes of epigenetic silencing mechanisms exist; histone modifications and DNA methylation, and they are often concurrent with one another. Histone modifications are believed to control the packaging and access of the DNA to other regulatory factors such as transcription factors and polymerases. Histone proteins that package the DNA into higher order structures are regulated through post-translational modifications on their N-terminal tails. The properties of these chemical moieties affect the binding affinity of the tails for DNA. For instance, histone acetylation on lysine residues reduces the positive charge on the tails and thusly decreases their affinity for the negatively charged DNA backbone. Therefore, histone acetylation is associated with active transcription while histone deacetylation is associated with transcriptional repression. Another histone modification, methylation, can cause transcriptional repression. Histone three lysines nine and twenty seven, when

methylated, result in a robust inhibition of transcription and an efficiently silenced state [Weinberg, 2007, pgs. 226-232].

DNA hypermethylation is another characteristic of silenced chromatin and occurs at the 5' position of the dinucleotide cytosine-phospho-guanine [CpG] residues, thus generating two 5-methylcytosine nucleotides anti-parallel to one another. However, it must occur at CpG dinucleotides so that the mark can be deposited on both strands of DNA and be stably inherited upon DNA synthesis. Furthermore, cytosine is inherently less stable than the three other base nucleotides and can spontaneously deaminate into uracil. This results in a point mutation if it is not discovered by DNA surveillance mechanisms and repaired. This spontaneous deamination has created a depletion of CpG dinucleotides in the genome yet some areas are unusually rich in Cpgs.. These so called CpG islands have an overabundance of CpG dinucleotides and are typically found near the transcriptional start site [TSS] of genes. Hypermethylation within these CpG islands results in a silenced chromatin state and loss of gene expression [Weinberg, 2007, pgs. 226-232].

Despite the fact that there is a global hypomethylation of the genome that takes place in cancer progression, CpG island hypermethylation typically occurs at the promoters of TSGs and has been attributed to supporting cancer progression [Laird, P.W. and Jaenisch, R. 1994]. While existing as a prevalent phenomenon

in both cell culture and human cancers, the factors responsible for directing and silencing TSGs via CpG island hypermethylation remain to be elucidated.

The discovery of ribonucleic acid interference [RNAi] or post-transcriptional gene silencing [PTGS] has greatly expanded the abilities of researchers to interrogate biological processes. The discovery of RNAi resulted in Andrew Fire and Craig Mello receiving the 2006 Nobel Prize in Physiology and Medicine. RNAi is a biological process where short double stranded RNA [dsRNA] molecules inhibit the expression of a gene in a sequence specific manner and promote the degradation of its messenger RNA [mRNA] [Mello, C.C. and Conte, D. Jr, 2004]. There are multiple endogenous and exogenous forms of RNAi that rely on slightly different short RNA species. For instance cells naturally harbor non-coding microRNAs [miRNAs], which are the products of transcription yet they form characteristic secondary structures and are processed by the RNA-induced silencing complex [RISC]. Conversely synthetic short interfering RNAs [siRNAs] can be transfected into cells and are loaded into the RISC machinery and facilitate silencing of their target mRNA. Finally, there are short hairpin RNAs [shRNAs] that display some of the properties of miRNAs and siRNAs and can be conveniently cloned into viral vectors. These vectors [often retroviral or lentiviral backbone vectors for stable expression] carry a miRNA-like promoter sequence and transcribe a single-stranded RNA that has a characteristic stem-loop structure similar to a miRNA's secondary structure. However, the stem-loop

dsRNA is cleaved and gives rise to a siRNA-like molecule and executes gene silencing in a manner more similar to siRNAs.

RNAi has become a tremendous tool due to its sequence-specificity and efficiency at silencing gene expression. There are now entire libraries of RNAi molecules for both siRNAs and shRNAs that target every gene in the genome with multiple independent dsRNAs. Therefore researchers can perform systematic loss of function screens where every gene in the genome is interrogated individually and with multiple independent RNAi molecules. Therefore any unknown biological process that can give a robust signal in an assay [such as cell survival or green fluorescence protein [GFP] fluorescence] can be coupled with an RNAi screen to determine the genes involved. In this way novel genes and pathways can be identified and systematically followed up for their biological mechanism and function.

With the acquisition of shRNA libraries I chose to investigate the biology of cancer using these tools. Here I describe the interrogation of two distinct processes in cancer. First I investigate the molecular players involved in OIS in melanocytes. I find that upon introduction of the oncogene $BRAF^{V600E}$, melanocytes undergo rapid apoptosis and senescence. However, I identified 17 factors that upon knockdown confer survival to the cells. Therefore these genes that are knocked down are involved in the $BRAF^{V600E}$ induced senescence

process. I identify and characterize a secreted protein called IGFBP7 that I find to play a critical role in melanomagenesis prevention.

Secondly I investigated the factors responsible for epigenetically silencing the TSG *p14*^{ARF} in colorectal cancer using a genome-wide shRNA screen. I identify a novel zinc finger transcription factor, ZNF304, which directs a silencing complex to the promoter of *p14*^{ARF}. I find that ZNF304 overexpression is dependent upon RAS activation. RAS signaling upregulates the deubiquitinase USP28 that antagonizes ZNF304 proteasome-mediated degradation, thus resulting in ZNF304 overexpression in human K-RAS-positive colorectal cancer. Furthermore, I find that ZNF304 is responsible for directing the epigenetic silencing of a group of ~50 genes known as Group 2 CIMP marker genes in K-RAS-positive cancers.

These two sets of studies identify and explore the interrelated relationship between oncogenes and TSGs. I have elucidated a set of genes that respond to oncogene activation and act to shut down cell growth to prevent melanomagenesis. When melanoma does occur it must circumvent this response and it does so through epigenetic silencing of the TSG, IGFBP7. Through my second set of studies I have explored this process of epigenetic silencing of TSG. I have found key players that preferentially silence these TSGs and how they are dependent upon oncogene signaling. Taken together, I have

revealed a novel regulatory network that contributes to our understanding of cancer biology.

CHAPTER II: BRAF^{V600E} INDUCED SENESCENCE SCREEN

Preface

The majority of this research chapter derives from the work I performed with Narendra Wajapeyee, Ph.D. while we were in Michael Green, M.D./Ph.D.'s lab at UMass Medical School. It was subsequently published in the journal Cell in 2008 entitled "Oncogenic BRAF Induces Senescence and Apoptosis through Pathways Mediated by the Secreted Protein IGFBP7." Narendra was the first author and I was the second author and the remaining co-authors were Xiaochun Zhu, Meera Mahalingham and Michael Green. Narendra and I came up with the concept for the screen and performed preliminary experiments using a variety of cell lines and oncogene combinations before settling on human fibroblasts with BRAF^{V600E} introduction. Narendra largely performed the cell culture component of the screen with my assistance making the BRAF^{V600E} virus and sequence identifying candidate shRNAs. Both Narendra and myself carried out validation of the candidate genes. Narendra performed all Annexin V and BrdU incorporation experiments and I performed most of the proliferation experiments and senescence-associated beta-galactosidase [SA-βGal] experiments and imaging. Xiaochun Zhu and myself performed the generation and purification of recombinant IGFBP7 [rIGFBP7]. Narendra and myself performed the quantitative real-time polymerase chain reactions [qRT-PCRs], chromatin immunoprecipitations [ChIPs] and sodium bisulfite sequencing [NaB-Seq] analysis throughout the paper either working alone or in concert. Both Narendra

and myself, given the needs of the experiments, performed cell culture of fibroblasts, melanocytes and melanoma cell lines as well as drug treatments and generation of knockdown [KD] cell lines. Narendra and myself often performed mouse xenograft experiments in tandem, however Narendra was usually responsible for the injections of rIGFBP7. Meera Mahalingham, a trained dermatopathologist facilitated our studies with human melanomas and naevis. She provided us with tissue sections that were characterized by disease status and Narendra and I performed the genotyping and NaB-Seq analysis together. The immunohistochemistry staining for IGFBP7 was carried out at the UMass DERC Histology core facility and the results were photographed by myself and scored for expression by Meera. Sarah Deibler [at the time, Sara Evans] facilitated the figure generation for the manuscript and edited the writing. The paper was co-written by Narendra, Michael and myself. Narendra and myself addressed the reviewers' comments and performed all requested experiments in tandem.

Subsequent to publication of this manuscript, work from the lab of Helen Rizos at the Westmead Institute for Cancer Research in Australia challenged some of our findings. According to their work, they did not find any link between $BRAF^{V600E}$, IGFBP7, the IGFBP7 target gene expression [SMARCB1, BNIP3L and PEA15] and senescence induction in human melanomas and melanocyte cultures.

Following the publication of our Cell paper on IGFBP7, the lab of Helen Rizos at the Westmead Institute for Cancer Research in Australia refuted certain key aspects of our work and published a “Matters Arising” article entitled “IGFBP7 is Not Required for B-RAF-Induced Melanocyte Senescence” [Scurr, L.L., et al. 2010]. Namely, they found there to be no correlation between expression of IGFBP7, PEA15 or BNIP3L upon $BRAF^{V600E}$ introduction in melanocytes and fibroblasts. Furthermore, they analyzed numerous cell lines, melanoma and nevi samples and again found no correlation between BRAF status and IGFBP7 expression. They concluded that IGFBP7 is unnecessary for BRAF induced senescence.

Unsurprisingly, we refuted their claims and presented a rebuttal shortly thereafter as a “Leading Edge Correspondence” in Cell entitled “Role for IGFBP7 in Senescence Induction by BRAF.” There were many aspects of Scurr, L.L. et. al. [2010] that were of concern to our group. For one, they repeatedly fail to reproduce well-established and published results such as the induction of TP53 post infection with $BRAF^{V600E}$. As a basic objection to their claims it is also noteworthy to mention they fail to use positive controls in most of their experiments that show negative data raising the possibility that their assays were not fully functional. Furthermore their analysis of IGFBP7, BNIP3L and PEA15 was performed using immunoblots and not qRT-PCR as we had done.

In addition, their analysis of melanomas and IGFBP7 expression failed to stratify primary versus metastatic melanomas. In fact, our results reveal that metastatic melanoma lose IGFBP7 expression more frequently yet it does not correlate with BRAF status. Therefore if primary and metastatic melanoma were not analyzed separately you would fail to see the correlation present in primary melanomas. Finally, the panel of cell lines they analyzed for IGFBP7 expression was a diverse collection of melanoma, non-melanoma and primary cells. In our report we chose to focus on melanocytes and melanoma and never expanded our results to other cell types. Above and beyond our results that refute their claims, there have been a number of independent groups that have verified and expanded upon our results. Importantly two groups have shown a loss of IGFBP7 expression that correlates with BRAF status in colorectal cancer, a cancer type that frequently harbors a BRAF mutation [Hinoue et al., 2009; Suzuki et al., 2010].

In summary, the work of Helen Rizos' group has raised important questions about our original Cell paper. It is our belief that their experiments were not rigorously designed and that they failed to recognize the scope of our claims. In response we repeated many experiments in additional cell lines and patient samples using a variety of assays that reinforce our original conclusions. Finally the scientific literature bears several examples of other independent labs that have reproduced and expanded upon our original results. We conclude that our

original results remain that IGFBP7 is a critical tumor suppressor in the process of BRAF-induced senescence and in the biology of melanoma.

Introduction

Expression of an oncogene in a primary cell can, paradoxically, block proliferation by inducing senescence or apoptosis through pathways that remain to be elucidated. Here I perform genome-wide RNAi screening to identify 17 genes required for an activated BRAF oncogene [$BRAF^{V600E}$] to block proliferation of human primary fibroblasts and melanocytes. Surprisingly, I find a secreted protein, IGFBP7, has a central role in $BRAF^{V600E}$-mediated senescence and apoptosis. Expression of $BRAF^{V600E}$ in primary cells leads to synthesis and secretion of IGFBP7, which acts through autocrine/ paracrine pathways to inhibit BRAF-MEK-ERK signaling and induce senescence and apoptosis. Apoptosis results from IGFBP7-mediated upregulation of BNIP3L, a proapoptotic BCL2 family protein. Recombinant IGFBP7 [rIGFBP7] induces apoptosis in $BRAF^{V600E}$-positive human melanoma cell lines, and systemically administered rIGFBP7 markedly suppresses growth of $BRAF^{V600E}$-positive tumors in xenografted mice. Immunohistochemical analysis of human skin, nevi, and melanoma samples implicates loss of IGFBP7 expression as a critical step in melanomagenesis.

When expressed in primary cells, activated oncogenes can block cellular proliferation by inducing senescence or apoptosis [reviewed in Campisi, 2005; Mooi and Peeper, 2006]. OIS and apoptosis are thought to play important roles in suppressing tumorigenesis by preventing proliferation of cells at risk for neoplastic transformation [Campisi, 2005; Michaloglou et al., 2005].

The BRAF proto-oncogene provides a paradigm for studying OIS and apoptosis. BRAF is a serine-threonine protein kinase that functions as an immediate downstream effector of RAS [reviewed in Dhomen and Marais, 2007]. BRAF activates the MAPK extracellular signal regulated kinase [MEK], which in turn phosphorylates and activates extracellular signal-regulated kinases 1 and 2 [ERK1 and ERK2].

Activating BRAF mutations are found at high frequency in human cancers and are particularly prevalent in melanoma where they occur at a frequency of 50%–70% [Davies et al., 2002]. Approximately 90% of activating BRAF mutations is glutamic acid to valine substitution at position 600 [V600E; formally identified as V599E] [Davies et al., 2002]. This mutation substantially increases protein kinase activity, resulting in constitutive BRAF-MEK- ERK signaling [Davies et al., 2002]. In $BRAF^{V600E}$-positive melanoma cell lines and mouse xenografts, $BRAF^{V600E}$ has been shown to be required for cell viability, proliferation, and tumor growth [Hingorani et al., 2003; Hoeflich et al., 2006; Satyamoorthy et al., 2003; Sharma et al., 2005].

Activating BRAF mutations are also present in up to 82% of melanocytic nevi [Pollock et al., 2003], which are benign skin lesions that rarely progress to melanoma [Bennett, 2003; Chin et al., 1998]. Nevi are growth arrested and display classical hallmarks of senescence, including expression of SA-β-Gal and

the cell-cycle inhibitor $p16^{INK4A}$ [Michaloglou et al., 2005; Sparrow et al., 1998; Wang et al., 1996]. Expression of $BRAF^{V600E}$ also induces senescence in cultured primary human melanocytes [Michaloglou et al., 2005].

How, then, does an activated BRAF oncogene induce uncontrolled proliferation in melanoma and senescence in benign nevi? One hypothesis is that melanomas contain a second oncogenic lesion that inactivates the BRAF-mediated senescence pathway [reviewed in Campisi, 2005]. Although attractive, this hypothesis remains to be proven largely because the downstream factors and signaling pathways involved in BRAF-mediated senescence have not been characterized. Here I perform a genome-wide RNA-interference [RNAi] screen to identify factors required for $BRAF^{V600E}$ to block cellular proliferation.

Results

To identify genes required for $BRAF^{V600E}$ to block proliferation of primary cells, I performed a genome-wide small hairpin RNA [shRNA] screen [Figure 2-1]. The primary screen was performed in human primary foreskin fibroblasts [PFFs]. A human shRNA library comprising ~62,400 shRNAs directed against ~28,000 genes was divided into 10 pools, which were packaged into retrovirus particles and used to stably transduce PFFs. The cells were then infected with a retrovirus expressing $BRAF^{V600E}$ under conditions in which all cells were infected. Cells that bypassed the $BRAF^{V600E}$-mediated cellular proliferation block formed colonies, which were pooled and expanded, and the shRNAs identified by sequence analysis. Positive candidates were confirmed by stable transduction of PFFs with single shRNAs directed against the candidate genes, infection with the $BRAF^{V600E}$-expressing retrovirus, and quantitation of cellular proliferation. Confirmed candidate shRNAs were then tested in a secondary screen for their ability to bypass the proliferation block in $BRAF^{V600E}$-expressing primary human melanocytes.

The screen identified 17 genes that, following shRNA-mediated knockdown, enabled $BRAF^{V600E}$-expressing PFFs [$BRAF^{V600E}$/PFFs] and melanocytes [$BRAF^{V600E}$/melanocytes] to proliferate. These genes are listed in Table 2-1 and proliferation assays of the 17 $BRAF^{V600E}$/PFF knockdown [KD] cell lines are shown in Figure 2-2 and Figure 2-3

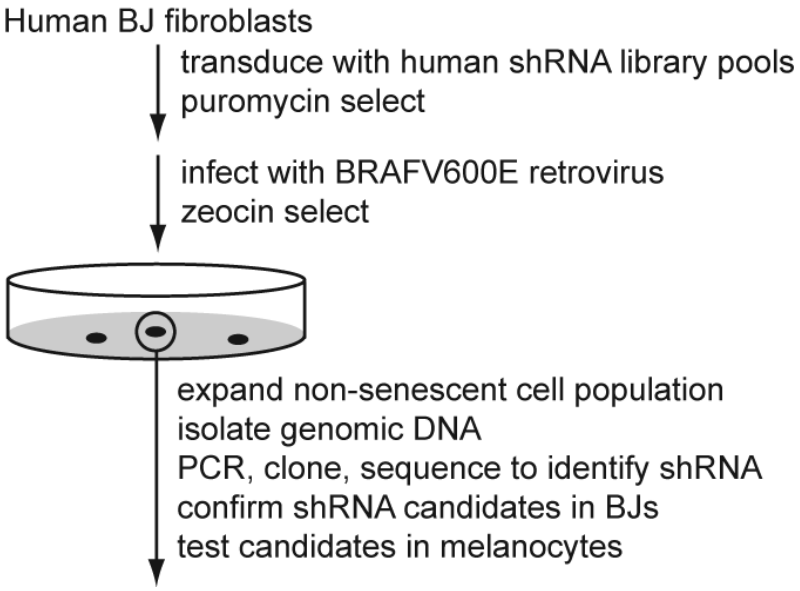

Figure 2-1. Schematic summary of the genome-wide shRNA screen.

Biological process	Accession number	Gene symbol	Gene name
Apoptosis	NM_004331	*BNIP3L*	BCL2/adenovirus E1B 19kDa interacting protein 3-like
Cell cycle regulation	NM_004336	*BUB1*	budding uninhibited by benzimidazoles 1 homolog (yeast)
Signal transduction	NM_004305	*BIN1*	bridging integrator 1
	NM_004134	*HSPA9*	heat shock 70 kDa protein 9 (mortalin)
	NM_001553	*IGFBP7*	insulin-like growth factor binding protein 7
	NM_000877	*IL1R1*	interleukin 1 receptor, type I
	NM_003768	*PEA15*	phosphoprotein enriched in astrocytes 15
	NM_002885	*RAP1GAP*	RAP1 GTPase activating protein
Transcription regulation	NM_021145	*DMTF1*	cyclin D binding myb-like transcription factor 1
	NM_004496	*FOXA1*	forkhead box A1
	NM_002198	*IRF1*	interferon regulatory factor 1
	NM_000244	*MEN1*	multiple endocrine neoplasia 1
	NM_000546	*TP53*	tumor protein p53 (Li-Fraumeni syndrome)
Chromatin remodeling	NM_003325	*HIRA*	HIR histone cell cycle regulation defective homolog A (*S. cerevisiae*)
	NM_001007468	*SMARCB1*	SWI/SNF related, matrix associated, actin dependent regulator of chromatin, subfamily b, member 1
Genome stability	NM_000268	*NF2*	neurofibromin 2 (bilateral acoustic neuroma)
Unknown	NM_024735	*FBXO31*	F-box protein 31

Table 2-1. Genes required for $BRAF^{V600E}$ to block proliferation of human PFFs and melanocytes

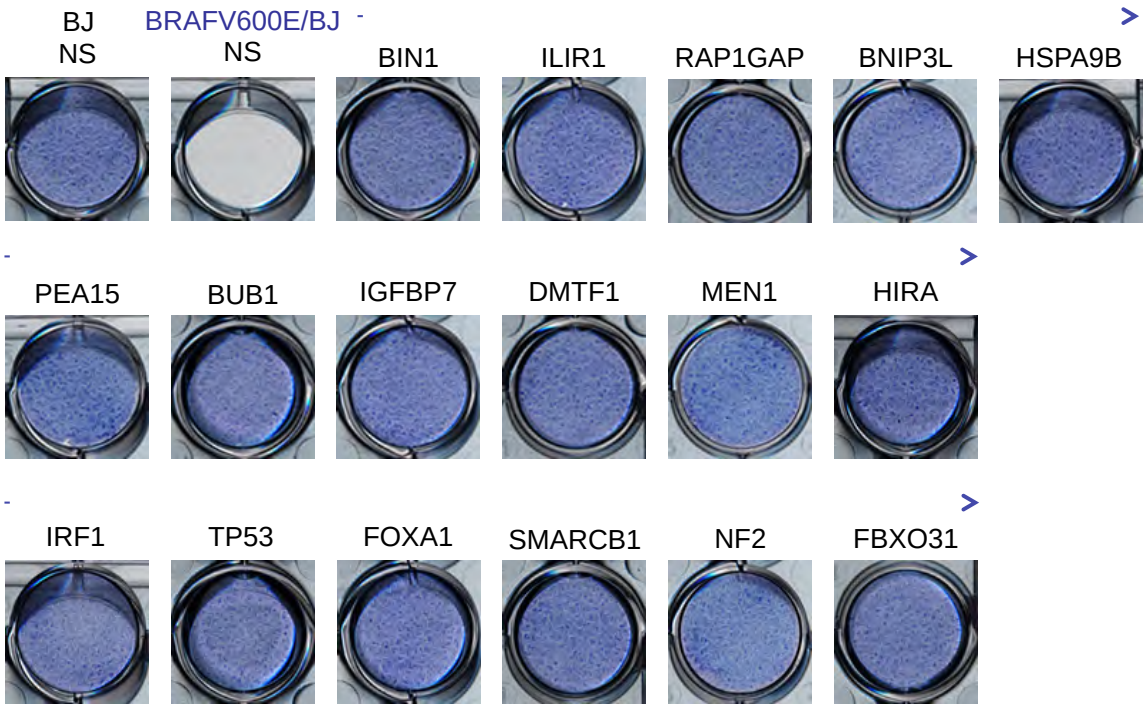

Figure 2-2. Proliferation of the 17 BRAF^{V600E}/PFF KD cell lines.
1 x 10^4 PFF fibroblasts stably expressing the indicated shRNA were cultured in 12-well plates, infected with the BRAF^{V600E}-expressing retrovirus, and after 14 days stained with crystal violet.

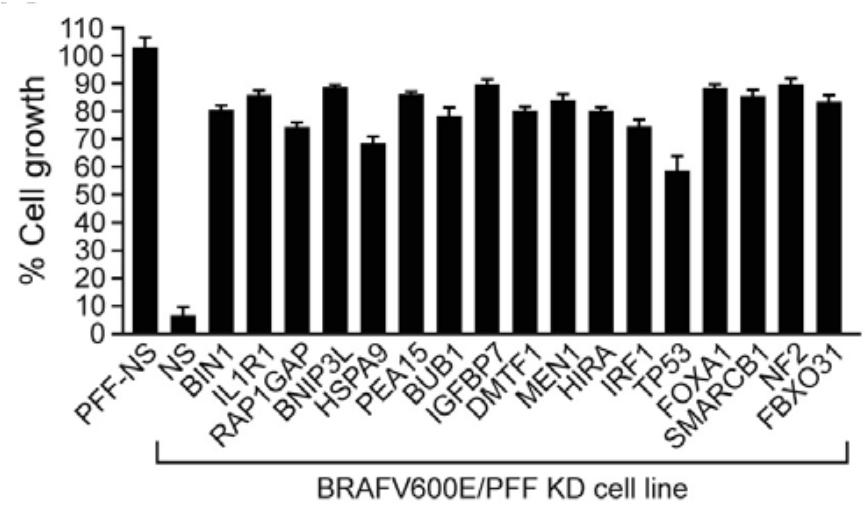

Figure 2-3. Quantitative proliferation assays of the 17 BRAF^{V600E}/PFF KD cell lines shown in Figure 2-2.
PFFs stably expressing the indicated shRNA were infected with the BRAF^{V600E} expressing retrovirus and after 14 days analyzed by the trypan blue exclusion assay. Growth of PFFs expressing a non-silencing shRNA [PFF-NS] relative to growth of untreated PFFs is shown. For the BRAF^{V600E}/PFF KD cell lines, values were normalized to the growth of the corresponding PFF KD cell line in the absence of BRAF^{V600E} expression. Error bars represent standard error.

Expression of $BRAF^{V600E}$ in PFFs containing a control non-silencing [NS] shRNA [Figure 2-2] efficiently inhibited cellular proliferation. Significantly, however, this block was overcome in all 17 $BRAF^{V600E}$/PFF KD cell lines. Quantitative real-time RT-PCR [qRT-PCR] confirmed in all cases that expression of the target gene was decreased in the corresponding KD cell lines [Figure 2-4]. For all 17 genes, a second, unrelated shRNA directed against the same target gene also enabled PFFs to proliferate following $BRAF^{V600E}$ expression [Figure 2-5].

As expected from previous studies [Michaloglou et al., 2005], expression of $BRAF^{V600E}$ in primary PFFs efficiently blocked cellular proliferation [Figure 2-3]. By contrast, $BRAF^{V600E}$ failed to block cellular proliferation in all 17 PFF KD cell lines.

Following expression of $BRAF^{V600E}$ in melanocytes, the majority of cells became senescent [Figure 2-6], consistent with previous studies [Michaloglou et al., 2005], although I found that ~10% of cells underwent apoptosis [Figure 2-7]. To determine the role of the 17 genes in these two pathways, apoptosis and senescence assays were performed in each melanocyte KD cell line following $BRAF^{V600E}$ expression. Figure 2-7 shows that only 3 of the 17 genes were required for apoptosis: BNIP3L, which encodes a proapoptotic BCL2 family protein; SMARCB1, which encodes a component of the

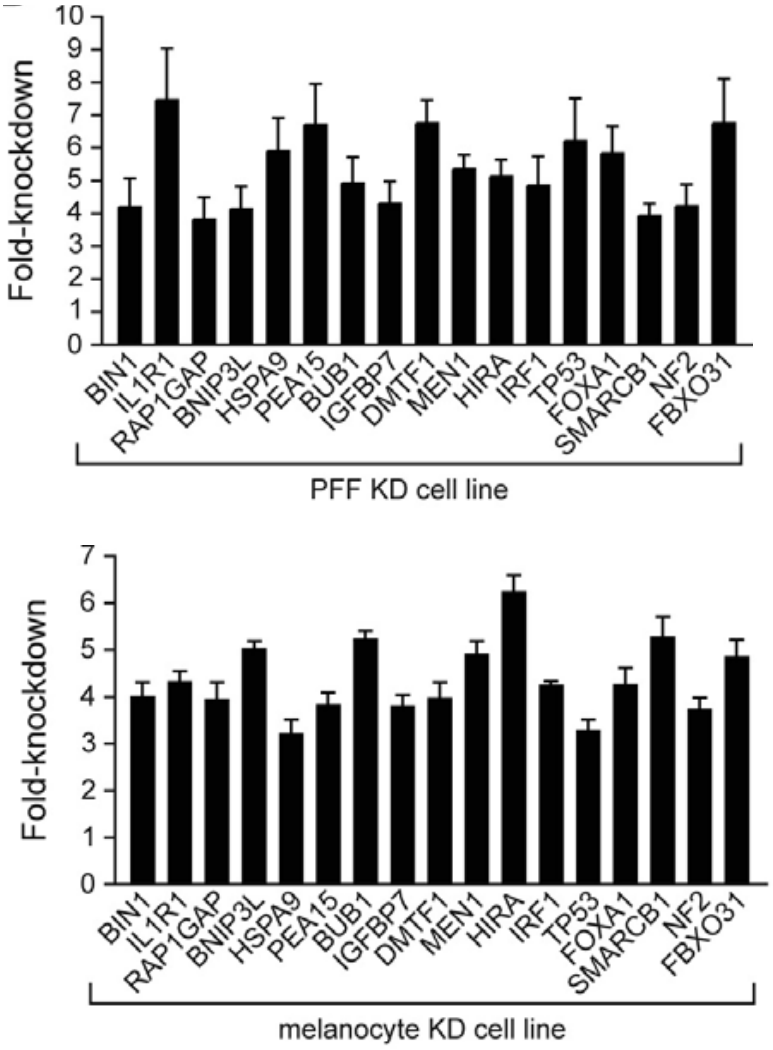

Figure 2-4. Analysis of target gene expression in the PFF and melanocyte KD cell lines. Quantitative real-time RT-PCR was used to analyze target gene expression in each of the 17 PFF [Top] or melanocyte [Bottom] KD cell lines.

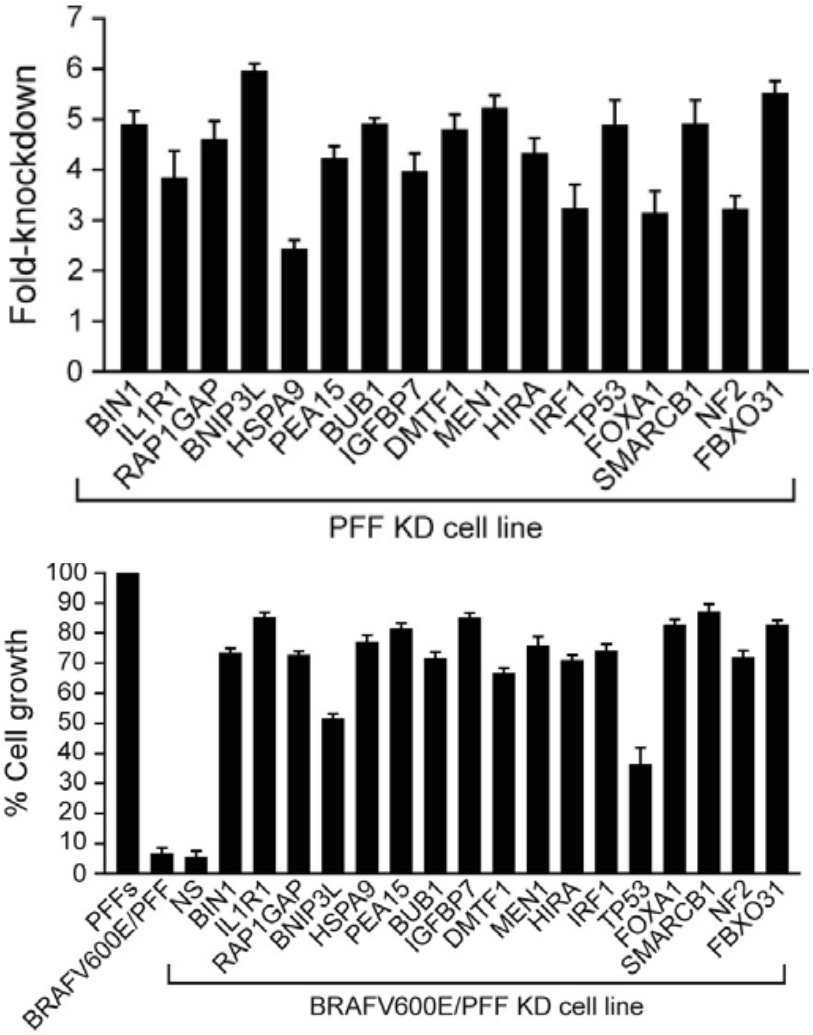

Figure 2-5. Confirmation of all 17 candidate genes using a second, unrelated shRNA directed against the target gene.
[Top] Quantitative proliferation assays. For each of the 17 candidate genes, a second, unrelated shRNA directed against the same target gene was used to derive an independent PFF KD cell line. Each PFF KD cell line was infected with the $BRAF^{V600E}$ expressing retrovirus and proliferation monitored after 14 days. Growth of $BRAF^{V600E}$/PFFs is expressed relative to the growth of normal PFFs. For the $BRAF^{V600E}$/PFF KD cell lines, values were normalized to the growth of the corresponding PFF KD cell line in the absence of $BRAF^{V600E}$ expression.
[Bottom] Quantitative real-time RT-PCR was used to analyze target gene expression in each of the 17 PFF KD cell lines.

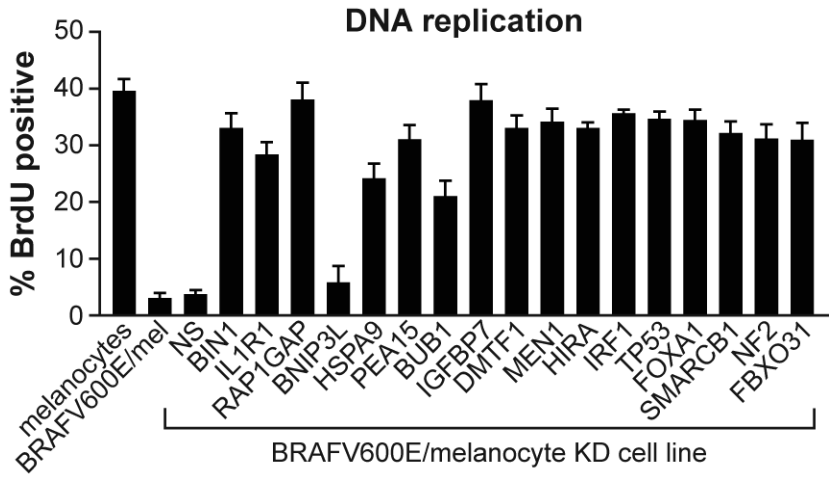

Figure 2-6. DNA replication assays of the 17 $BRAF^{V600E}$/melanocyte KD cell lines, monitored by BrdU incorporation. Error bars represent standard error.

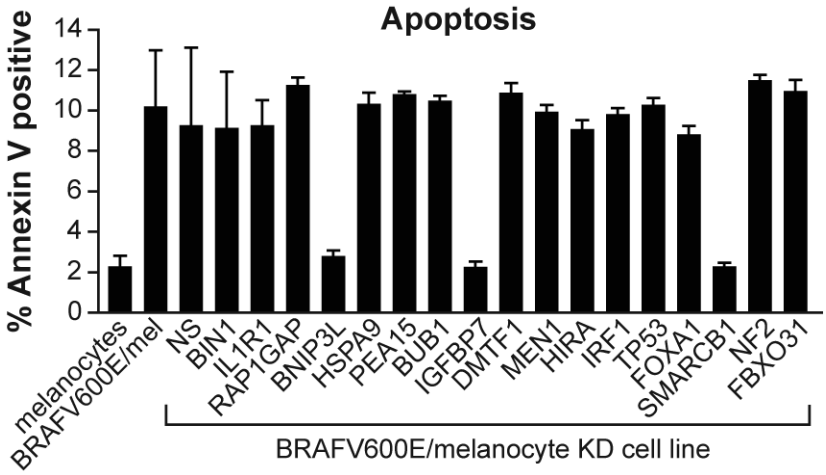

Figure 2-7. Apoptosis assays of the 17 $BRAF^{V600E}$/melanocyte KD cell lines, monitored by Annexin V-PE staining. Error bars represent standard error.

SWI/SNF chromatin-remodeling complex; and insulin growth factor binding protein 7 [IGFBP7], which encodes a secreted protein with weak homology to IGF-binding proteins. By contrast, all but 1 of the 17 genes, BNIP3L, are required for $BRAF^{V600E}$ to induce growth arrest [Figure 2-6] and characteristic markers of senescence [see below]. Presumably the BNIP3L shRNA was picked up in the screen due to its ability to an inability to induce apoptosis upon $BRAF^{V600E}$ introduction, yet the cells still fail to proliferate. Identical results were obtained using $BRAF^{V600E}$/melanocyte KD cell lines that had undergone an additional 15 population doublings [Figure 2-8] and in PFFs [Figure 2-9].

$p16^{INK4A}$ has been proposed to play an important role in replicative and oncogene-induced senescence [reviewed in Ben-Porath and Weinberg, 2005]. I was therefore interested in determining whether the genes identified in my screen were required for $p16^{INK4A}$ induction. Figure 2-10 shows, as expected, that $p16^{INK4A}$ levels increased substantially following $BRAF^{V600E}$ expression in control melanocytes expressing an NS shRNA. Significantly, $p16^{INK4A}$ expression was not induced by $BRAF^{V600E}$ in 16 of the 17 melanocyte KD cell lines. The sole exception was the cell line knocked down for BNIP3L, which, as described above, is specifically involved in apoptosis [Figure 2-10]. The failure to pick up $p16^{INK4A}$ as a candidate gene indicates that my shRNA screen, like other large-scale shRNA screens [see, for example Mullenders, 2009], was not saturating.

Loss of histone H3 lysine 9 [H3K9] acetylation, another well characterized

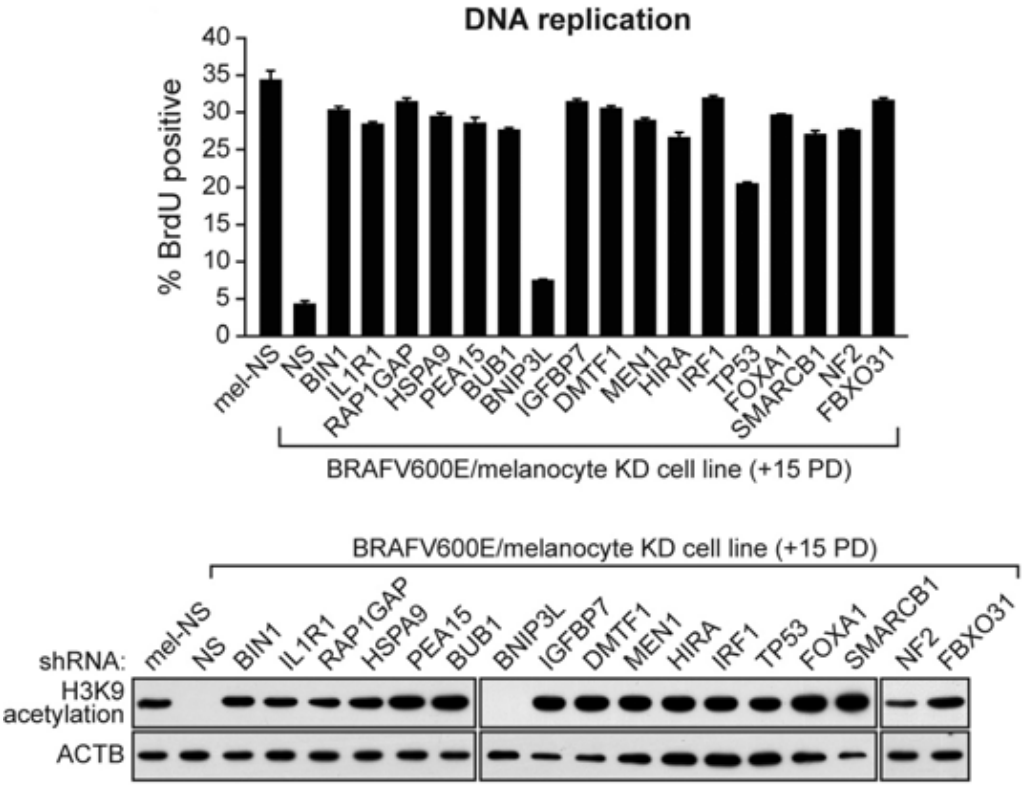

Figure 2-8. Analysis of the BRAF^{V600E}/Melanocyte KD Cell Lines After an Additional 15 Population Doublings, and Further Characterization of the BRAF^{V600E}/PFF KD Cell Lines.
[Top] DNA replication assays. The BRAF^{V600E}/melanocyte KD cell lines were allowed to undergo an additional 15 population doublings [+15 PD] and then analyzed for BrdU incorporation. Error bars represent standard error.
[Bottom] Immunoblot analysis monitoring acetylation of histone 3 lysine 9 [H3K9] after an additional 15 population doublings. β-ACTIN [ACTB] was monitored as a loading control.

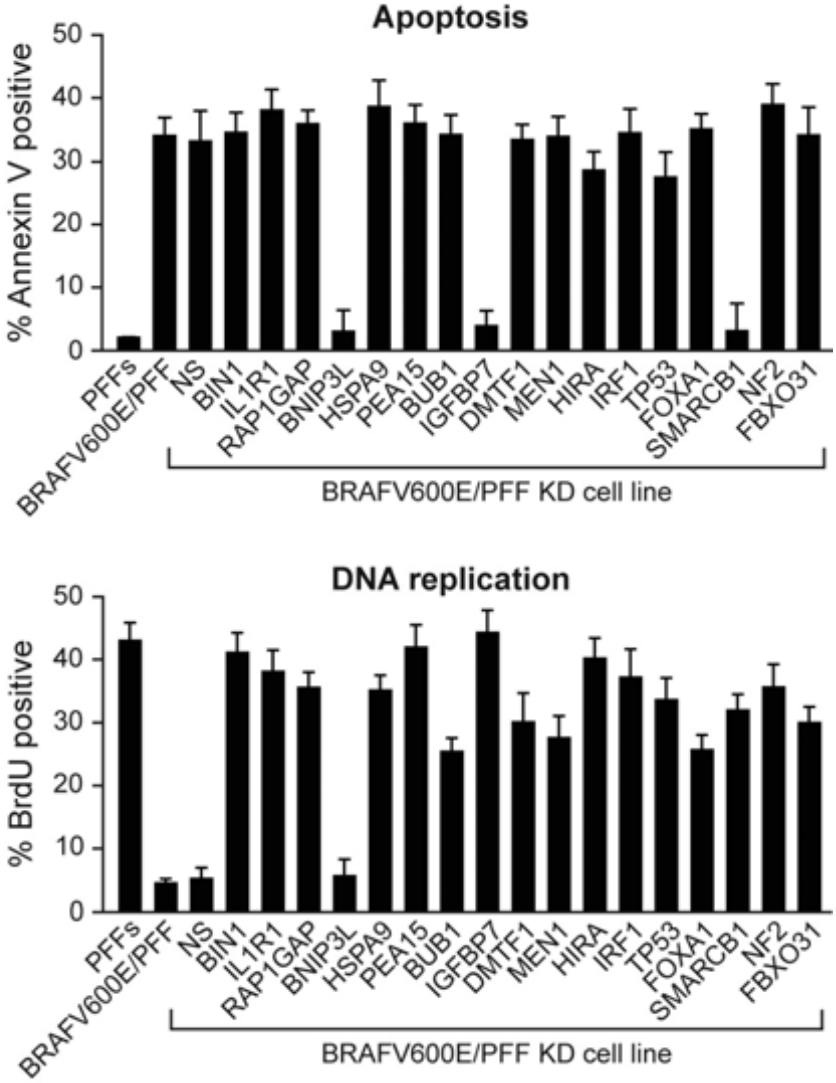

Figure 2-9. Apoptosis assays [top] and DNA replication assays [bottom] of the $BRAF^{V600E}$/PFF KD cell lines.
Apoptosis was monitored by Annexin V-PE staining 4 days after $BRAF^{V600E}$ expression; DNA replication was monitored by BrdU incorporation 4 days after $BRAF^{V600E}$ expression.

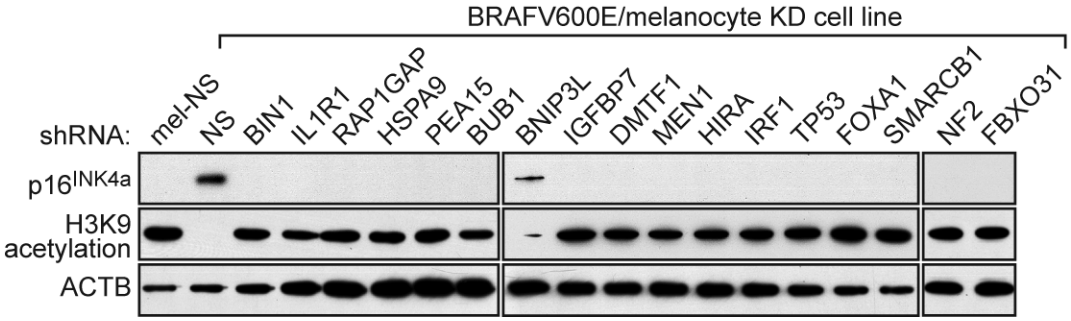

Figure 2-10. Immunoblot analysis monitoring induction of $p16^{INK4A}$ and H3K9 acetylation in each of the 17 $BRAF^{V600E}$/melanocyte KD cell lines. β-ACTIN [ACTB] was monitored as a loading control.

senescence marker [Narita et al., 2006], also occurred following $BRAF^{V600E}$ expression in control melanocytes but not in any of the melanocyte KD cell lines except for the BNIP3L KD cell line [Figures 2-10 and Figure 2-8].

One of the genes required for the induction of both senescence and apoptosis was IGFBP7, which encodes a secreted protein [Wilson et al., 1997], raising the possibility that the $BRAF^{V600E}$mediated block to cellular proliferation might occur through an autocrine/paracrine pathway. To determine whether IGFBP7 is secreted and functions extracellularly, I analyzed the ability of conditioned medium [CM] from $BRAF^{V600E}$/melanocytes to induce senescence. Figure 2-11 [top panel] shows that following expression of $BRAF^{V600E}$ in melanocytes, the level of IGFBP7 in CM increased substantially. Addition of CM from $BRAF^{V600E}$/melanocytes to naive melanocytes blocked cellular proliferation, primarily resulting from the induction of senescence [Figure 2-11, bottom panel and see Figure 2-19 below].

Two experiments verified that IGFBP7 activation was downstream of BRAF-MEK-ERK signaling. First, $BRAF^{V600E}$-mediated induction of IGFBP7 was blocked by addition of a MEK inhibitor [Figure 2-12]. Second, expression of a constitutively activated ERK mutant [$ERK2^{Q103A}$ or $ERK2^{L73P,S151D}$] was sufficient to activate IGFBP7 transcription [Figure 2-13].

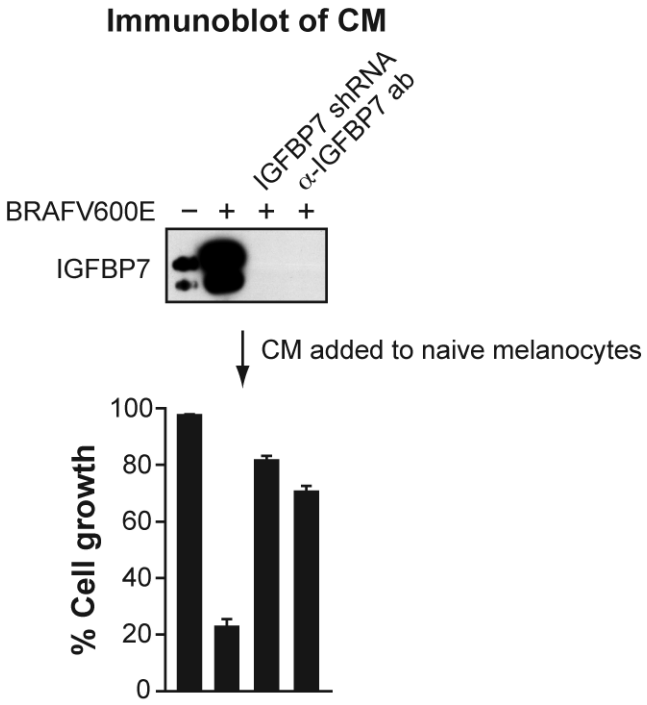

Figure 2-11. The secreted protein, IGFBP7, inhibits cell growth
[Top] Immunoblot analysis of IGFBP7 levels in CM from normal melanocytes, $BRAF^{V600E}$/melanocytes, $BRAF^{V600E}$/melanocytes stably expressing an IGFBP7 shRNA, or $BRAF^{V600E}$/melanocyte CM treated with an α-IGFBP7 antibody.
[Bottom] Proliferation assays on naive melanocytes following addition of the different CMs described above. Proliferation was measured and normalized to the growth of untreated melanocytes. Error bars represent standard error.

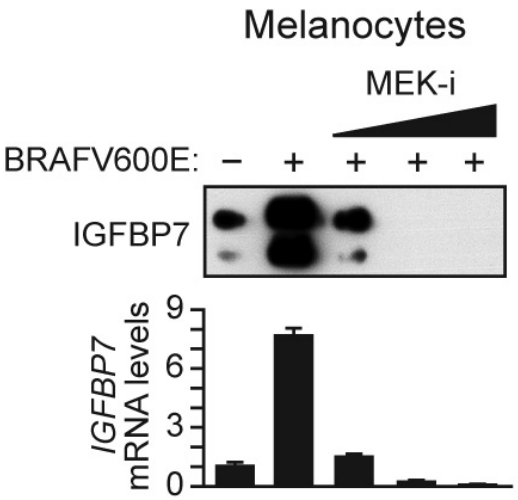

Figure 2-12. IGFBP7 Upregulation Occurs Downstream of BRAF-MEK-ERK Signaling.
IGFBP7 protein levels in CM from $BRAF^{V600E}$-expressing melanocytes [top] or mRNA expression in $BRAF^{V600E}$-expressing melanocytes [bottom] was monitored in the presence of increasing amounts of a MEK inhibitor. The results show that $BRAF^{V600E}$-mediated induction of IGFBP7 was blocked by addition of a MEK inhibitor. Error bars represent standard error.

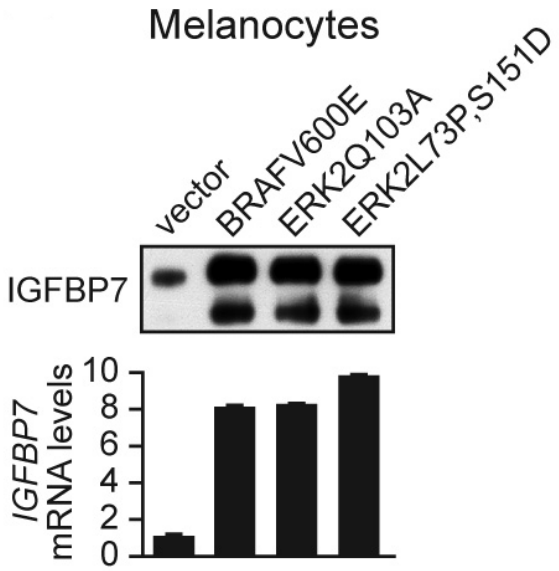

Figure 2-13. IGFBP7 protein levels in CM from melanocytes
[top] or mRNA expression in melanocytes [bottom] was monitored in the presence of $BRAF^{V600E}$ or a constitutively activated ERK mutant [$ERK2^{Q103A}$ or $ERK2^{L73P,S151D}$]. The results show that expression of a constitutively activated ERK mutant was sufficient to activate IGFBP7 transcription. Collectively, these results demonstrate that IGFBP7 induction is downstream of BRAF-MEK-ERK signaling. Error bars represent standard error.

The IGFBP7 promoter contains a consensus binding site for the dimeric AP-1 [JUN/FOS] transcription factor [Figure 2-14]. Significantly, JUN [also known as c-Jun] is activated through RAF-MEK-ERK signaling [Leppa et al., 1998], raising the possibility that AP-1 is involved in $BRAF^{V600E}$-mediated induction of IGFBP7. Chromatin immunoprecipitation [ChIP] analysis verified that JUN bound to the IGFBP7 promoter in response to $BRAF^{V600E}$ expression [Figure 2-15], and siRNA-mediated knockdown of JUN abrogated induction of IGFBP7 transcription in $BRAF^{V600E}$/melanocytes [Figure 2-16]. Again, the failure to pick up c-Jun as a candidate gene indicates that my shRNA screen, like other large-scale shRNA screens [see, for example Mullenders, 2009], was not saturating.

I next sought to verify that IGFBP7 was the secreted protein responsible for the $BRAF^{V600E}$-mediated cellular proliferation block. In one experiment, I treated $BRAF^{V600E}$/melanocytes with an shRNA targeting IGFBP7. Figure 2-11 shows that IGFBP7 was absent from the CM of $BRAF^{V600E}$/melanocytes expressing an IGFBP7 shRNA [top panel], and that this CM did not inhibit cellular proliferation of naive melanocytes [bottom panel]. In a second experiment, immunodepletion with an α-IGFBP7 antibody efficiently removed IGFBP7 from CM of $BRAF^{V600E}$/ melanocytes [top panel], and this immunodepleted CM failed to inhibit cellular proliferation of naive melanocytes [bottom panel].

To confirm that IGFBP7 could block cellular proliferation, I purified recombinant

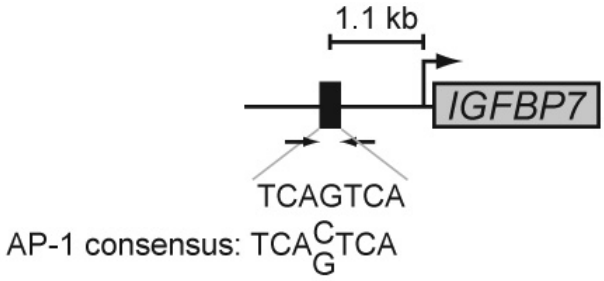

Figure 2-14. A Role for the AP-1 Transcription Factor in $BRAF^{V600E}$-Mediated Upregulation of IGFBP7 Expression.
Schematic of the IGFBP7 promoter showing a consensus binding site for the dimeric AP-1 [JUN/FOS] transcription factor located ~1 kb upstream of the transcription start-site.

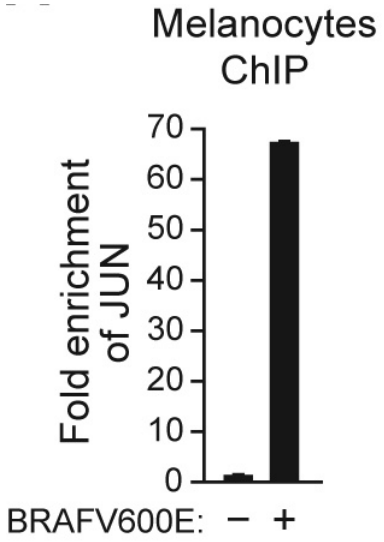

Figure 2-15. A Role for the AP-1 Transcription Factor in $BRAF^{V600E}$-Mediated Upregulation of IGFBP7 Expression.
Chromatin immunoprecipitation [ChIP] analysis. ChIP assays were performed using extracts prepared 4 days following $BRAF^{V600E}$ retroviral infection. Error bars represent standard error. The results show that JUN binds to the IGFBP7 promoter in response to $BRAF^{V600E}$ expression in melanocytes.

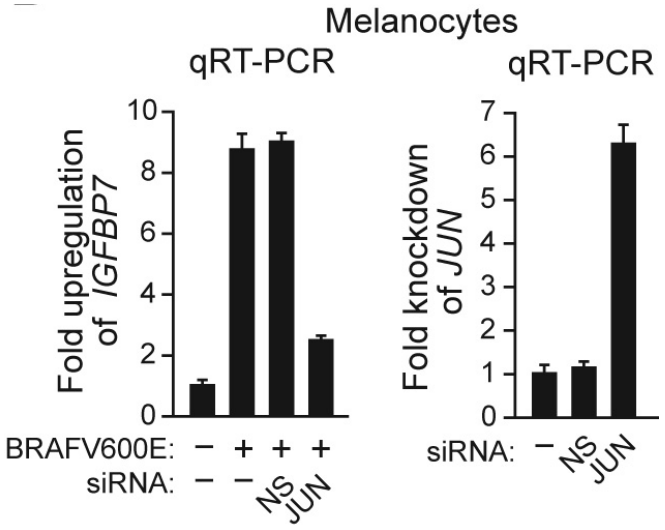

Figure 2-16. AP-1 is required for $BRAF^{V600E}$-mediated upregulation of IGFBP7 expression.

[Left] Quantitation of IGFBP7 mRNA levels in $BRAF^{V600E}$-expressing melanocytes following treatment with a non-silencing [NS] or JUN siRNA. The results demonstrate that JUN is required for $BRAF^{V600E}$-mediated induction of IGFBP7 transcription.

[Right] Quantitative real-time RT-PCR was used to analyze JUN mRNA levels following siRNA treatment. The results of Figures 2-15 and 2-16, in conjunction with my other results, indicate that $BRAF^{V600E}$ induces expression of IGFBP7, at least in part, through activation of ERK, which in turn activates AP-1, resulting in binding of AP-1 to the IGFBP7 promoter and stimulation of transcription.

IGFBP7 [rIGFBP7] from baculovirus-infected insect cells. Figure 2-17 shows that following expression and purification, a polypeptide of ~33 kDa was detected, the expected size of IGFBP7. Addition of rIGFBP7 blocked proliferation of primary melanocytes in a dose-dependent manner [Figure 2-18]. The growth-arrested cells had an enlarged flat morphology, characteristic ofsenescent cells, and stained positively for senescence-associated β-galactosidase [Figure 2-19].

The finding that primary melanocytes expressed IGFBP7 [Figure 2-11 and see below] raised the possibility that under normal conditions IGFBP7 might regulate melanocyte proliferation. To test this idea, I compared the proliferation rates of untreated melanocytes, control melanocytes expressing an NS shRNA, and melanocytes expressing an IGFBP7 shRNA. Figure 2-20 shows that melanocyte proliferation increased following IGFBP7 knockdown. Thus, normal melanocytes express low levels of IGFBP7, which restrains proliferation. When present at high levels, such as following expression of $BRAF^{V600E}$, IGFBP7 induces senescence.

I next analyzed the ability of IGFBP7 to block cellular proliferation in a panel of human melanoma cell lines. The cells contained either an activating BRAF mutation [$BRAF^{V600E}$; SK-MEL-28, MALME-3M, WM793B, WM39, and WM278] or an activating RAS mutation [RAS^{Q61R}; SK-MEL-2, SK-MEL-103, and WM1366]

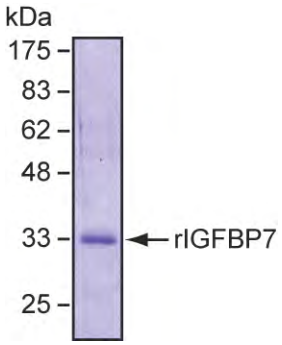

Figure 2-17. Coomassie-stained gel of purified, recombinant IGFBP7 [rIGFBP7]. Molecular weight markers are shown on the left, in kDa.

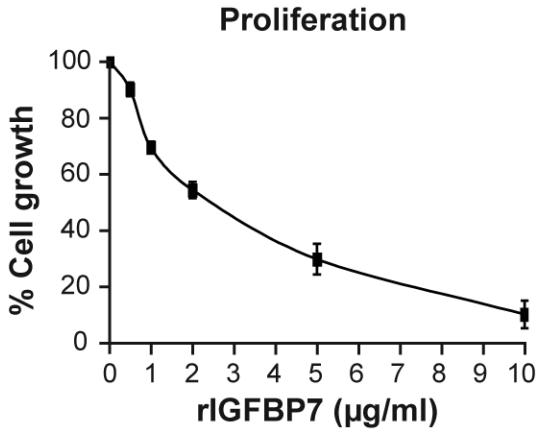

Figure 2-18. Proliferation assay monitoring the effect of rIGFBP7 on the growth of melanocytes 14 days after treatment. Error bars represent standard error.

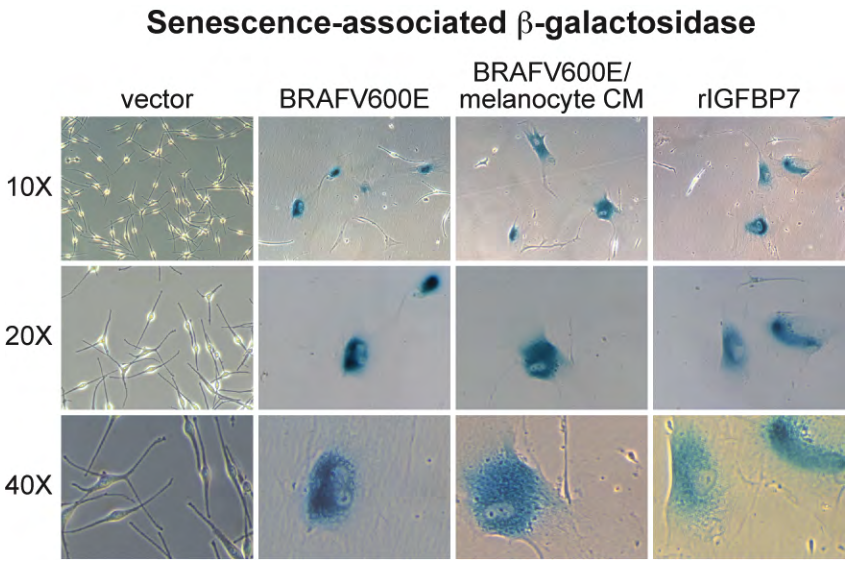

Figure 2-19. β-galactosidase staining of melanocytes infected with a retrovirus expressing either empty vector or $BRAF^{V600E}$ or melanocytes treated with CM from $BRAF^{V600E}$/melanocytes or rIGFBP7. Images are shown at a magnification of 10X, 20X, and 40X.

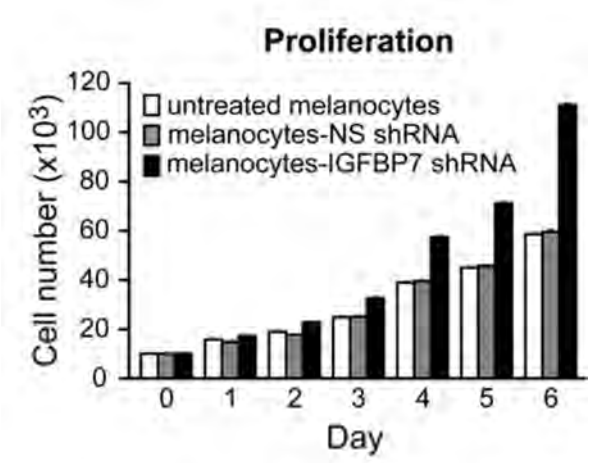

Figure 2-20. Proliferation assay monitoring growth rates of untreated melanocytes or melanocytes stably expressing an NS or IGFBP7 shRNA. Error bars represent standard error.

or were wild-type for both BRAF and RAS [CHL, SK-MEL-31, WM1321, and WM3211]. For each cell line, the presence of IGFBP7 in the CM was determined by immunoblot analysis [Figure 2-21] and sensitivity to IGFBP7-induced growth inhibition was measured in a proliferation assay [Figure 2-22]. The results reveal a striking inverse correlation between IGFBP7 expression and sensitivity to IGFBP7-mediated growth inhibition that correlates with the status of BRAF or RAS. Most importantly, melanoma cell lines harboring an activating BRAF mutation fail to express IGFBP7 and are highly sensitive to IGFBP7-mediated growth inhibition. By contrast, cells that are wild-type for BRAF and RAS express IGFBP7 and are relatively insensitive to IGFBP7-mediated growth inhibition for reasons that remain to be determined. Finally, melanoma cell lines containing an activating RAS mutation express low levels of IGFBP7 and are partially sensitive to IGFBP7-mediated growth inhibition. I further analyzed the IGFBP7-mediated cellular proliferation block with regard to apoptosis and senescence. Significantly, in melanoma cell lines harboring an activating BRAF mutation, rIGFBP7 strongly induced apoptosis and surviving senescent cells were undetectable [Figure 2-23]. Thus, IGFBP7 primarily induced senescence in melanocytes and apoptosis in $BRAF^{V600E}$-positive melanoma cells.

To understand the basis of this differential response, I analyzed expression of the 17 genes in primary melanocytes and SK-MEL-28 melanoma cells. Figure 2-24 [top panel] shows that in primary melanocytes, expression of $BRAF^{V600E}$ resulted

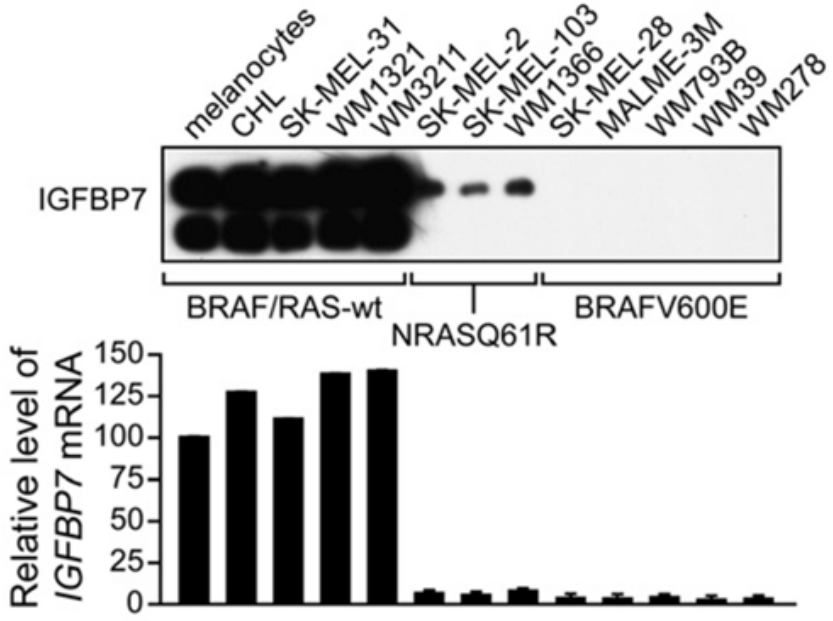

Figure 2-21. [Top] Immunoblot analysis monitoring IGFBP7 levels in the CM from a panel of human melanoma cell lines. [Bottom] Quantitative real-time RT-PCR analysis of IGFBP7 expression. Error bars represent standard error.

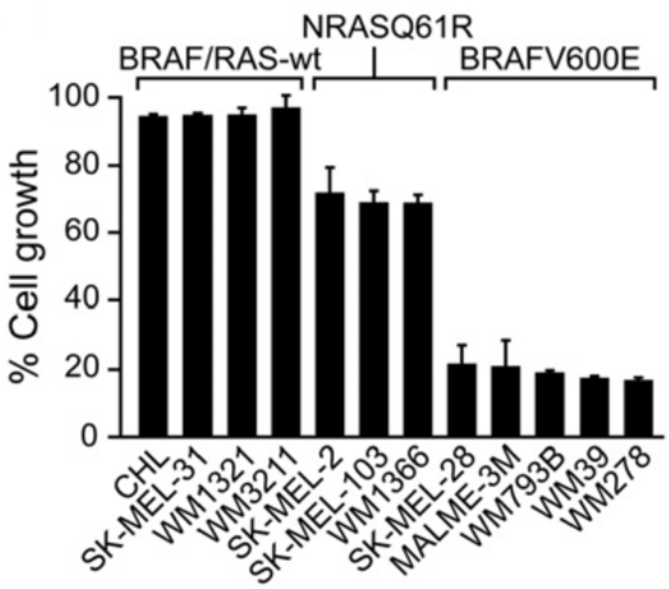

Figure 2-22. Proliferation assays of human melanoma cell lines 24 hr after rIGFBP7 treatment. Proliferation was normalized to the growth of the corresponding cell line in the absence of rIGFBP7 addition. Error bars represent standard error.

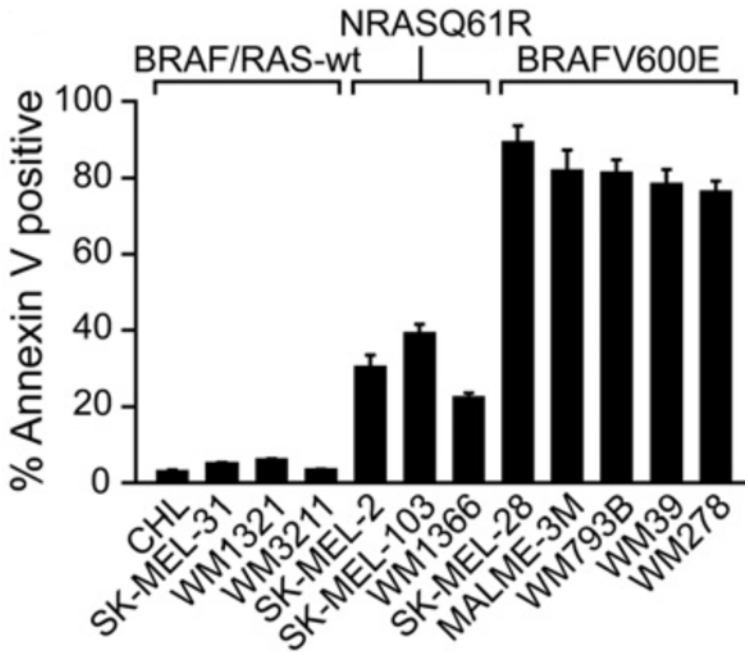

Figure 2-23. Apoptosis assays of human melanoma cell lines treated with rIGFBP7. Error bars represent standard error.

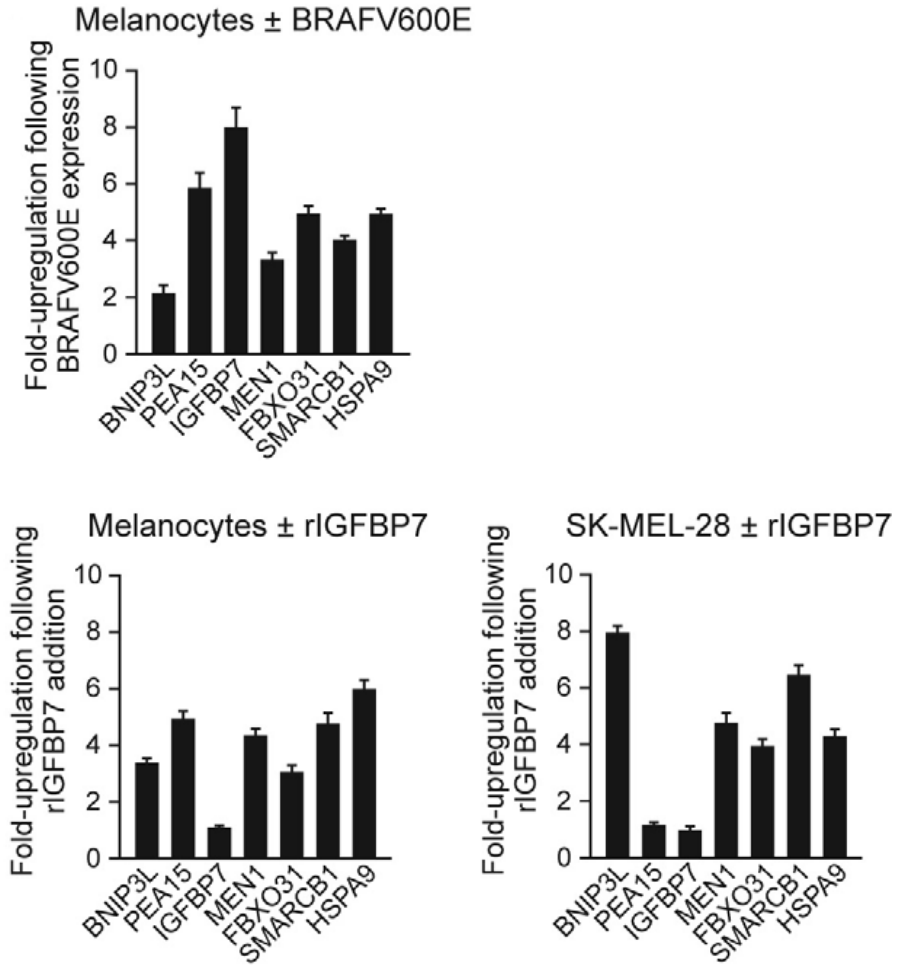

Figure 2-24. Induction of Gene Expression by $BRAF^{V600E}$ and IGFBP7.
Quantitation of gene expression in $BRAF^{V600E}$/melanocytes compared to melanocytes [Top], rIGFBP7-treated melanocytes compared to untreated melanocytes [Bottom left], and rIGFBP7-treated SK-MEL-28 cells compared to untreated cells [Bottom right]. Gene expression was monitored by qRT-PCR in untreated and treated cells, and expressed as fold-upregulation.

in the transcriptional upregulation of seven genes, which are involved in apoptosis [BNIP3L, IGFBP7, and SMARCB1] and senescence [PEA15, IGFBP7, MEN1, FBXO31, SMARCB1, and HSPA9]. $BRAF^{V600E}$-mediated induction of all seven genes did not occur following knockdown of IGFBP7 [Figure 2-25]. Following addition of rIGFBP7 to melanocytes, six of the seven genes were induced, IGFBP7 being the exception [Figure 2-24, bottom left panel]. Significantly, following addition of rIGFBP7 to SK-MEL-28 cells, neither IGFBP7 nor PEA15 was upregulated [Figure 2-24, bottom right panel]. PEA15, a known regulator of BRAF-MEK- ERK signaling [Formstecher et al., 2001], is required for senescence [see Figure 2-10]. Thus, the lack of PEA15 induction in IGFBP7-treated SK-MEL-28 cells can explain their failure to undergo senescence. I note that BNIP3L is only modestly upregulated in primary melanocytes following expression of $BRAF^{V600E}$ or addition of rIGFBP7, consistent with the relatively low level of apoptosis in IGFBP7-treated melanocytes [see Figure 2-7]

As described above, $BRAF^{V600E}$-mediated apoptosis was dependent upon IGFBP7, SMARCB1, and BNIP3L, raising the possibility that these three proteins were components of a common pathway required for apoptosis. I performed a series of experiments to confirm this idea and establish the order of the pathway. Figure 2-26 shows that following addition of rIGFBP7 to SK-MEL-28 cells, expression of SMARCB1 and BNIP3L were significantly increased, and apoptosis occurred as evidenced by caspase 3 activation. Expression of a

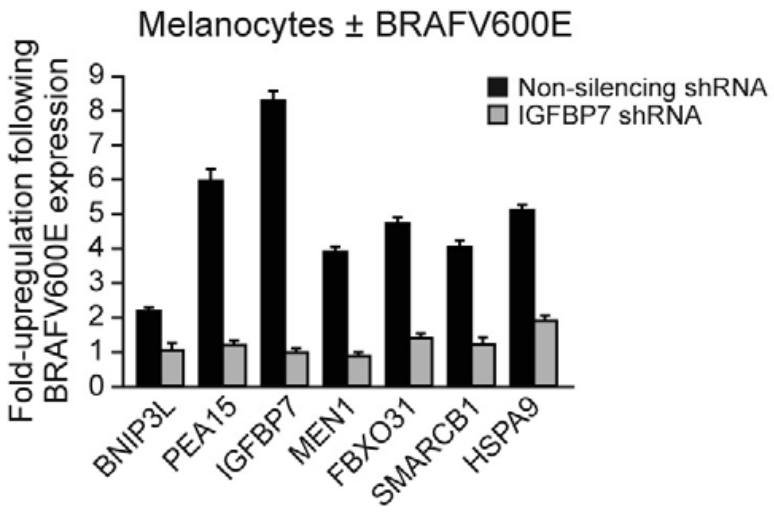

Figure 2-25. Melanocytes expressing either a non-silencing or IGFBP7 shRNA were monitored for $BRAF^{V600E}$-induced expression of seven genes by quantitative real-time RT-PCR. Error bars represent standard error. The results show that $BRAF^{V600E}$-mediated induction of all seven genes did not occur following knockdown of IGFBP7.

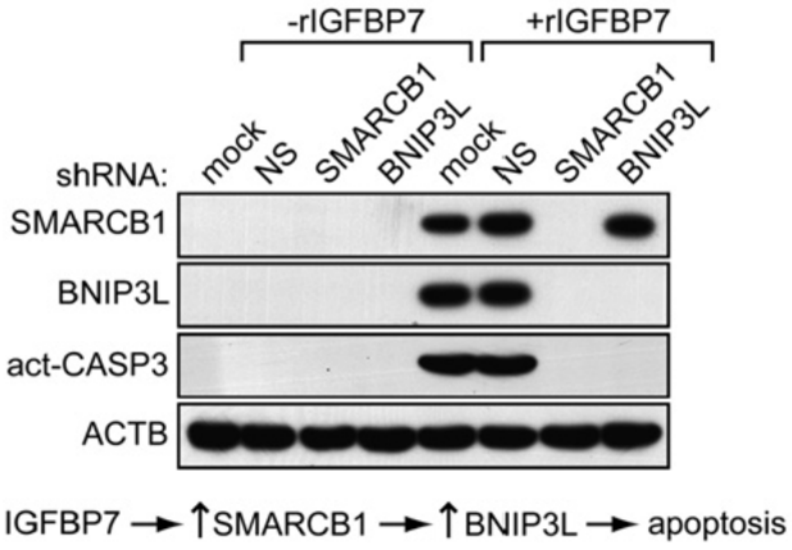

Figure 2-26. [Top] Immunoblot analysis in SK-MEL-28 cells in the presence or absence of rIGFBP7 and stably expressing either an NS, SMARCB1, or BNIP3L shRNA.
[Bottom] Schematic summary of the IGFBP7-mediated apoptotic pathway.

SMARCB1 shRNA [identified in primary screen] blocked induction of BNIP3L and apoptosis. By contrast, expression of a BNIP3L shRNA [identified in primary screen] still resulted in induction of SMARCB1 following rIGFBP7 addition although apoptosis did not occur. Collectively, these results reveal a pathway in which IGFBP7 increases expression of SMARCB1, which in turn leads to increased expression of BNIP3L culminating in apoptosis [Figure 2-26, bottom panel].

In $BRAF^{V600E}$/melanocytes, induction of SMARCB1 and BNIP3L was blocked following IGFBP7 knockdown [Figure 2-27]. Moreover, addition of CM from $BRAF^{V600E}$-expressing melanocytes to naive melanocytes substantially upregulated SMARCB1 and BNIP3L, which did not occur with various control CMs that lacked IGFBP7 [Figure 2-28]. Thus, in $BRAF^{V600E}$/melanocytes induction of SMARCB1 and BNIP3L is also dependent upon and downstream of IGFBP7.

I next sought to determine the mechanistic basis for IGFBP7-mediated induction of BNIP3L and SMARCB1. A previous study analyzing genome-wide targets of STAT proteins had provided evidence that STAT1 was involved in certain SMARCB1-inducible transcription responses and had shown that the SMARCB1 promoter contains a STAT1 binding site located ~2.4 kb upstream of the transcription start site [Hartman et al., 2005]. I therefore investigated the

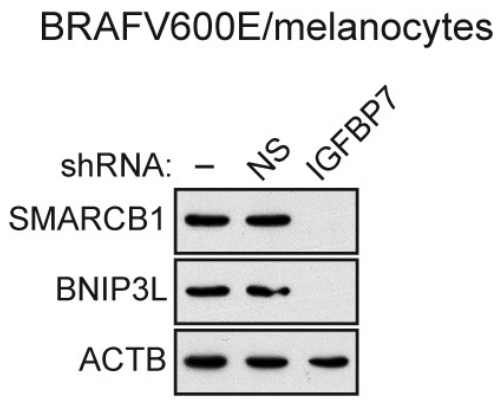

Figure 2-27. $BRAF^{V600E}$-Mediated Induction of SMARCB1 and BNIP3L is Dependent Upon and Downstream of IGFBP7.
Immunoblot analysis showing SMARCB1 and BNIP3L induction in $BRAF^{V600E}$expressing melanocytes in the presence of a non-silencing [NS] or IGFBP7shRNA. β-ACTIN [ACTB] was monitored as a loading control. The results show that induction of SMARCB1 and BNIP3L was blocked following IGFBP7 knockdown.

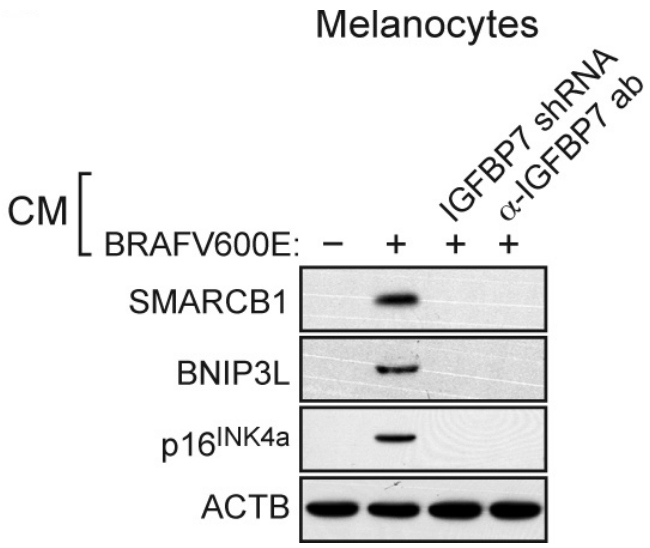

Figure 2-28. Immunoblot analysis monitoring SMARCB1, BNIP3L and $p16^{INK4A}$ in naïve melanocytes following addition of CM from normal melanocytes, $BRAF^{V600E}$/melanocytes, $BRAF^{V600E}$/melanocytes stably expressing an IGFBP7 shRNA or in $BRAF^{V600E}$/melanocyte CM immunodepleted of IGFBP7.

The results show that addition of CM from $BRAF^{V600E}$expressing melanocytes to naïve melanoctyes substantially upregulated SMARCB1 and BNIP3L, which did not occur with CM from $BRAF^{V600E}$/melanocytes expressing an IGFBP7 shRNA or with CM from $BRAF^{V600E}$/melanocytes following immunodepletion of IGFBP7. Collectively,the results of Figures 2-27 and 2-28 demonstrate that $BRAF^{V600E}$-mediated induction of SMARCB1 and BNIP3L is dependent upon and downstream of IGFBP7.

potential role of STAT1 in IGFBP7-mediated induction of SMARCB1 transcription. ChIP experiments revealed that following addition of rIGFBP7 to SK-MEL-28 cells, STAT1 was recruited to the SMARCB1 promoter [Figure 2-29], and shRNA-mediated knockdown experiments confirmed that STAT1 was required for IGFBP7-mediated upregulation of SMARCB1 [Figure 2-30].

As described above, SMARCB1 is required for upregulation of BNIP3L by IGFBP7 [Figure 2-26]. ChIP experiments revealed that following addition of rIGFBP7, SMARCB1 as well as BRG1, an essential subunit of the SWI/SNF complex [Bultman et al., 2000], were recruited to the BNIP3L promoter near the transcription start site [Figure 2-31]. Following knockdown of SMARCB1, BRG1 [and, as expected, SMARCB1] failed to associate with the BNIP3L promoter. Collectively, these results indicate that IGFBP7 stimulates BNIP3L transcription, at least in part, by increasing intracellular levels of SMARCB1, leading to formation of a SMARCB1-containing SWI/SNF chromatin-remodeling complex, which is recruited to the BNIP3L promoter and facilitates BNIP3L transcriptional activation.

Finally, I asked whether apoptosis was dependent upon the continual presence of rIGFBP7 or was irreversible following transient exposure to rIGFBP7. SK-MEL-28 cells were incubated with rIGFBP7 for various lengths of time, following which the cells were washed and cultured in medium lacking rIGFBP7, and

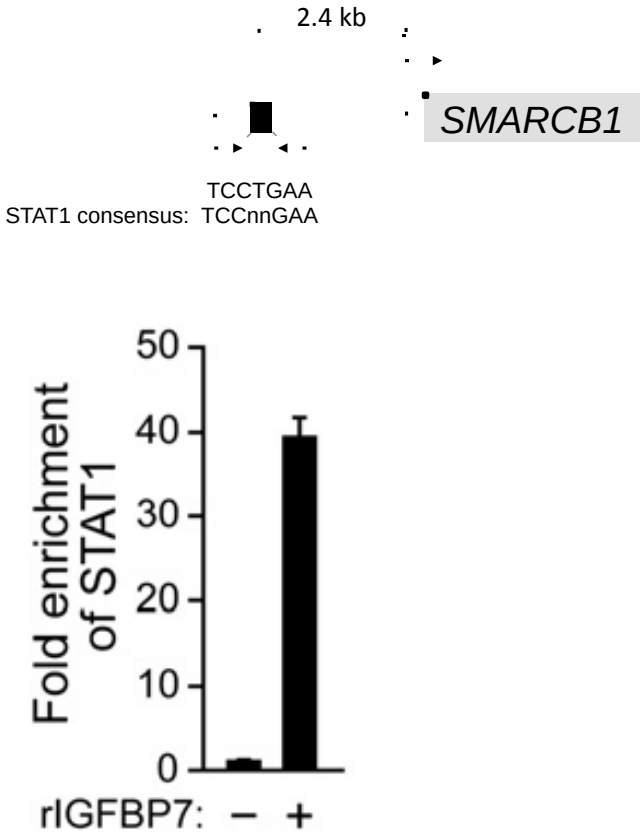

Figure 2-29. [Top] Schematic of STAT1 binding site location in SMARCB1 promoter.
[Bottom] ChIP analysis monitoring STAT1 recruitment to the SMARCB1 promoter in SK-MEL-28 cells. [lower] Error bars represent standard error.

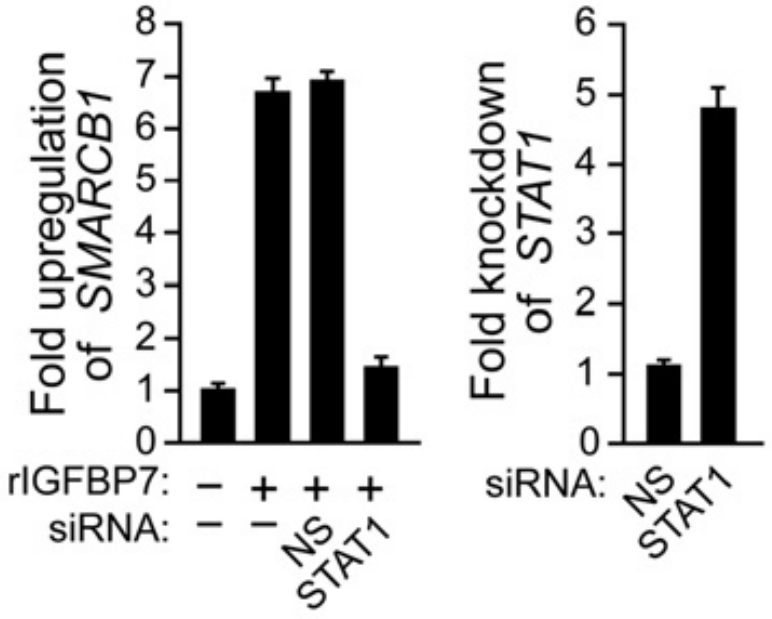

Figure 2-30. qRT-PCR analysis of SMARCB1 [left] or STAT1 [right] mRNA levels in SK-MEL-28 cells following treatment with an NS or STAT1 siRNA. Error bars represent standard error.

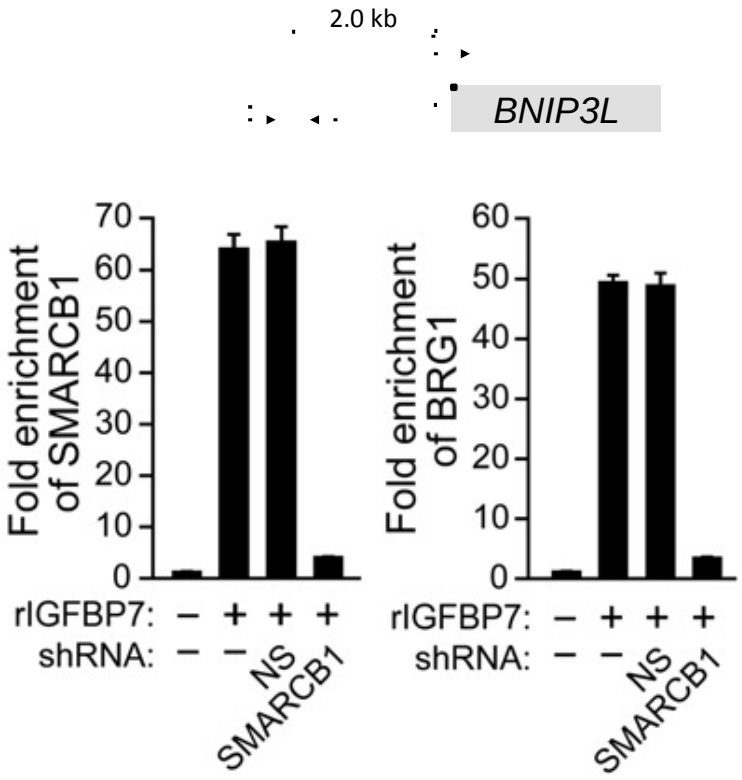

Figure 2-31. [Top] Schematic of putative SMARCB1/BRG1 binding site in BNIP3L promoter.
[Bottom, left] ChIP analysis monitoring SMARCB1 or [Bottom, right] BRG1 recruitment to the BNIP3L promoter in SK-MEL-28 cells. Error bars represent standard error.

apoptosis was quantitated after 24 hr. Figure 2-32 shows that following 6 hr of incubation with rIGFBP7, the cells were irreversibly committed to apoptosis, which occurred even after removal of rIGFBP7.

In $BRAF^{V600E}$-positive melanoma cells BRAF-MEK-ERK signaling is hyperactivated, rendering the cells highly dependent on this pathway. Thus, treatment of $BRAF^{V600E}$-positive melanoma cells with a BRAF shRNA [Hoeflich et al., 2006] or an inhibitor of BRAF [Sharma et al., 2005] or MEK [Solit et al., 2006] blocks cellular proliferation. I therefore considered the possibility that IGFBP7 blocks cellular proliferation, at least in part, by inhibiting BRAF-MEK-ERK signaling.

To test this idea I added rIGFBP7 to SK-MEL-28 cells and analyzed the levels of total and activated ERK [phospho-ERK]. Figure 2-33 shows that addition of rIGFBP7 resulted in a dose-dependent loss of phospho-ERK. Similarly, expression of $BRAF^{V600E}$ in melanocytes markedly decreased phospho- ERK levels, which did not occur in $BRAF^{V600E}$/melanocytes expressing an IGFBP7 shRNA [Figure 2-34]. Moreover, addition of CM from $BRAF^{V600E}$/melanocytes to naive melanocytes substantially decreased the levels of phospho-ERK, which did not occur with various control CMs that lacked IGFBP7 [Figure 2-35]. rIGFBP7 also blocked growth factor-induced ERK activation [Figure 2-36]. Collectively, these results indicate that IGFBP7 inhibits BRAF-MEK-ERK signaling.

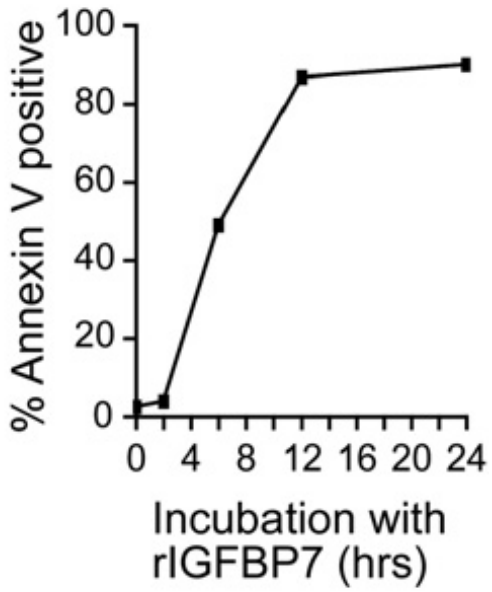

Figure 2-32. SK-MEL-28 cells were incubated with rIGFBP7 for 0, 2, 6, 12, or 24 hr, following which the cells were washed and cultured in medium lacking rIGFBP7 and apoptosis was quantitated.

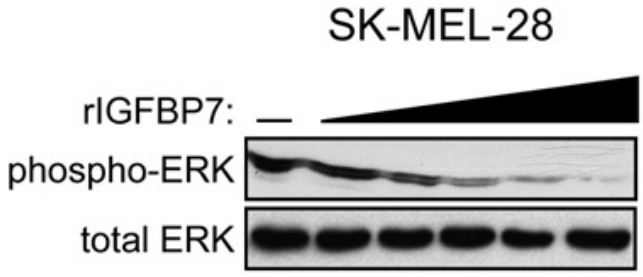

Figure 2-33. Immunoblot analysis in SK-MEL-28 cells treated with increasing concentrations of rIGFBP7 [0.2, 1.0, 2.0, 5.0, or 10 μg/ml] for 24 hr.

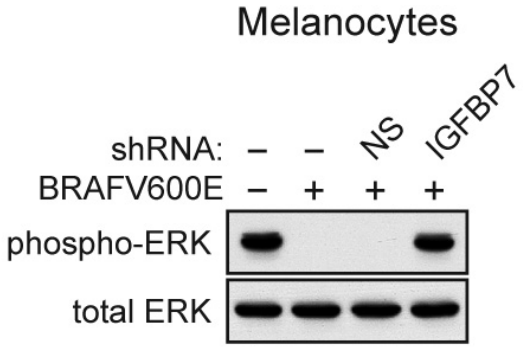

Figure 2-34. IGFBP7-Dependent Inhibition of BRAF-MEK-ERK Signaling in Melanocytes Following $BRAF^{V600E}$ Expression or Growth Factor Stimulation. Immunoblot of phospho-ERK and total ERK in $BRAF^{V600E}$-expressing melanocytes compared to $BRAF^{V600E}$-expressing melanocytes containing a non-silencing [NS] or IGFBP7 shRNA. The results confirm that phospho-ERK levels are markedly decreased in $BRAF^{V600E}$/melanocytes, which are senescent. This decrease in phospho-ERK levels did not occur in $BRAF^{V600E}$/melanocytes expressing an IGFBP7 shRNA.

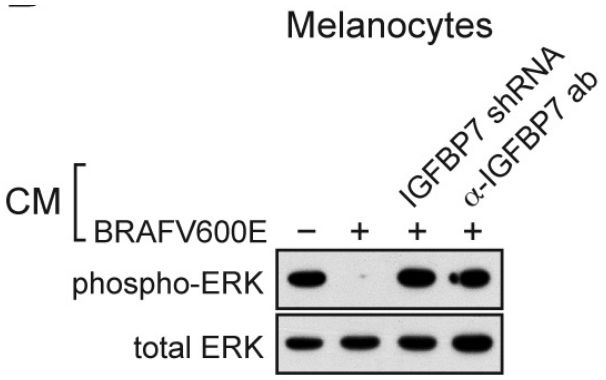

Figure 2-35. Immunoblot analysis of phospho-ERK and total ERK in naïve melanocytes following addition of CM from normal melanocytes, $BRAF^{V600E}$/melanocytes, $BRAF^{V600E}$/melanocytes stably expressing an IGFBP7 shRNA or in $BRAF^{V600E}$/melanocyte CM immunodepleted of IGFBP7.
The results show that addition of CM from $BRAF^{V600E}$expressing melanocytes to naïve melanocytes substantially decreased the level of phospho-ERK, which did not occur with the various control CMs that lacked IGFBP7.

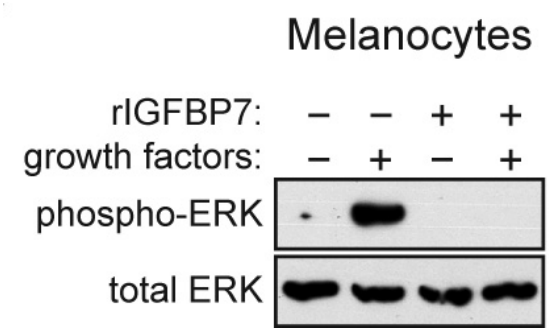

Figure 2-36. Immunoblot analysis of phospho-ERK and total ERK levels in melanocytes treated in the presence or absence of rIGFBP7 [10 µg/ml], or the presence or absence of melanocyte growth factors [1X Human Melanocyte Growth Supplement [Cascade Biologics]. Cells were treated or 48 hrs prior to harvesting cells. The results demonstrate that rIGFBP7 also blocked growth factor-induced ERK activation.

Addition of rIGFBP7 to SK-MEL-28 cells resulted in decreased levels of activated MEK1/2, corresponding with the reduced phospho-ERK levels and apoptosis [Figure 2-37]. Moreover, ectopic expression of a constitutively activated MEK1 mutant [MEK1-EE] prevented IGFBP7 from blocking ERK activation [Figure 2-38]. These results demonstrate that IGFBP7 blocks phosphorylation of MEK by BRAF. Finally, I found that addition of IGFBP7 to SK-MEL-28 cells resulted in upregulation of RAF inhibitory protein [RKIP] [Figures 2-37 and 2-39], which has been shown to interact with several RAF proteins, including BRAF, and inhibit RAF-mediated phosphorylation of MEK [see, for example, Park et al., 2005]. Following knockdown of RKIP in SK-MEL-28 cells, rIGFBP7 failed to block activation of MEK or ERK [Figure 2-39]. Collectively, these results indicate that IGFBP7 inhibits BRAF-MEK-ERK signaling by inducing RKIP, which prevents BRAF from phosphorylating MEK.

To establish the relationship between inhibition of BRAF-MEK-ERK signaling and the IGFBP7-mediated block to cellular proliferation, I ectopically expressed a constitutively activated ERK2 or MEK1 mutant and analyzed sensitivity to rIGFBP7. Figure 2-40 shows that expression of either an ERK2 [left] or MEK1 [right] mutant in SK-MEL-28 cells substantially overcame the IGFBP7-mediated cellular proliferation block. Expression of a constitutively activated ERK2 mutant also blocked $BRAF^{V600E}$ and IGFBP7-induced senescence in melanocytes

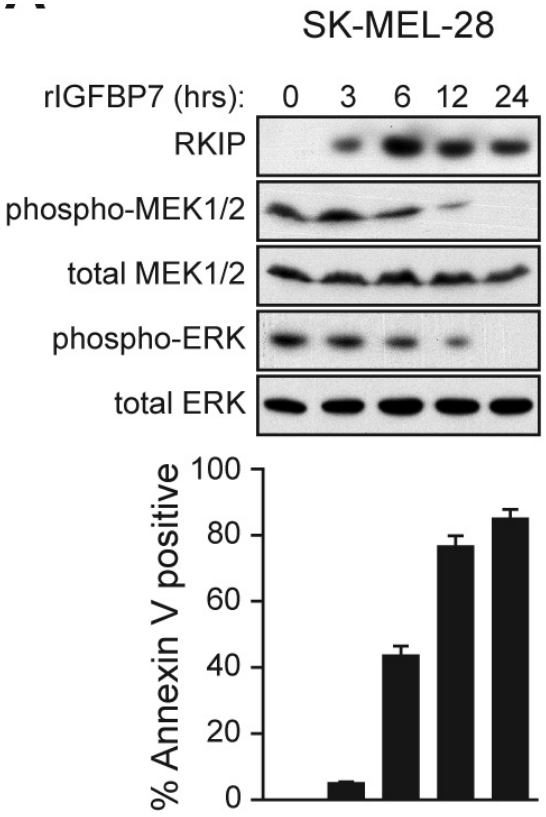

Figure 2-37. Mechanism of IGFBP7-Mediated Inhibition of BRAF-MEK-ERK Signaling.
[Top] Immunoblot analysis monitoring expression of RAF inhibitory protein [RKIP], phospho-MEK1/2, total MEK1/2, phospho-ERK and total ERK in $BRAF^{V600E}$-positive SKMEL-28 cells following addition of rIGFBP7 for 0, 3, 6, 12 or 24 hours.
[Bottom] Apoptosis of rIGFBP7-treated SK-MEL-28 cells was monitored by Annexin V-PE staining. Error bars represent standard error. The results show that addition of rIGFBP7 to SK-MEL-28 cells resulted in induction of RKIP and decreased levels of activated MEK1/2, corresponding with the reduced phospho-ERK levels and apoptosis.

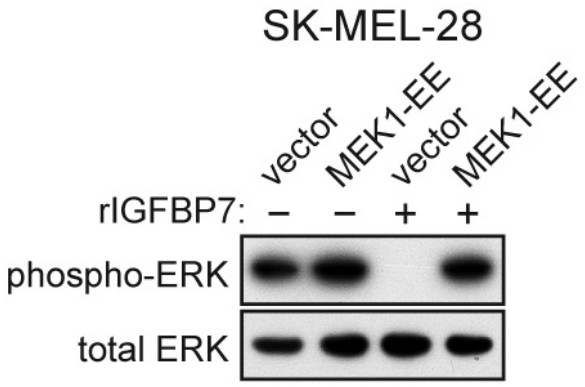

Figure 2-38. Immunoblot analysis of phospho-ERK and total ERK levels in SK-MEL-28 cells treated in the presence or absence of rIGFBP7, and following expression of a constitutively activated MEK1 mutant. The results show that ectopic expression of a constitutively activated MEK1 mutant prevented the ability of IGFBP7 to block ERK activation.

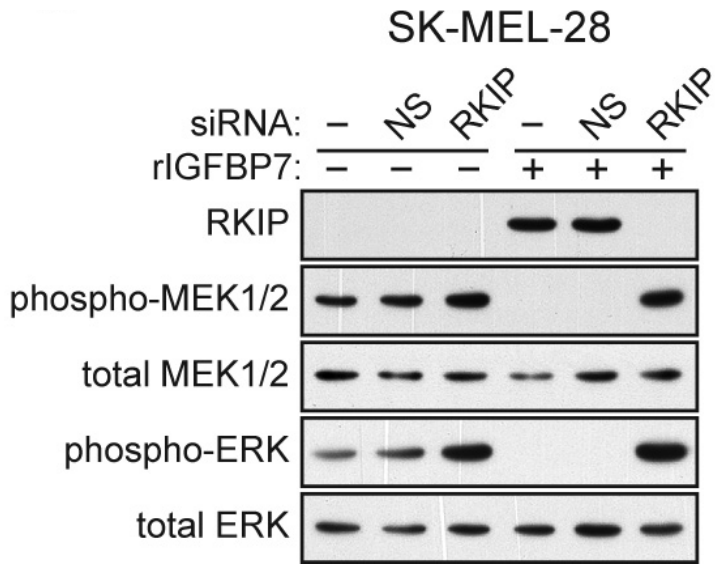

Figure 2-39. Immunoblot analysis monitoring expression of RKIP, phospho-MEK1/2, total MEK1/2, phospho-ERK and total ERK in SK-MEL-28 cells treated in the presence or absence of rIGFBP7, and with a non-silencing [NS] or RKIP siRNA.

The results show that following knockdown of RKIP in SK-MEL-28 cells, rIGFBP7 failed to block activation of MEK or ERK. Collectively, the results of Figures 2-37, 2-38 and 2-39 indicate that IGFBP7 inhibits ERK activation by inducing RKIP, which prevents BRAF from phosphorylating MEK.

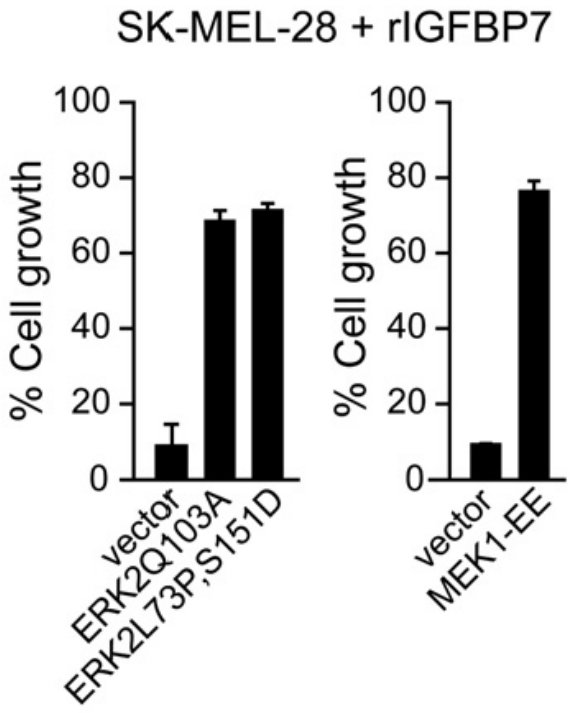

Figure 2-40. Proliferation assays monitoring sensitivity of SK-MEL-28 cells to rIGFBP7.

Cells were transfected with an empty expression vector or a constitutively activated ERK2 or MEK1 mutant. Cell growth was analyzed 24 hr after treatment with rIGFBP7 and normalized to the growth of the corresponding cell line in the absence of rIGFBP7 addition. Error bars represent standard error.

[Figure 2-41]. In addition, ectopic expression of a constitutively activated ERK2 mutant in SK-MEL-28 cells increased phospho-ERK2 levels and prevented the IGFBP7- mediated upregulation of BNIP3L and induction of apoptosis [Figure 2-42].

The above results allowed us to draw two conclusions. First, IGFBP7 blocks cellular proliferation, at least in part, by inhibiting BRAF-MEK-ERK signaling. Second, inhibition of BRAF-MEK-ERK signaling is required for activation of the IGFBP7-mediated apoptotic pathway. This latter observation prompted us to ask whether inhibition of BRAF-MEK-ERK signaling was sufficient to induce apoptosis. Figure 2-43 shows, as expected, that addition of a MEK or RAF inhibitor blocked BRAF-MEK-ERK signaling. However, unlike rIGFBP7, MEK and RAF inhibitors did not increase BNIP3L levels or efficiently induce apoptosis. Thus, inhibition of BRAF-MEK-ERK signaling is necessary but not sufficient for IGFBP7-mediated upregulation of BNIP3L and induction of apoptosis.

The ability of IGFBP7 to inhibit proliferation of $BRAF^{V600E}$-positive human melanoma cell lines [see Figure 2-22] raised the possibility that IGFBP7 could suppress growth of tumors containing an activating BRAF mutation. As a first test of this possibility, human melanoma cells that contained [SK-MEL-28] or lacked [SK-MEL-31] an activating BRAF mutation were injected subcutaneously into the flanks of nude mice. Three, six, and nine days later, the mice were

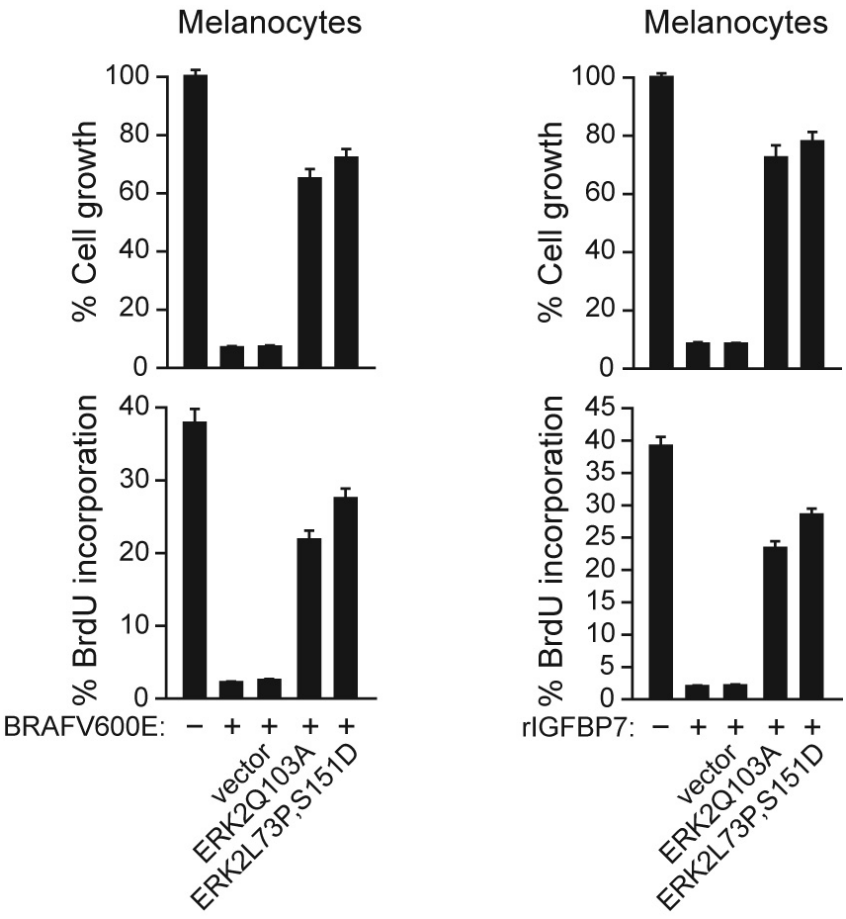

Figure 2-41. Inhibition of BRAF-MEK-ERK Signaling is Required for $BRAF^{V600E}$- and IGFBP7-Induction of Senescence in Melanocytes.
Quantitative proliferation assays showing that constitutively activated ERK2 mutants block $BRAF^{V600E}$-induced [left] or IGFBP7-induced [right] senescence in melanocytes. Error bars represent standard error.

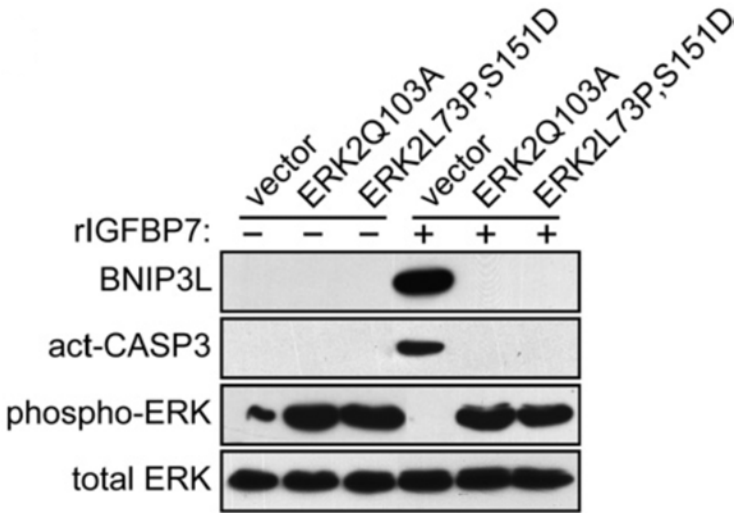

Figure 2-42. Immunoblot analysis in SK-MEL-28 cells stably transfected with an empty expression vector or a constitutively activated ERK2 mutant.
SK-MEL-28 cells were either untreated or treated with 10 μg/ml of rIGFBP7, as indicated, for 24 hr prior to harvesting cells.

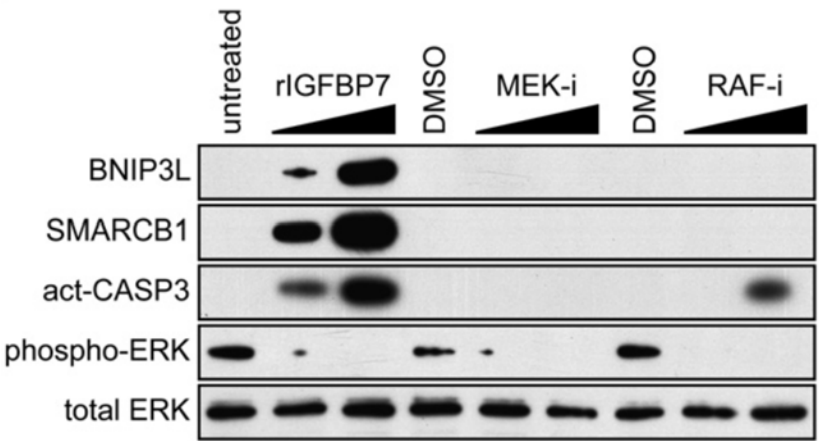

Figure 2-43. Immunoblot analysis in SK-MEL-28 cells 24 hr after treatment with rIGFBP7, a MEK inhibitor [MEK-i], or a RAF inhibitor [RAF-i].

injected at the tumor site with either rIGFBP7 or, as a control, PBS. Figure 2-44 shows that rIGFBP7 substantially suppressed growth of $BRAF^{V600E}$-positive tumors but had no effect on tumors containing wild-type BRAF.

I next asked whether tumor growth could also be suppressed by systemic administration of rIGFBP7. SK-MEL-28 or SK-MEL-31 cells were injected into the flanks of nude mice and when tumors reached a size of 100 mm^3, 100 µg rIGFBP7 was delivered by tail vein injection at days 6, 9, and 12. Figure 2-45 shows that systemic administration of rIGFBP7 completely suppressed growth of $BRAF^{V600E}$-positive tumors, whereas tumors containing wild-type BRAF were unaffected. In mice treated with rIGFBP7, $BRAF^{V600E}$-positive tumors were deoxyuridine triphosphate nick-end labeling [TUNEL] positive [Figure 2-46], indicating that suppression of tumor growth resulted from apoptosis. Suppression of tumor growth by systemically administered rIGFBP7 was dose dependent, and concentrations higher than that required for inhibition of tumor growth could be delivered without apparent adverse effects [Figure 2-47].

As shown above, $BRAF^{V600E}$-positive melanoma cell lines fail to express IGFBP7 and are highly sensitive to IGFBP7-mediated apoptosis. These results raised the possibility that IGFBP7 functions as a tumor suppressor and loss of IGFBP7 might be required for development of $BRAF^{V600E}$-positive melanoma. To

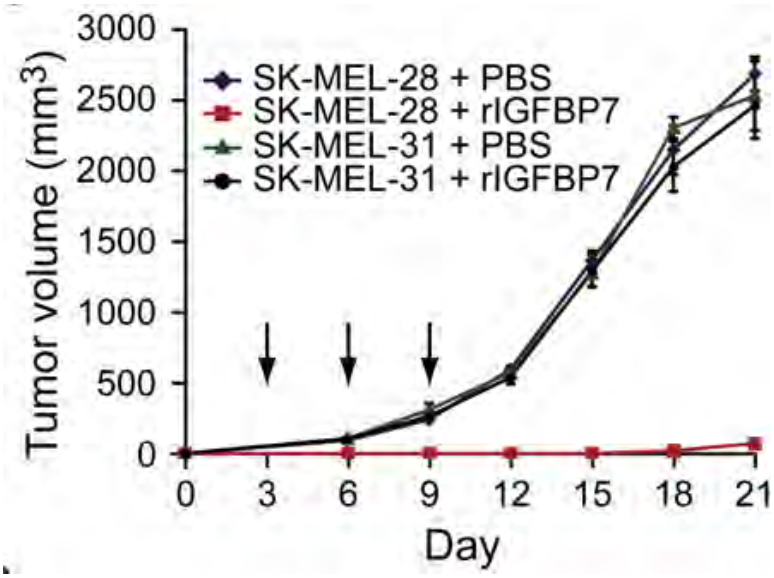

Figure 2-44. SK-MEL-28 or SK-MEL-31 cells were injected subcutaneously into the flanks of nude mice, and 3, 6, and 9 days later [denoted by arrows], the mice were injected at the tumor site with rIGBP7 or, as a control, PBS. Error bars represent standard error.

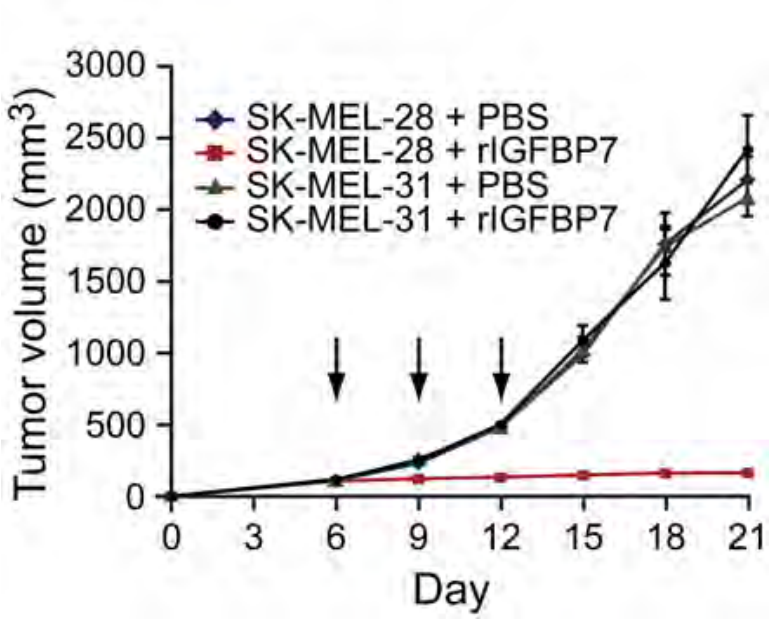

Figure 2-45. SK-MEL-28 or SK-MEL-31 cells were injected into the flanks of nude mice. When tumors reached a size of 100 mm^3, 100 µg rIGFBP7 was systemically administered by tail vein injection at days 6, 9, and 12 [indicated by arrows]. Error bars represent standard error.

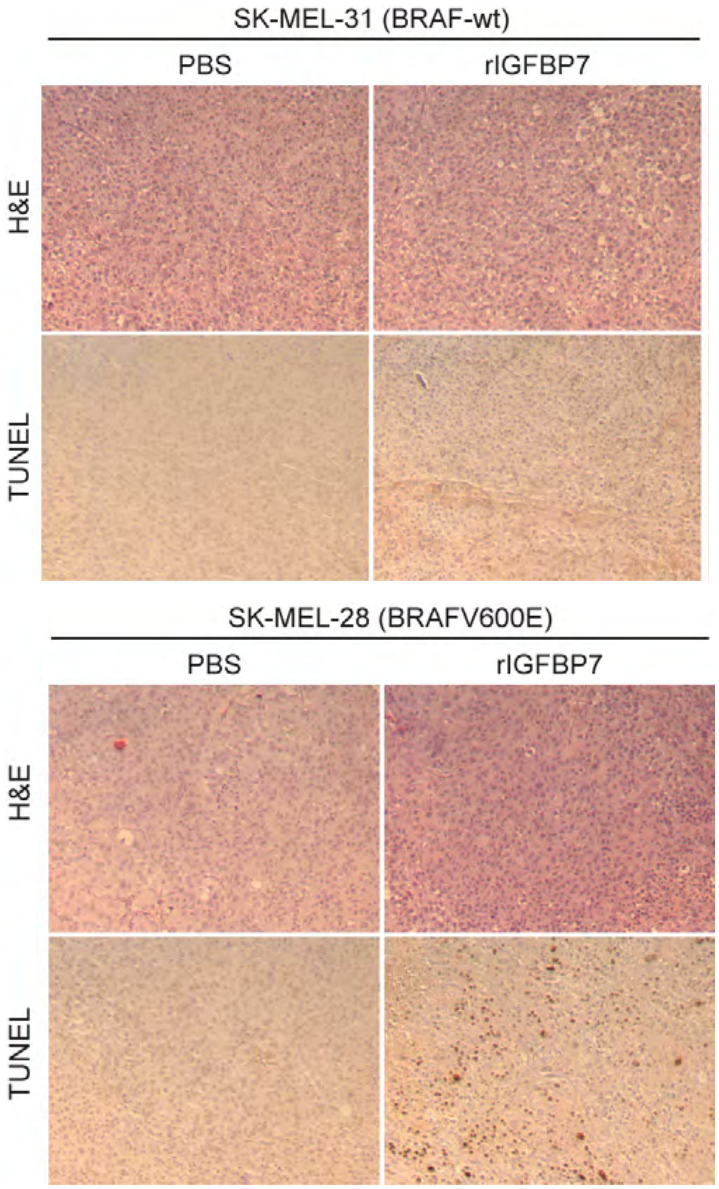

Figure 2-46. Systemic Administration of rIGFBP7 Induces Apoptosis in $BRAF^{V600E}$Positive Mouse Xenografts.
Tumors derived from the rIGFBP7 systemic administration experiment shown in Figure 5B were analyzed in a deoxyuridine triphosphate nick-end labeling [TUNEL] assay. The results show that following treatment with rIGFBP7, $BRAF^{V600E}$-positive tumors were TUNEL-positive, indicating that suppression of tumor growth resulted from apoptosis.

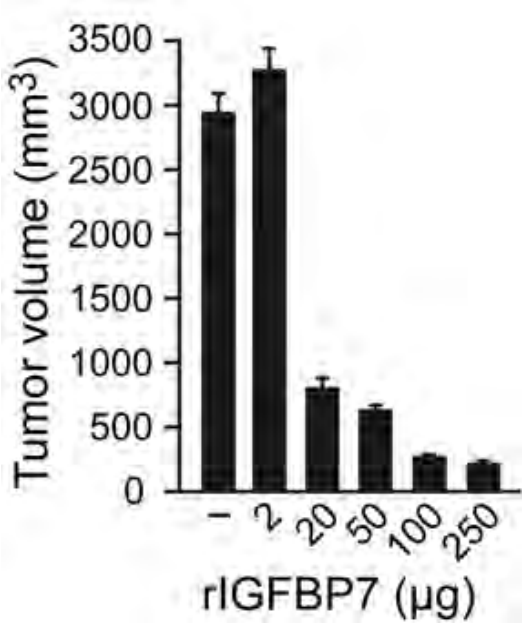

Figure 2-47. Dose-dependent suppression of tumor growth by rIGFBP7. SK-MEL-28 cells were injected into the flanks of nude mice as described in Figure 2-45, following which rIGFBP7 was systemically administered by tail vein injection. Tumor volume was measured at day 21. Error bars represent standard error.

investigate this possibility, I performed immunohistochemical analysis of IGFBP7 expression on a series of human skin, nevi, and melanoma samples.

Figure 2-48 and Table 2-2 show that normal skin melanocytes expressed low but detectable levels of IGFBP7. $BRAF^{V600E}$positive nevi expressed high levels of IGFBP7, consistent with the finding that expression of $BRAF^{V600E}$ in melanocytes increased IGFBP7 levels [Figure 2-11]. Significantly, expression of IGFBP7 was not detectable in $BRAF^{V600E}$-positive melanomas. By contrast, IGFBP7 was clearly expressed in melanomas lacking activated BRAF.

To determine whether loss of IGFBP7 expression was the result of epigenetic silencing, I performed bisulfite sequence analysis. Figure 2-49 shows that the IGFBP7 promoter was densely hypermethylated in $BRAF^{V600E}$-positive melanomas but not in $BRAF^{V600E}$-positive nevi or melanomas lacking activated BRAF. Similar analyses in a panel of melanoma cell lines showed that the IGFBP7 promoter was densely hypermethylated in $BRAF^{V600E}$-positive melanoma cell lines and modestly hypermethylated in $NRAS^{Q61R}$-positive melanoma cell lines [Figure 2-50]. Treatment of these cell lines with the DNA methyltransferase inhibitor 5-aza-2'-deoxycytidine restored IGFBP7 expression in $BRAF^{V600E}$- and $NRAS^{Q61R}$-positive cell lines but had no effect in BRAF/RAS wild-type cell lines [Figure 2-51]. Collectively, these results indicate that loss of

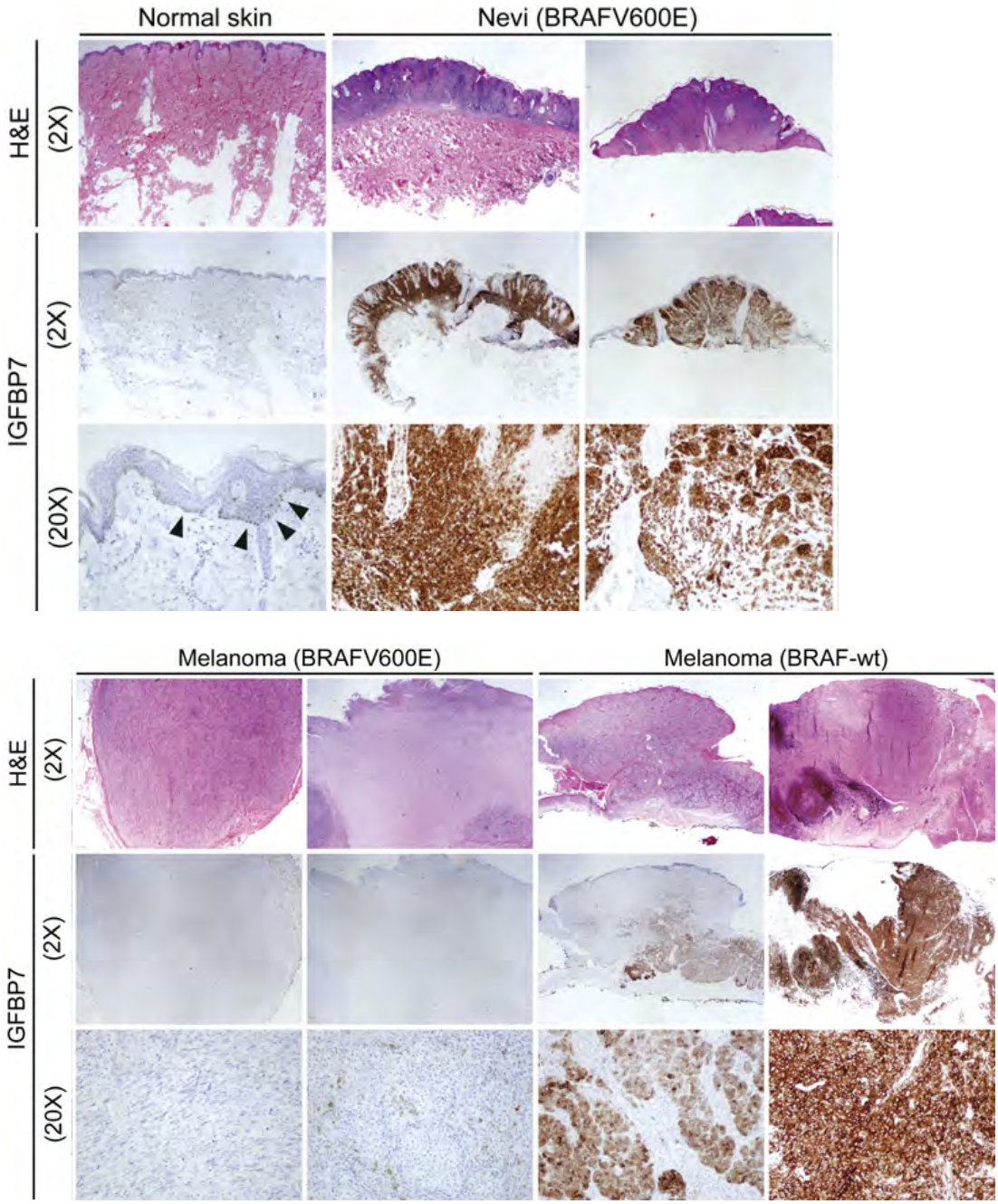

Figure 2-48. Immunohistochemical analysis of IGFBP7 expression in human tissue samples. Samples were stained with hematoxylin and eosin [H&E]. Arrowheads indicate IGFBP7-positive melanocytes. Images are shown at 2X and/or 20X.

Tissue sample	Number	BRAFV600E status	IGFBP7 status
Normal skin	5	–	+
Benign nevi	20	+	+
Melanoma	13	+	–
Melanoma*	7	–	+

* Genotyping showed that all BRAF-wild type melanomas were also wild type for RAS.

Table 2-2. IGFBP7 expression in human skin, nevi and melanoma samples.

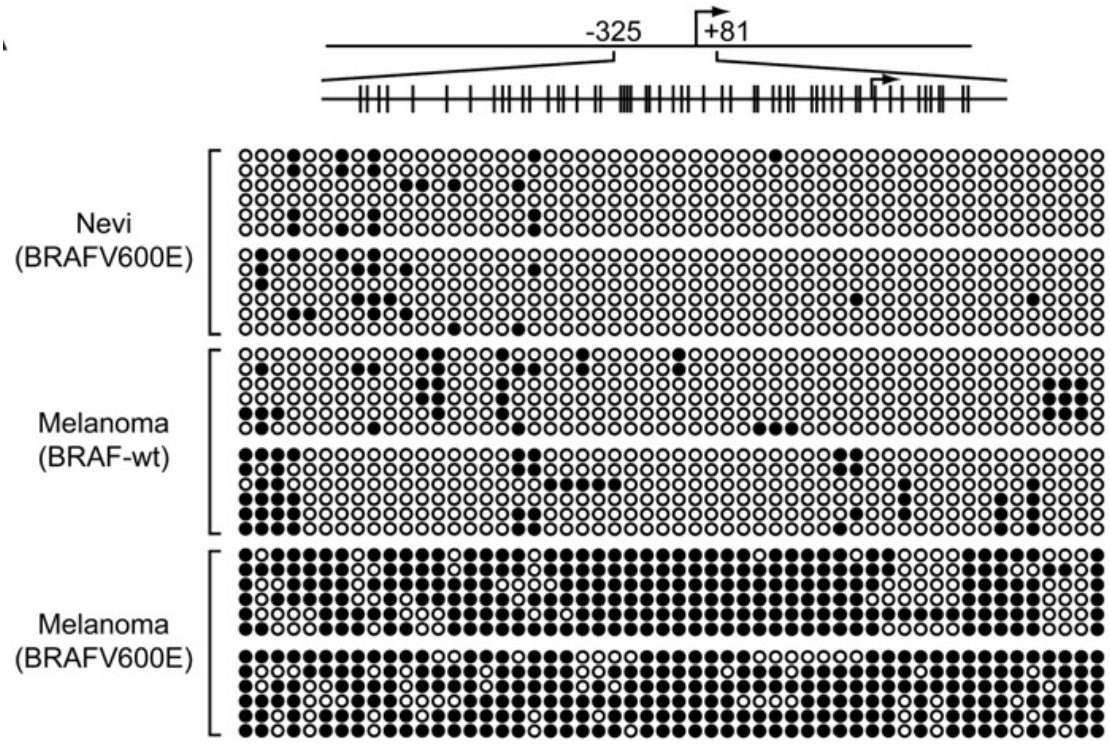

Figure 2-49. [Top] Schematic of the IGFBP7 promoter; positions of the CpG dinucleotides are shown to scale by vertical lines.

[Bottom] Each circle represents a CpG dinucleotide: open [white] circles denote unmethylated CpG sites and filled [black] circles indicate methylated CpG sites. Each row represents a single clone.

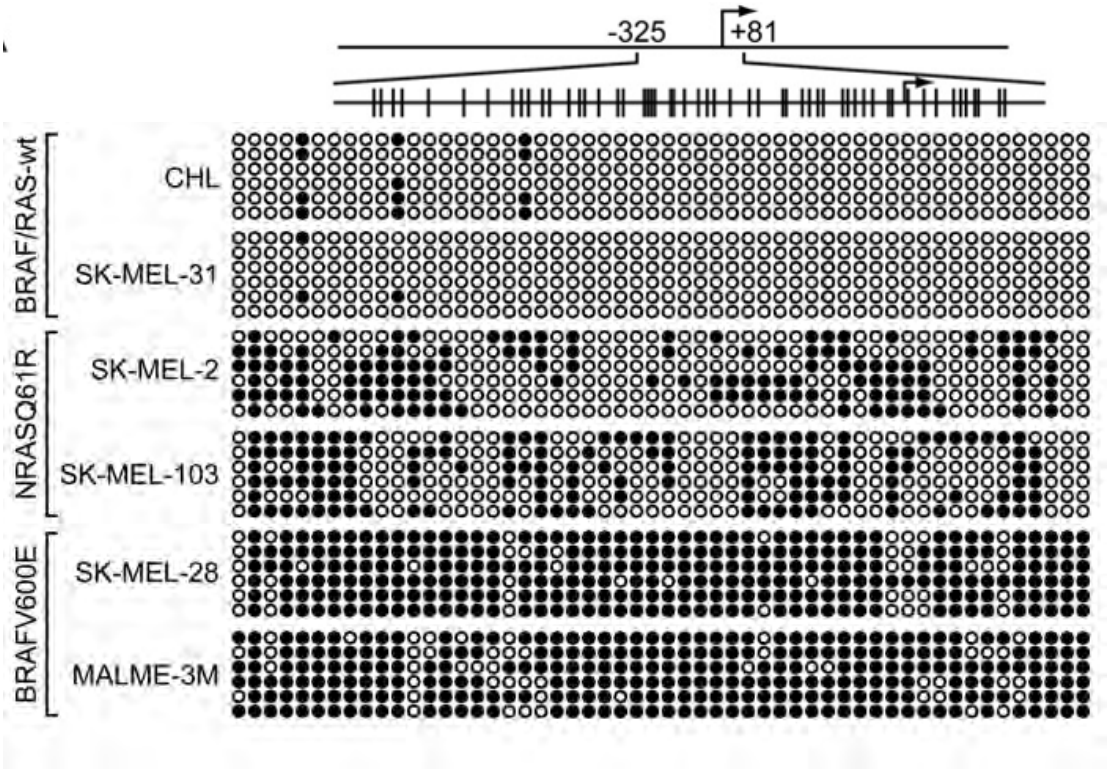

Figure 2-50. [Top] Schematic of the IGFBP7 promoter; positions of the CpG dinucleotides are shown to scale by vertical lines.

[Bottom] Bisulfite sequence analysis of the IGFBP7 promoter in a panel of melanoma cell lines.

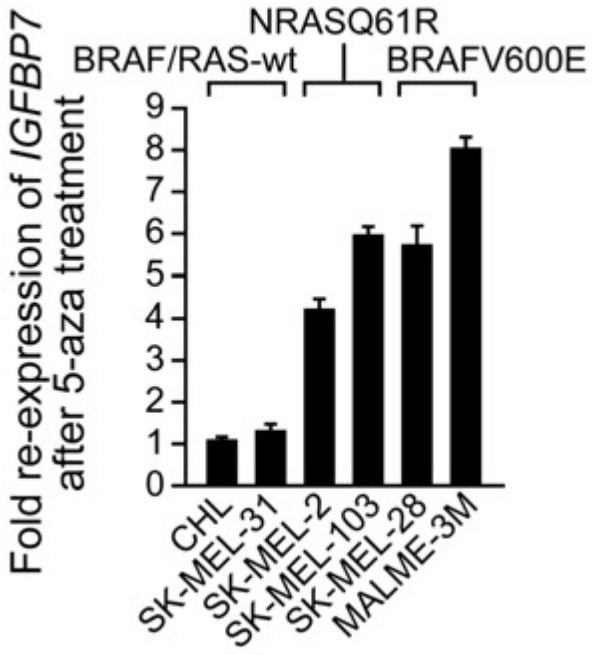

Figure 2-51. qRT-PCR analysis of IGFBP7 mRNA levels in melanoma cell lines following treatment with the DNA methyltransferase inhibitor 5-aza-2'-deoxycytidine [5-aza]. Error bars represent standard error.

IGFBP7 expression in $BRAF^{V600E}$-positive melanomas and cell lines results from epigenetic silencing involving promoter hypermethylation.

Conclusions I

By performing a genome-wide shRNA screen, I have identified 17 genes that are essential for $BRAF^{V600E}$ to induce senescence or apoptosis in primary cells. Unexpectedly, a critical component of the senescence and apoptotic pathways are a secreted protein, IGFBP7. Expression of $BRAF^{V600E}$ in primary cells induces synthesis and secretion of IGFBP7, which functions through autocrine/paracrine pathways to inhibit BRAF-MEK-ERK signaling and induce senescence or apoptosis. Consistent with my findings are previous reports that IGFBP7 [also called IGFBP-rP1 or MAC25] can inhibit proliferation of some cancer cell lines *in vitro* [see, for example, Hingorani et al., 2003; Mutaguchi et al., 2003; Ruan et al., 2006; Swisshelm et al., 1995; Wilson et al., 2002]. My results provide new insights into how activated BRAF promotes senescence, apoptosis and malignant transformation, which are schematically summarized in Figure 2-52 and discussed below.

I note that TP53 was one of the genes I identified as required for $BRAF^{V600E}$-mediated senescence. There have been several previous reports that loss of TP53 does not enable escape from oncogene-induced senescence [see, for example, Beausejour et al., 2003; Narita et al., 2006; Zhu et al., 1998]. However, these studies involved either a different cell type or oncogene than those used

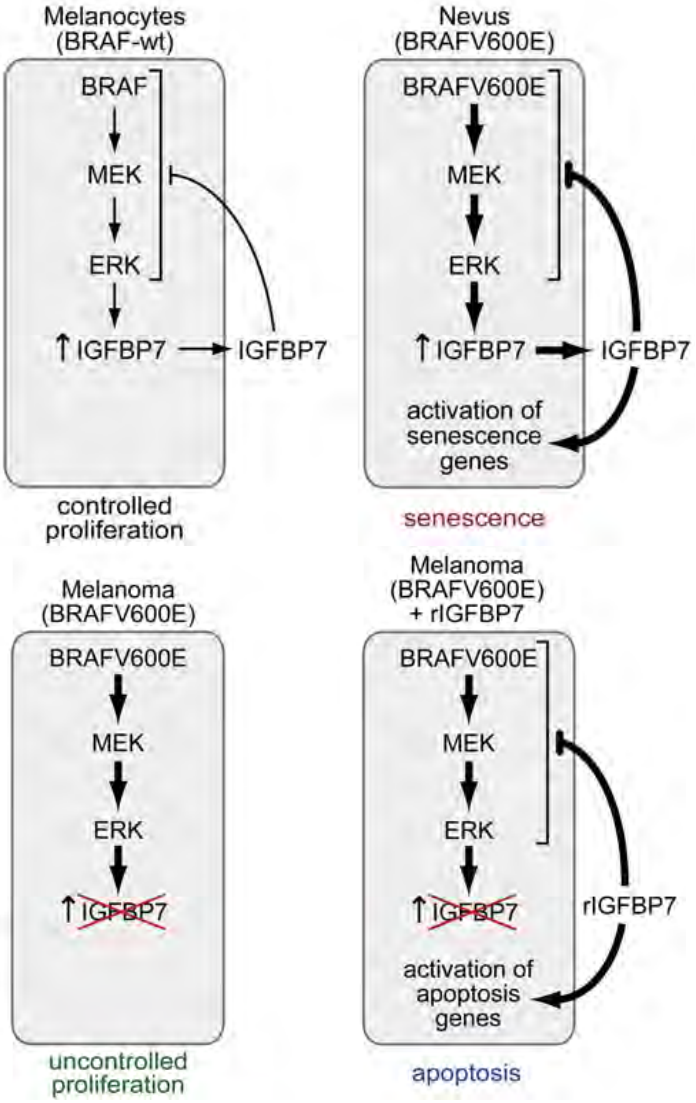

Figure 2-52. Schematic summary of $BRAF^{V600E}$-mediated senescence and melanoma progression.
Normal melanocytes [BRAF-wt] express and secrete low levels of IGFBP7, which inhibits BRAF-MEK-ERK signaling through an autocrine/paracrine pathway, thereby restraining proliferation. In $BRAF^{V600E}$-positive nevi, constitutive activation of the BRAF-MEK-ERK pathway increases expression and secretion of IGFBP7, and the resultant high levels of IGFBP7 inhibit BRAF-MEK- ERK signaling and activate senescence. In a $BRAF^{V600E}$-positive melanoma, IGFBP7 expression is lost, enabling the cells to escape from senescence and resulting in uncontrolled proliferation. Addition of exogenous IGFBP7 to $BRAF^{V600E}$-positive melanoma cells inhibits BRAF-MEK-ERK signaling and activates apoptosis.

in my study.

Previous studies have shown that expression of $BRAF^{V600E}$ in melanocytes results in an initial proliferative burst leading to clonal expansion followed by growth arrest [Michaloglou et al., 2005]. My results explain this biphasic response. In the first phase, the initial expression of $BRAF^{V600E}$ increases BRAF-MEK-ERK signaling, providing a transient proliferative signal. In the second phase, $BRAF^{V600E}$ expression results in the synthesis and secretion of IGFBP7, which acts through an autocrine/ paracrine pathway to inhibit BRAF-MEK-ERK signaling and activate a senescence program.

The non-uniform expression of $p16^{INK4A}$ in nevi has prompted speculation that senescent cells secrete a senescence-inducing agent that acts upon neighboring cells [Gray-Schopfer et al., 2007]. I find that $BRAF^{V600E}$-positive melanocytic nevi express high levels of IGFBP7 and propose that secreted IGFBP7 has a central role in the initiation and maintenance of the senescent state. A senescence-inducing secreted protein provides a powerful mechanism for tumor suppression because, following an initial oncogenic event in a single cell, neighboring cells is also protected.

$BRAF^{V600E}$ cannot fully transform human melanocytes, implying the existence of additional, cooperating events required for tumor development [Peeper and Mooi,

2002]. The 17 genes I have identified are potential tumor suppressors in malignancies involving an activating BRAF mutation. Unlike nevi, $BRAF^{V600E}$-positive melanomas do not express IGFBP7. On the basis of this observation and the other results presented in this study, I propose that loss of IGFBP7 expression allows escape from $BRAF^{V600E}$-mediated senescence and is a critical step in melanomagenesis.

Activated BRAF-positive metastatic melanoma is an aggressive disease that is refractory to conventional chemotherapeutic agents and lacks adequate treatment options [reviewed in Gray- Schopfer et al., 2007]. Inhibitors of BRAF have been developed but unfortunately have performed poorly in clinical trials. I have shown that IGFBP7, but not a RAF or MEK inhibitor, efficiently induces apoptosis in $BRAF^{V600E}$-positive melanoma cell lines. IGFBP7 may be a more efficacious anti-cancer agent than a BRAF or MEK inhibitor because it both inhibits BRAF-MEK-ERK signaling and irreversibly induces apoptosis following transient exposure. The selective sensitivity of $BRAF^{V600E}$-containing human cancer cell lines to IGFBP7, and the ability of IGFBP7 to suppress $BRAF^{V600E}$-positive tumor growth in mice, suggest that IGFBP7 may have a role in treating malignancies harboring activating BRAF mutations.

Scurr, L.L. et. al. [2010] Response:

In their recent Matters Arising article, Scurr, L.L., et al. [2010] questioned several of my conclusions regarding the role of IGFBP7 in $BRAF^{V600E}$-mediated senescence induction. In my original study in Cell [Wajapeyee et al., 2008], I used a genome-wide RNA interference [RNAi] screen to identify 17 genes required for an activated BRAF oncogene [$BRAF^{V600E}$] to block proliferation of primary melanocytes and melanoma cells. One of these genes encodes a secreted protein, IGFBP7, which I showed has a central role in $BRAF^{V600E}$-mediated senescence and apoptosis. Here, I reproduce several of the key findings of my earlier study and present new results that substantiate my original claims.

In my original study [Wajapeyee et al., 2008], I showed that expression of $BRAF^{V600E}$ in primary melanocytes increases synthesis and secretion of IGFBP7, which then acts through an autocrine/ paracrine pathway to induce senescence. $BRAF^{V600E}$-mediated induction of IGFBP7 expression was directly demonstrated in six independent experiments. By contrast, Scurr, L.L., et al. [2010] claim in their Matters Arising that $BRAF^{V600E}$ results in decreased IGFBP7. I introduced $BRAF^{V600E}$ into cultured human melanocytes by retroviral transduction, and in a series of new experiments now also show that transient transfection of a $BRAF^{V600E}$-expression plasmid results in increased IGFBP7 [Figure 2-53].

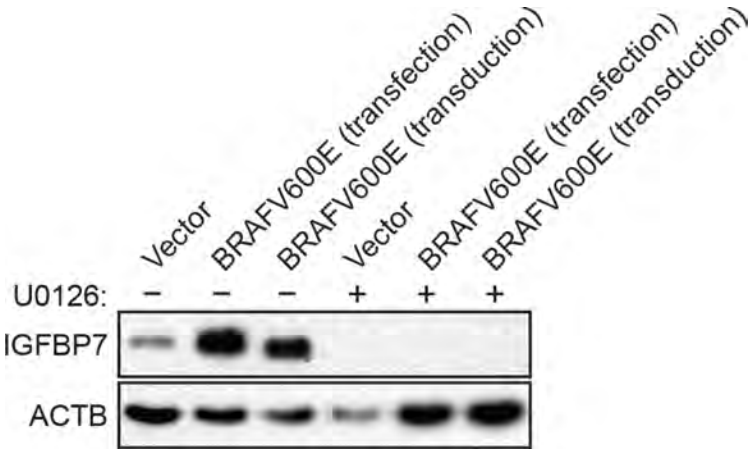

Figure 2-53. Immunoblot analysis monitoring IGFBP7 levels in human primary melanocytes transfected with an empty vector or $BRAF^{V600E}$-expression plasmid, or transduced with a $BRAF^{V600E}$expressing retrovirus.
Two days following introduction of $BRAF^{V600E}$, cells were cultured in the absence or presence of the MEK inhibitor U0126. Twenty-four hours later, conditioned medium was prepared and analyzed for IGFBP7. β-ACTIN [ACTB] was monitored as a loading control.

Furthermore, $BRAF^{V600E}$-mediated induction of IGFBP7 is, as expected, lost following addition of the MEK inhibitor U0126, which blocks BRAF-MEK-ERK signaling. Transfection of a $BRAF^{V600E}$expression plasmid into melanocytes also induces expression of a co-transfected IGFBP7 reporter plasmid [Figure 2-54].

Originally, I showed that $BRAF^{V600E}$ transcriptionally activates other genes involved in senescence or apoptosis, including PEA15, SMARCB1, and BNIP3L [Wajapeyee et al., 2008]. By contrast, Scurr, L.L., et al. [2010] claim that following introduction of $BRAF^{V600E}$ into primary melanocytes, PEA15, SMARCB1, BNIP3L, and p53 protein levels are reduced. Their p53 result is particularly surprising because activated oncogenes induce a DNA-damage response, which is expected to elevate p53 levels. Indeed, in direct contrast to Scurr, L.L., et al. [2010], another study has shown that $BRAF^{V600E}$ increases p53 levels in melanocytes [Yu et al., 2009]. To confirm my original conclusions, I performed a new immunoblot experiment, which shows that $BRAF^{V600E}$ activates the DNA-damage response and markedly upregulates expression of PEA15, SMARCB1, BNIP3L, and p53 in primary melanocytes [Figure 2-55].

Following the primary screen, I performed 11 independent experiments demonstrating that the $BRAF^{V600E}$mediated block to cellular proliferation requires IGFBP7 [Wajapeyee et al., 2008]. These experiments involved two different cell types, two unrelated IGFBP7 short-hairpin RNAs [shRNAs], and five different

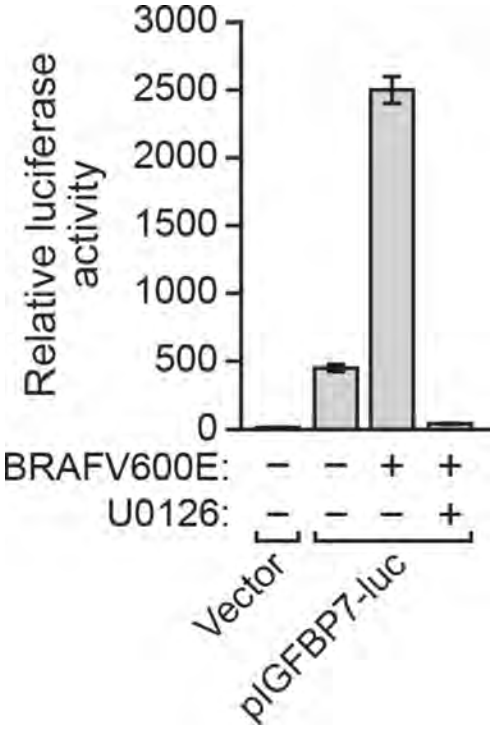

Figure 2-54. IGFBP7 reporter assays.
Human primary melanocytes were co-transfected with the $BRAF^{V600E}$-expression plasmid and a reporter plasmid containing the human IGFBP7 promoter cloned upstream of the luciferase gene [pIGFBP7-luc] and, as well as a plasmid expressing Renilla luciferase, which was used to normalize the transfection efficiency across different samples. Two days later cells were cultured in the presence or absence of U0126, and 24 hours later luciferase activity was quantified. Error bars represent standard error.

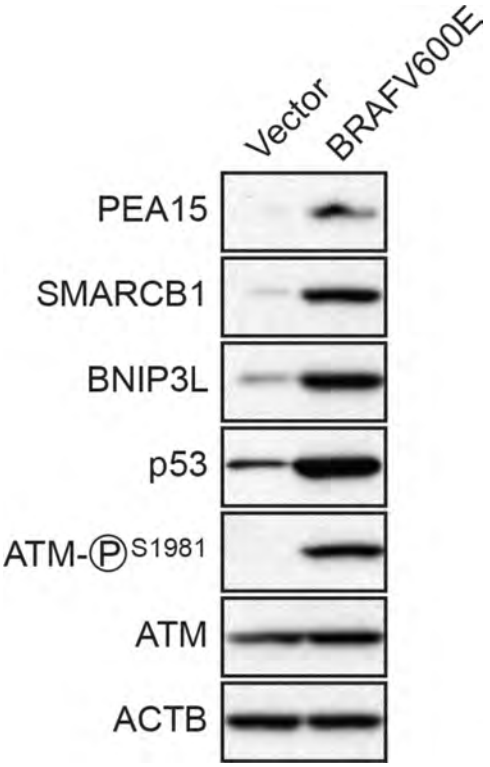

Figure 2-55. Immunoblot analysis monitoring levels of PEA15, SMARCB1, BNIP3L, p53, phosphorylated ATM and total ATM in primary melanocytes transduced with a retrovirus expressing vector or $BRAF^{V600E}$. As expected, $BRAF^{V600E}$ induces a DDR as evidenced by the appearance of phosphorylated ATM.

assays related to cellular proliferation. Finally, I showed that addition of IGFBP7 to melanocytes is sufficient to induce senescence.

In their Matters Arising, Scurr, L.L., et al. [2010] performed RNAi experiments and did not find a role for IGFBP7 in $BRAF^{V600E}$mediated senescence. To investigate this discrepancy, I repeated several of my original experiments [Wajapeyee et al., 2008], which confirmed that senescence in melanocytes is substantially reduced following shRNA-mediated knockdown of IGFBP7 [Figures 2-56 and 2-57].

Scurr, L.L., et al. [2010] suggested that my use of drug selection to introduce $BRAF^{V600E}$ and shRNAs may have inadvertently selected for senescence resistant cells. To address this concern, I transduced melanocytes with the $BRAF^{V600E}$-expressing retrovirus in the absence of drug selection. IGFBP7 knockdown was performed using two unrelated small-interfering RNAs [siRNAs] in the absence of drug selection, and induction of $p16^{INK4A}$ was analyzed as a marker of senescence. As expected, $BRAF^{V600E}$ results in enhanced expression of $p16^{INK4A}$ as well as IGFBP7 [Figure 2-58]. Moreover, the two IGFBP7 siRNAs substantially reduced IGFBP7 levels resulting in loss of $p16^{INK4A}$ induction.

Although I do not understand the failure of Scurr, L.L., et al. 2010 [2010] to observe a requirement for IGFBP7 in the induction of senescence by the BRAF

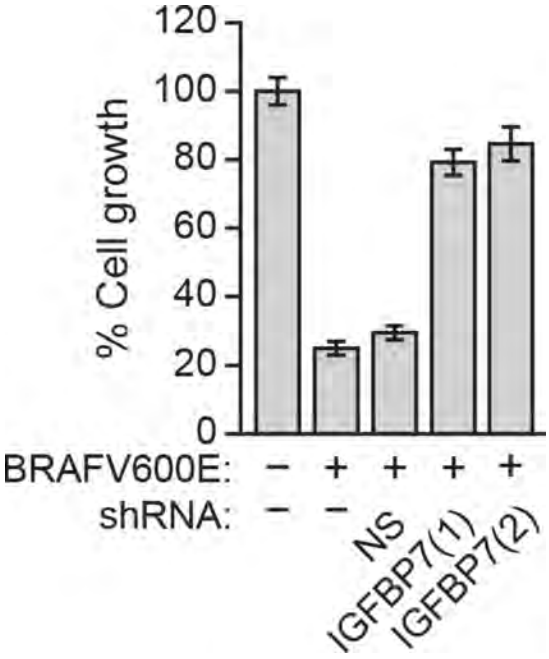

Figure 2-56. Quantitative proliferation assays.
Human primary melanocytes stably expressing a non-silencing [NS] shRNA or one of two different IGFBP7 shRNAs were infected with the $BRAF^{V600E}$-expressing retrovirus and after 7 days viable cells were counted using trypan blue exclusion. Growth of $BRAF^{V600E}$-expressing melanocytes in the absence of an shRNA is shown relative to that of mock-infected melanocytes. Growth of $BRAF^{V600E}$-expressing melanocyte cell lines expressing an shRNA has been normalized to that of the corresponding melanocyte knockdown cell line in the absence of $BRAF^{V600E}$ expression. Error bars represent standard error; experiments were performed in triplicate.

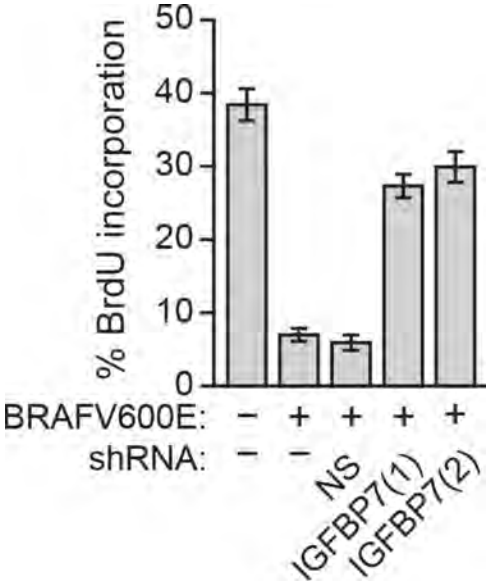

Figure 2-57. DNA replication assays monitored by BrdU incorporation.
Human primary melanocytes stably expressing a NS or IGFBP7 shRNA were infected with the $BRAF^{V600E}$-expressing retrovirus and after 7 days analyzed by BrdU incorporation assay. Error bars represent standard error.

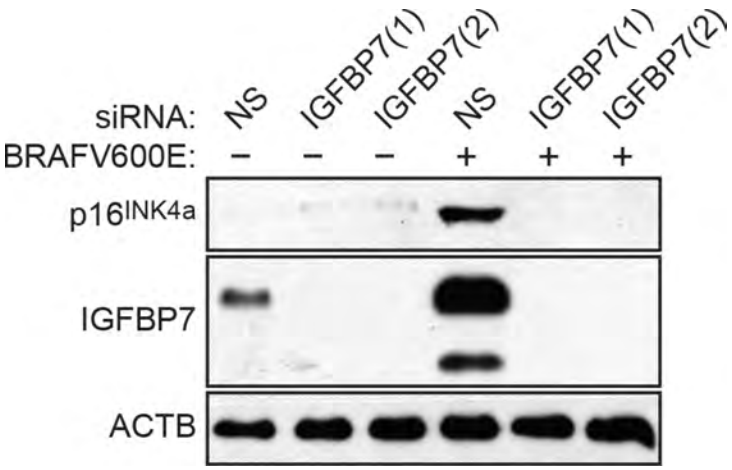

Figure 2-58. Immunoblot analysis monitoring induction of $p16^{INK4A}$. Human primary melanocytes transfected with a NS or IGFBP7 siRNA were infected with the $BRAF^{V600E}$-expressing retrovirus at a high multiplicity of infection and after 3 days cell extracts were prepared and immunoblotted for $p16^{INK4A}$, IGFBP7 or ACTB.

oncogene, it is clear that the populations of cells in which senescence is being analyzed are markedly different in the two studies. I analyzed senescence in $BRAF^{V600E}$-expressing cells that contain elevated levels of IGFBP7, PEA15, SMARCB1, BNIP3L, and p53; by contrast, in Scurr, L.L., et al. [2010] the cells analyzed for senescence contained reduced levels of these factors.

Finally, the inability of Scurr, L.L., et al. [2010] to observe a requirement for IGFBP7 is essentially a negative result; none of the experiments presented in Figure 4 of their Matters Arising included as a positive control an shRNA that knocks down a gene required for senescence induction. Scurr, L.L., et al. [2010] presented elsewhere an experiment purporting to show that knockdown of both p53 and pRb abrogates $BRAF^{V600E}$-mediated senescence [Figure S2]. However, examination of their results reveals that the level of $BRAF^{V600E}$ is substantially lower in the p53, pRb double-knockdown cells than in the control cells, which could account for the apparent difference in senescence induction.

In my original study [Wajapeyee et al., 2008], I showed by immunohistochemical analysis that IGFBP7 expression is lost at high frequency in primary melanoma cells containing $BRAF^{V600E}$. Subsequently, I showed that in metastatic melanomas IGFBP7 is lost at an even higher frequency and is independent of BRAF mutational status [Wajapeyee et al., 2009]. Scurr, L.L., et al. [2010] analyzed IGFBP7 expression in human metastatic, but not primary, melanoma

samples and failed to observe a correlation with the status of BRAF, which is in agreement with my metastatic melanoma results. To provide additional support for my original conclusions, I analyzed 14 new primary melanomas and found that IGFBP7 is expressed in all six primary melanomas containing wild-type BRAF but not in any of eight primary melanomas containing $BRAF^{V600E}$ [Figure 2-59]. As in my previous studies, I also provide independent support for the immunohistochemical results using bisulfite sequencing to determine the methylation status of the IGFBP7 promoter [Figure 2-50].

Scurr, L.L., et al. [2010] found that IGFBP7 is expressed in virtually all $BRAF^{V600E}$-containing benign melanocytic lesions [nevi], in agreement with my original immunohistochemical analysis [Wajapeyee et al., 2008]. Using tissue arrays, Scurr, L.L., et al. [2010] also found that IGFBP7 expression is not detectable in ~50% or more of the metastatic melanoma samples containing $BRAF^{V600E}$ or wild-type BRAF. The Figure 3B legend in the Scurr, L.L., et al. [2010] Matters Arising states that the median expression value for IGFBP7 is zero for both $BRAF^{V600E}$-containing and wild-type BRAF-containing metastatic melanoma samples, which is in excellent agreement with my immunohistochemistry results [Wajapeyee et al., 2009]. In summary, both my results and those of Scurr, L.L., et al. [2010] show that IGFBP7 is expressed in primary melanocytes and benign nevi, and that IGFBP7 expression is lost in a

high percentage of both $BRAF^{V600E}$-containing and wild-type BRAF-containing metastatic melanomas.

In my original study in Cell, I found that loss of IGFBP7 expression correlates with the presence of the $BRAF^{V600E}$ mutation in human melanoma cell lines [Wajapeyee et al., 2008]. Scurr, L.L., et al. [2010] also observed frequent loss of IGFBP7 expression in human cancer cell lines but without a correlation with BRAF status. However, whereas I analyzed only human melanoma cell lines, Scurr, L.L., et al. [2010] analyzed a diverse collection of melanoma and non-melanoma cell lines as well as primary cells. For example, of the 10 cell types containing wild-type BRAF and another oncogene RAS analyzed by Scurr, L.L., et al. [2010], only one [NM138] is a human melanoma cell line. The focus of my original study was melanoma and not other cancers, and thus the results of Scurr, L.L., et al. [2010] using non-melanoma cell lines are not directly relevant to my study or its conclusions. Notably, however, two other laboratories have found, analogous to my results in melanoma, that in primary colorectal cancers there is a loss of IGFBP7 expression that correlates with the presence of an activating BRAF mutation [Hinoue et al., 2009; Suzuki et al., 2010].

In summary, here I provide new results confirming several of the main conclusions of my original study in Cell [Wajapeyee et al., 2008], including [1] the transcriptional induction of IGFBP7 by $BRAF^{V600E}$, [2] the requirement of

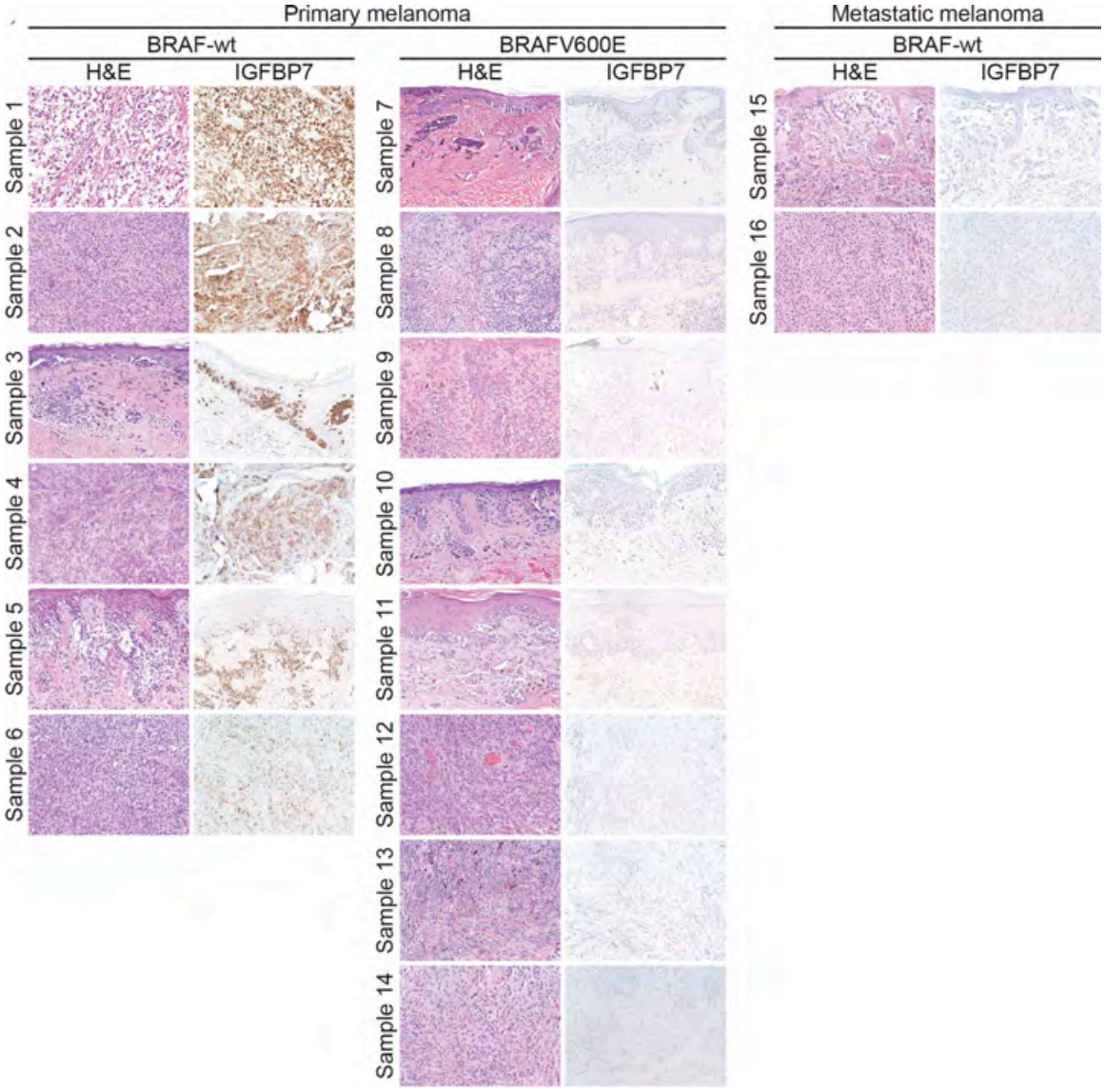

Figure 2-59. Immunohistochemical analysis of IGFBP7 expression in wild type BRAF- [BRAF-wt] and $BRAF^{V600E}$-containing human primary melanoma tissue samples.

Samples were stained with hematoxylin and eosin [H&E]. Images are shown at 20X. For reference, two new and BRAF-wt metastatic melanoma samples are included and, consistent with my previous findings [Wajapeyee et al., 2009], IGFBP7 expression is not detectable.

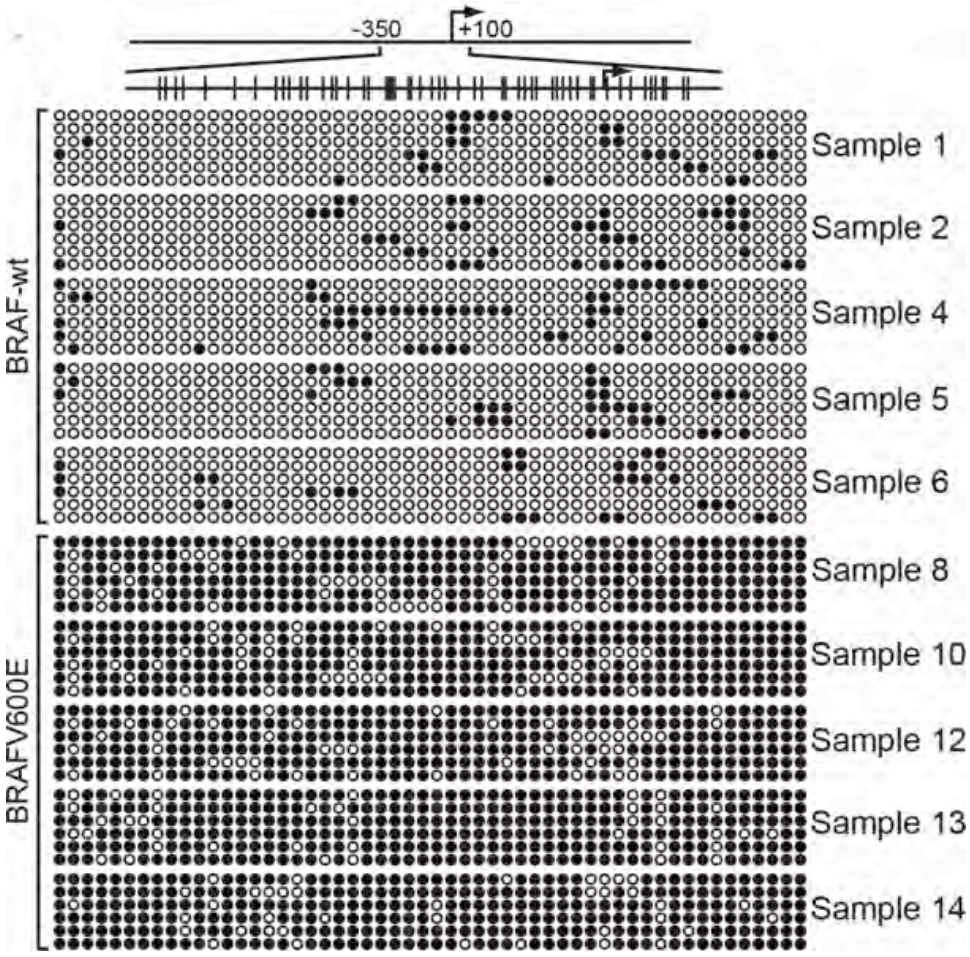

Figure 2-60. Bisulfite sequence analysis of the IGFBP7 promoter in human primary melanoma tissue samples.
[Top] Schematic of the IGFBP7 promoter; positions of the CpG dinucleotides are shown to scale by vertical lines.
[Bottom] Each circle represents a CpG dinucleotide: open [white] circles denote unmethylated CpG sites and filled [black] circles indicate methylated CpG sites. Each row represents a single clone. The results reveal a perfect correspondence between the immunohistochemical analysis of IGFBP7 expression and the methylation status of the IGFBP7 promoter.

IGFBP7 for $BRAF^{V600E}$-mediated senescence, and [3] the frequent loss of IGFBP7 expression in $BRAF^{V600E}$-containing primary melanomas. Collectively, these results implicate IGFBP7 as a tumor suppressor protein in melanomas.

Conclusions II

My studies of BRAF induced senescence have revealed an unexpected mechanism for limiting the growth of cells harboring an oncogene. The important role of senescence in tumor suppression has gradually gained momentum given the acquisition of *in vivo* results. For instance melanocytic nevi stain positively for SA-β-GAL and almost never progress into melanoma despite containing an activated BRAF allele. Furthermore my studies reveal the importance of secretory factors in promoting the senescence phenotype. Shortly after my publication, two other groups published findings that paralleled my own investigations into BRAF induced senescence. Acosta et al. [2008] and Kuilman et al. [2008] revealed the prevalence of secretory molecules in senescence induction.

Acosta et al. [2008] performed a loss of function screen to identify genes required for replicative and oncogene induced senescence in IMR-90 fibroblasts. They identified the chemokine receptor CXCR2 as a critical mediator of senescence induction. Importantly the extracellular ligands for CXCR2, interleukin-8 [IL-8] and GROα/Gro-1, also mediated the response. These findings underline the importance of the interleukin secretory response in OIS and the overall importance of secretion in tumor suppression.

The work of Kuilman et al [2008] utilized a different approach to study BRAF induced senescence. Similar to the studies of Judith Campisi's group, they employed whole-genome transcriptional analysis and identified interleukin-6 [IL-6] as being upregulated in BRAF-positive cells. Similar to Acosta et al.'s [2008] findings that CXCR2 or IL-8 depletion causes senescence bypass, Kuilman et al. [2008] show that IL-6 or the IL-6 receptor, IL-6R, depletion facilitates senescence bypass. Furthermore, additional genes involved in the chemokine signaling were also upregulated suggesting a general role in senescence induction that parallels the work of Acosta et al. [2008].

From these three studies a common theme emerges that speaks to the importance of a secreted response to oncogenic stimuli. Despite identifying different factors in each of the studies, all three define an autocrine regulatory mechanism for halting cell growth. Importantly, the factors that were identified are all potential targets for inactivation in cancer and represent a novel tumor suppression system in cells. Given the lack of identification and understanding of the exact inducers of each of these responses, it will be interesting to see how other research groups explore the similarities and differences found in these studies.

Methods

Cell Lines and Culture

Primary foreskin fibroblasts [BJ] and human melanoma cell lines were obtained from ATCC, and human primary melanocytes were obtained from Cascade Biologics; all cells were grown as recommended by the supplier.

Retroviruses and Plasmids

Retroviruses expressing empty vector or $BRAF^{V600E}$ were generated from plasmids pBABE-zeo [Addgene] or pBABE-zeo/$BRAF^{V600E}$ [Michaloglou et al., 2005], respectively. Plasmids expressing ERK2Q103A and ERK2L73P, S151D [Emrick et al., 2006] and MEK1EE [Tournier et al., 1999] have been described. shRNA Screen

The human shRNAmir library [release 1.20; Open Biosystems] was obtained through the UMass Medical School shRNA library core facility. Retroviral pools were generated and used to transduce PFFs as described [Gazin et al., 2007]. Cells were then infected with a retrovirus carrying $BRAF^{V600E}$ at MOI 20. Cells that bypassed the $BRAF^{V600E}$-induced cellular proliferation block formed colonies, which were pooled and expanded, and the shRNAs identified by sequence analysis as previously described [Gazin et al., 2007]. Individual knockdown cell lines were generated by stable transduction of 6×10^4 cells with a single shRNA followed by infection with the $BRAF^{V600E}$-expressing retrovirus. Individual

shRNAs were either obtained from the Open Biosystems library or synthesized [see Table 2-3 and Table 2-4].

Quantitative Real-Time RT-PCR

Total RNA was isolated and reverse transcription was performed as described [Gazin et al., 2007], followed by quantitative real-time PCR using Platinum SYBR Green qPCR SuperMix-UDG with Rox [Invitrogen]. Expression of GAPDH was used as an internal reference gene. Primer sequences are provided in Table 2-6.

Quantitative Proliferation Assay

Cell viability was measured by trypan blue exclusion at the time point indicated in the relevant figure legend. The number of viable cells was quantitated, and the values were expressed as percent cell growth, as described in the relevant figure legend. For the assay shown in Figures 2-11, CM was replenished every 3 days and proliferation was measured after a total of 14 days of CM treatment. Unless otherwise stated, rIGFBP7 was added to the culture medium at 10 μg/ml.

Apoptosis and DNA Replication Assays

PFFs, melanocytes, or shRNA knockdown derivatives [5 x 10^5 cells] were infected with $BRAF^{V600E}$-expressing retrovirus, and 4 days later the total cell population was stained for Annexin V-PE [BD Biosciences]. To monitor apoptosis

in melanoma cells following rIGFBP7 treatment, 5 x 10^5 cells were treated with rIGFBP7 [10 μg/ml] for 24 hr and stained for Annexin V-PE. For DNA replication assays, cells were treated as described above, except 4 hr prior to the end of the 4 day retroviral infection, cells were incubated with 20 μM BrdU [Sigma] and processed as previously described [Wajapeyee and Somasundaram, 2003].

Antibodies and Immunoblot Analysis

Cell extracts were prepared by lysis in Laemmli buffer in the presence or absence of a phosphatase inhibitor cocktail [Sigma], as needed. To prepare CM, cells were grown in Opti-MEM [Invitrogen] for 24 hr and media were harvested and concentrated using Centricon plus 20 tubes [Millipore]. CM was normalized to cell number prior to loading the gel. For the experiments shown in Figures 2-29 and 2-42, rIGFBP7 was added to the culture medium at 10 μg/ml. For the experiment of Figure 2-43, SK-MEL-28 cells were treated with 2 μg/ml or 10 μg/ml rIGFBP7, 20 μM or 40 μM of the MEK inhibitor PD98054 [Calbiochem], or 5 nM or 10 nM of the RAF inhibitor GW5074 [Sigma] for 24 hr prior to harvesting cells. Blots were probed with the following antibodies: α-p16 [Abcam]; α-acetylated H3K9 [Upstate]; α-IGFBP7, α-$BRAF^{V600E}$, cleaved caspase-3 p11 [Santa Cruz]; αSMARCB1 [Abnova]; α-BNIP3L [Proscience]; α- β-actin [Sigma]; or α-phospho-ERK or α-ERK [Cell Signaling Technology].

Recombinant IGFBP7 Expression and Purification

The human IGFBP7 expression vector pFASTBAC-1/IGFBP7, expressing a C-terminal Flag-tagged fusion protein [Oh et al., 1996], was used to generate recombinant baculovirus using the Bac-to-Bac Baculovirus Expression System [Invitrogen]. The recombinant baculovirus construct was then transfected into Sf9 cells [Invitrogen], and CM was collected and incubated with α-Flag M2 beads [Sigma], and the bound IGFBP7 protein was eluted using an α-Flag peptide [synthesized by CFAR, UMass Medical School, USA].

Senescence-Associated β-galactosidase Assay

Melanocytes infected with a retrovirus expressing either vector or $BRAF^{V600E}$ or melanocytes treated with $BRAF^{V600E}$/melanocyte CM or rIGFBP7[10 μg/ml] for 14 days were processed as previously described [Dimri et al., 1995]. Cells were visualized on a Zeiss Axiovert 40 CFL microscope. Images were captured using QCapture Pro version 5 software [QImaging Corporation].

ChIP Assays

ChIP assays were performed using extracts prepared 24 hr following rIGFBP7 treatment. The following antibodies were used: αBRG1 [a gift from A. Imbalzano, UMass Medical School], α-phospho-STAT1 [Upstate], and α-SMARCB1 and α-STAT1 [Santa Cruz]. For ChIP experiments on the SMARCB1 promoter, primers spanning a STAT1 binding site located ~2.4 kb upstream of the transcription start

site were used. For ChIP experiments on the BNIP3L promoter, a series of primer pairs that covered ~2 kb of the BNIP3L promoter were used; following addition of rIGFBP7, SMARCB1 and BRG1 were recruited to the BNIP3L promoter near the transcription start site. shRNA/siRNA sequences are provided in Table 2-4 and Table 2-5, and primer sequences used for amplifying the ChIP products are provided in Table 2-7. ChIP products were analyzed by quantitative real-time PCR using Platinum SYBR Green qPCR SuperMix- UDG with Rox [Invitrogen]. Calculation of fold-differences was done as previously described [Pfaffl, et al. 2001].

Tumor Formation Assays

5 x 10^6 SK-MEL-28 or SK-MEL-31 cells were suspended in 100 µl of serum-free MEM and injected subcutaneously into the right flank of athymic Balb/c [nu/nu] mice [Taconic]. At days 3, 6, and 9, mice were injected at the tumor site with either rIGBP7 [20 µg in 100 µl total volume] or, as a control, PBS. Tumor dimensions were measured every three days and tumor volume was calculated using the formula: $\pi/6$ x [length] x $[\text{width}]^2$. For the systemic administration experiments, cells were injected into the flank as described above and when tumors reached a size of 100 mm3, 100 µg rIGFBP7 in a total volume of 100 µl was delivered by tail vein injection at days 6, 9, and 12. Tumor dimensions were measured every 3 days. Animal experiments were performed in accordance with the Institutional Animal Care and Use Committee [IACUC] guidelines.

Immunohistochemistry

The study was approved by the UMass Medical Center institutional review board [IRB #12543]. Archival materials from normal skin [n = 5], nevi [n = 20], and malignant melanoma [primary [n = 7] and metastatic [n = 13]] were retrieved from the pathology files of UMass Medical Center, Worcester, MA. The histologic sections of all cases were re-reviewed and the diagnoses confirmed by a dermatopathologist [MM]. All patient data were de-identified. Five micrometer-thick sections were cut for immunohistochemical studies, which were performed, using standard techniques, with heat-induced epitope retrieval buffer and an α-IGFBP7 antibody [1:20 dilution; Santa Cruz]. Appropriate positive and negative controls were included such as cell lines containing an shRNA against the antigen [ie IGFBP7] and a cell line over-expressing the antigen. Positive staining was noted by ascertaining expression of IGFBP7 in the cytoplasm; significant nuclear staining was not noted. All stained slides were reviewed by the dermatopathologist [MM] in a blind fashion with respect to genotype. Genomic DNA was isolated and quantitated, followed by PCR amplification [see Table 2-8 for primer sequences] and TA cloning [Promega]. Multiple clones were sequenced or identifying the ^{V600E} mutation [T1796A] in exon 15 of the BRAF gene.

Bisulfite Sequencing

Bisulfite modification was carried out essentially as described [Frommer et al., 1992] except that hydroquinone was used at a concentration of 125 mM during bisulfite treatment [carried out in the dark] and DNA was desalted on Qiaquick columns [QIAGEN] after the bisulfite reaction. Six clones were sequenced for each cell line or human tissue sample [see Table S4 for primer sequences]. For 5-aza-2’-deoxycytidine [5-aza] treatment, melanoma cell lines were treated with 10 µM 5-aza [Calbiochem] for 48 hr.

Deoxyuridine Triphosphate Nick-End Labeling [TUNEL] Assays

Paraffin sections of 5 micrometer thickness were tested for DNA fragmentation by the non-isotopic in situ TUNEL method using the ApopTag Peroxidase in situ Apoptosis Detection Kit Apo-DirectTM TUNEL Assay Kit [Chemicon International].

Open Biosystems shRNAs

Gene	Source ID	Clone Location
BIN1	V2HS_192552	SH2136-G-11
	V2HS_238893	SH2490-D-11
BNIP3L	V2HS_15157	SH2240-F-2
	V2HS_15153	SH2117-G-8
BUB1	V2HS_15109	SH2335-D-10
	V2HS_15112	SH2123-B-6
CDKN2A (p16)	V2HS_195839	SH2517-C-6
DMTF1	V2HS_18765	SH2249-A-4
	V2HS_18766	SH2114-C-10
FBXO31	V2HS_15701	SH2119-C-4
	V2HS_25023	SH2497-B-9
FOXA1	V2HS_16780	SH2118-F-5
	V2HS_16813	SH2260-H-2
HIRA	V2HS_179296	SH2205-H-3
	V2HS_171670	SH2526-G-6
HSPA9	V2HS_173169	SH2210-F-7
	V2HS_263034	SH2661-D-2
IGFBP7	V2HS_132291	SH2710-D-9
	V2HS_132289	SH2094-C-3
IRF1	V2HS_133394	SH2096-C-1
	V2HS_133391	SH2095-E-6
IL1R1	V2HS_131082	SH2445-F-2
	V2HS_131085	SH2517-E-6
MEN1	V2HS_76534	SH2523-E-5
	V2HS_76605	SH2638-A-12
NF2	V2HS_115769	SH2336-C-2
	V2HS_115768	SH2563-F-9
PEA15	V2HS_23701	SH2137-E-11
	V2HS_23702	SH2320-C-5
RAP1GAP	V2HS_175368	SH2458-H-11
SMARCB1	V2HS_153159	SH2218-F-3
TP53	V2HS_93615	SH2423-C-10

Table 2-3. shRNA information

Gene	Sequence (5' -> 3')
RAP1GAP	TGCTGTTGACAGTGAGCGCGCCACCAGTGTGACCCTGTTATAGTGAAGC CACAGATGTATAACAGGGTCACACTGGTGGCTTGCCTACTGCCTCGGA
SMARCB1	TGCTGTTGACAGTGAGCGCTCACTGATTGTCCCTGGGAAGTAGTGAAGC CACAGATGTACTTCCCAGGGACAATCAGTGATTGCCTACTGCCTCGGA
TP53	TGCTGTTGACAGTGAGCGACCTGTGCAGCTGTGGGTTGATTAGTGAAGC CACAGATGTAATCAACCCACAGCTGCACAGGGTGCCTACTGCCTCGGA

Table 2-4. Synthesized shRNA information, hairpins were cloned into the pSM2-shRNA backbone [Open Biosystems].

Gene	Sequence (5' -> 3')
JUN	GGAACAGGTGGCACAGCTT
RKIP	CACTCACTCTGATTTATGT
STAT1	CCCAGAATGCCCTGATTAA
Non-silencing	AACACCGAACGAGACACGA

Table 2-5. Synthesized siRNA information

RT-PCR

Gene	Forward or reverse primer	Sequence (5' → 3')
BIN1	forward	TCTCCAGAAGCTGGGGAAGG
	reverse	TCCATCCACAGCAGGTCGTT
BNIP3L	forward	CGGACTCGGCTTGTTGTGTT
	reverse	ATGGGTAGCTCCACCCAGGA
BUB1	forward	GATGCTTGAAGCCCACATGC
	reverse	AGGGGATGACAGGGTTCCAA
JUN	forward	GGTAGCAGATAAGTGTTGAG
	reverse	GGCGCTAGCTCTGGGCAGTT
DMTF1	forward	AGCCAAGAGGCCAACCTGTC
	reverse	CCTGGCTGGAGCTGTTCTCA
FBXO31	forward	AATCCGGCCTTTTGACCAGA
	reverse	TCCGCTCACAGGAAGAGCAC
FOXA1	forward	GGAGCCGGCGTACTACCAAG
	reverse	TTTTGCACTGGGGGAAAGGT
HIRA	forward	ACACTCTCGCCGCTGATGAC
	reverse	GGGGCTAGTGTCCACCTTGG
HSPA9	forward	ACGGGAAGCTGCTGAAAAGG
	reverse	TGGGGCTCTGCCAAAAAGAT
IGFBP7	forward	GGCATGGAGTGCGTGAAGAG
	reverse	CTTGCTGACCTGGGTGATGG
IRF1	forward	CCGTTCTTGCCCTCCTGAGT
	reverse	TCCATGGCCTCTGCCTTACA
IL1R1	forward	TCTTGCCTCGACCCTTCCTC
	reverse	TGCTCCTGGAAGGCAGTGAG
MEN1	forward	CAGGGGCCAGACAGTCAATG
	reverse	GGTGGGCTCCAGCTCCTCTA
NF2	forward	TCGGGCCCTGAATTTTCTGT
	reverse	GAGGTTGCAGTGAGCCGAGA
PEA15	forward	CTAGGGGAGGGGGCTGAGTT
	reverse	GGTGGGGGTTGAGTGGTCTC
RAP1GAP	forward	GGCAGACCTCCGAGGAAGAA
	reverse	GGAAGACCACAGCCACGATG
SMARCB1	forward	TCTGGATTTGAACCCGCTGA
	reverse	TGCTGTATGCGATGGTGGTG
STAT1	forward	GTTAGAAAAGCAAGACTG
	reverse	CATCTGGATTGGGTCTTCC
TP53	forward	AGCTCCCAGAATGCCAGAGG
	reverse	AAGCCCAGACGGAAACCGTA

Table 2-6. Primers used for quantitative real time RT-PCR

ChIP

Gene	Forward or reverse primer	Sequence (5' → 3')
BNIP3L	forward	CCTCATTCCGTTTCTCCTCA
	reverse	GCCCAGGCCACGTGATGA
IGFBP7	forward	GATTGGAGGATGTTTCCC
	reverse	CATGTCACATTGTGGTTCTT
SMARCB1	forward	TGCTACAGTGGCTTCTTAAC
	reverse	TTCTACCCGAGGTTAGT

Table 2-7. Primers used for ChIP

BRAF Genotyping
Forward primer: 5'-TCATAATGCTTGCTCTGATAGGA-3'
Reverse primer: 5'-GGCCAAAATTTAATCAGTGGA-3'

Bisulfite Sequencing
Forward primer: 5'-GAGAAATTAGAGGGTGGAAG-3'
Reverse primer: 5'-AACAAAAACAACAACCCAAC-3'

Table 2-8. Primers used for *BRAF* genotyping and bisulfite sequencing

CHAPTER III: $p14^{ARF}$ EPIGENETIC SILENCING SCREEN

Preface

This body of work was completed over the entire length of my graduate studies, eight years. This research was my first and last project with the Green lab. It began with the assistance of Claude Gazin and Narendra Wajapeyee. Each of us initiated a reporter cell line based screen using vector backbones generated by Claude. Unfortunately Claude's attempts were unsuccessful but Narendra's resulted in a publication entitled "Epigenetic Silencing of the RASSF1A Tumor Suppressor Gene through HOXB3-Mediated Induction of DNMT3B Expression" in the journal Molecular Cell in 2009. This publication combined with Claude and Narendra's 2007 Nature paper entitled "An Elaborate Pathway Required for Ras-Mediated Epigenetic Silencing" proved formative in my development of this work. Narendra and I had daily informal discussions related to my results and experiments.

As time went on, I sought the help and expertise of others within and outside my lab. Minggang Fang had developed a very similar project concerning the epigenetic silencing of MLH1 in a BRAF-positive cell line. Minggang and I converged on the concept that our projects, for the first time, defined the connection between an oncogene and its consequences on the epigenetic profile of a colorectal cancer cell. This link between the oncogenotype and epigenotype had been observed over a decade prior and has since been better characterized.

However the basis of this link has never been explained in molecular detail until my results. The serendipity and complexity of our results drove us to work together on the molecular basis of the CIMP profile and the bulk of the CIMP-based results were performed in concert. Furthermore, Sung Mi Park, with her adept ability to purify proteins and perform beautiful *in vitro* experiments was utilized to investigate the specificity of the PRKD1 phosphorylation of USP28 via kinase assays.

Introduction

The tumor suppressor $p14^{ARF}$, encoded within the *INK4-ARF* locus, is epigenetically silenced in 30-45% of colorectal cancers [CRCs] through a mechanism[s] that remains to be determined. Here I perform a large-scale RNA interference [RNAi] screen and identify ZNF304, a zinc-finger DNA binding protein, as the initiator of $p14^{ARF}$ epigenetic silencing in CRCs containing activated RAS. ZNF304 binds directly to the $p14^{ARF}$ promoter and recruits a co-repressor complex that includes the histone methyltransferase, SETDB1, and the DNA methyltransferase, DNMT1. Knockdown of ZNF304 derepresses $p14^{ARF}$ and markedly decreases tumor growth in mouse xenografts. Significantly, I find that ZNF304 is over-expressed in KRAS-positive CRC cell lines and human CRC samples. Over-expression of ZNF304 is dependent upon USP28, a deubiquitinase isolated in my original RNAi screen, which is upregulated by RAS signaling and antagonizes ZNF304 proteolytic degradation. KRAS-positive CRCs frequently have a CpG island methylator phenotype [CIMP] characterized by aberrant DNA hypermethylation of a specific set of CIMP marker genes. I find that ZNF304 binds directly to and is required for epigenetic silencing of these CIMP marker genes both *in vitro* and *in vivo*. $p14^{ARF}$ is also silenced in human embryonic stem cells [hESCs] and becomes poised for expression following differentiation. Remarkably, I show that this same ZNF304-directed pathway also mediates epigenetic silencing of $p14^{ARF}$ in undifferentiated hESCs.

Epigenetic silencing represents an important mechanism by which tumor suppressor genes are inactivated during cancer development, and is believed to be a critical event in cancer progression [Esteller et al., 2002]. In many instances, epigenetic silencing occurs by DNA hypermethylation in CpG-rich promoter regions [Baylin et al., 2005]. A well-studied example is the *INK4-ARF* locus , which harbors a cluster of three tumor suppressor genes: $p14^{ARF}$, $p15^{INK4B}$ [also known as *CDKN2B*] and $p16^{INK4A}$ [also called *CDKN2A*] [reviewed in Gil et al., 2006]. The three genes are located in close proximity to one another on chromosome 9, yet each is transcribed from a distinct promoter. Notably, $p14^{ARF}$ and $p16^{INK4A}$ share exons two and three, yet each is translated in a different reading frame yielding unrelated polypeptides. The tumor suppressor activities of the encoded proteins derive from their ability to act as negative regulators of the cell cycle. For instance, $p15^{INK4B}$ and $p16^{INK4A}$ both function in the retinoblastoma [Rb] tumor suppressor pathway and act by inhibiting the cyclin-dependent kinases CDK4 and CDK6, which in turn induces G1 arrest. By contrast, $p14^{ARF}$ functions in the p53 tumor suppressor pathway and abrogates MDM2-mediated ubiquitination of p53, leading to an increase in p53 abundance [Sherr, C.J., 2006].

Inactivation of the *INK4-ARF* locus through chromosomal deletion or epigenetic silencing is a common event in cancer and yields cells with increased proliferative capacity and a predisposition to tumorigenesis. Disabling the

functions of *p14*^{ARF}, *p15*^{INK4B} or *p16*^{INK4A} by promoter hypermethylation occurs at high frequency in numerous types of human cancers including colon [Burri et al., 2001, Lind et al., 2004, Shen et al., 2003], primary central nervous system lymphomas [Nakamura et al., 2001, Zhang et al., 2005], chronic myeloid leukemia [Nagy et al., 2003] and bladder cancer [Chang et al., 2003, Dominguez et al., 2003, Kawamoto et al., 2006]. In general, the factors and pathways responsible for aberrant tumor suppressor hypermethylation have yet to be identified. Epigenetic silencing of the *p14*^{ARF} gene provides a paradigm for studying the mechanisms involved in tumor suppressor silencing in cancer. Notably, *p14*^{ARF} is silenced due to DNA methylation in approximately 30% of human colon cancer samples analyzed [Dominguez et al., 2003]. Identifying the genes responsible for *p14*^{ARF} silencing and understanding how they function may reveal novel mechanisms of cancer progression and identify new therapeutic targets. Here I perform a genome-wide RNA-interference [RNAi] screen to identify factors required for *p14*^{ARF} epigenetic silencing. Using this approach, I identified the KRAB-containing zinc finger transcription factor, ZNF304, required for efficient *p14*^{ARF} epigenetic silencing. Here I describe the mechanism and regulation of ZNF304-mediated silencing of tumor suppressor genes in human colorectal cancer.

Results

To screen for factors involved in epigenetic silencing of *p14^{ARF}*, I generated a reporter construct in which the *p14^{ARF}* promoter was used to direct expression of a gene encoding the blasticidin-resistance [Blast^{R}] gene [Figure 3-1]. This *p14^{ARF}*-Blast^{R} reporter construct was linearized by restriction enzyme digest and stably transfected into DLD-1 cells, a human CRC cell line in which endogenous *p14^{ARF}* is epigenetically silenced [Zheng et al., 2000] and Figure 3-2]. I then selected cells in which the reporter gene had been silenced as evidenced by acquisition of blasticidin sensitivity. Transcriptional repression of the reporter gene was due to DNA methylation of the *p14^{ARF}* promoter as evidenced by the appearance of blasticidin-resistant colonies following treatment with the DNA methyltransferase inhibitor 5-aza-2'-deoxycytidine [5-AZA] [Figure 3-3]. Furthermore, methylation of the endogenous *p14^{ARF}* promoter and that of the reporter were confirmed by bisulfite sequencing. Treatment with 5-AZA demethylates the endogenous promoter as well as that of the reporter [Figure 3-4].

A human shRNA library [Silva et al., 2005] comprising ~62,400 shRNAs directed against ~28,000 genes was divided into 10 pools, which were packaged into retrovirus particles and used to stably transduce the DLD-1/*p14^{ARF}*-Blast^{R} reporter cell line. Blasticidin-resistant colonies, indicative of de-repression of the

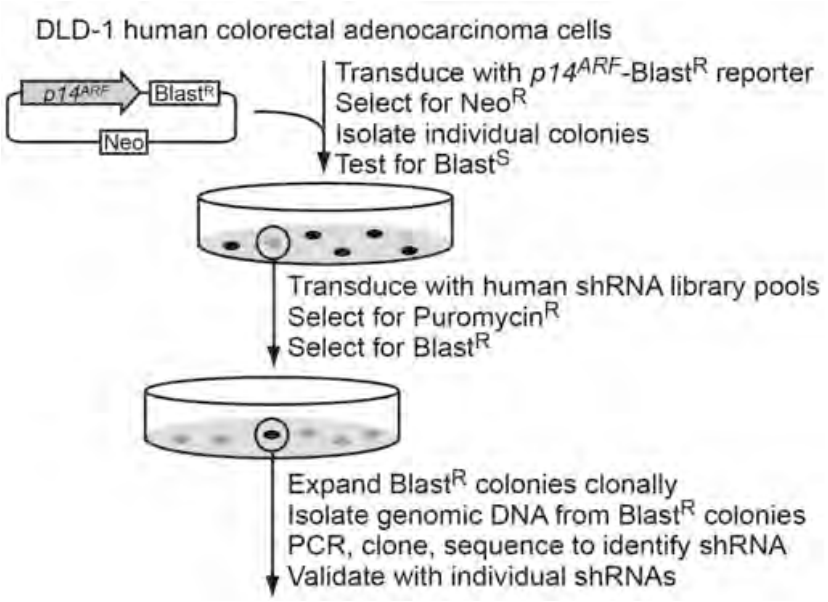

Figure 3-1. Schematic of the generation of the DLD-1/*p14*^{ARF}-Blast^{R} reporter cell line and subsequent shRNA screen.

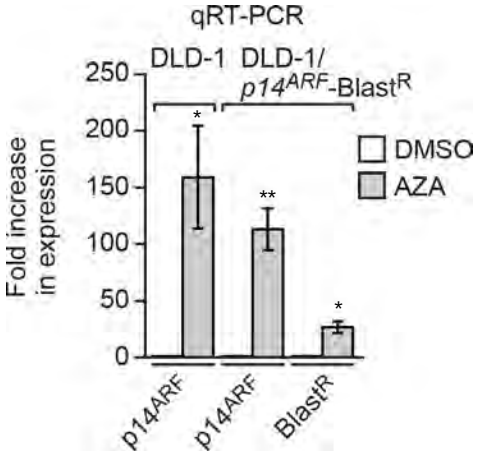

Figure 3-2. Validation of DLD-1/*p14*^{ARF}-Blast^{R} reporter cell line.
qRT-PCR analysis for p14^{ARF} and/or Blast^{R} mRNA expression in parental DLD-1 cells [left] or the DLD-1/*p14*^{ARF}-Blast^{R} reporter cell line [right] treated with either DMSO or 10 μM 5-AZA for three days. Data was normalized to the DMSO control. Data were collected from experiments performed in at least triplicate, and expressed as mean ± standard deviation. Differences between groups were assayed using two-tailed student *t*-test using Excel [Microsoft]. Significant differences were considered when $P < 0.05$. n.s., not significant [$P > 0.05$]; *$P \leq 0.05$ and **$P \leq 0.01$ indicate statistical significance.

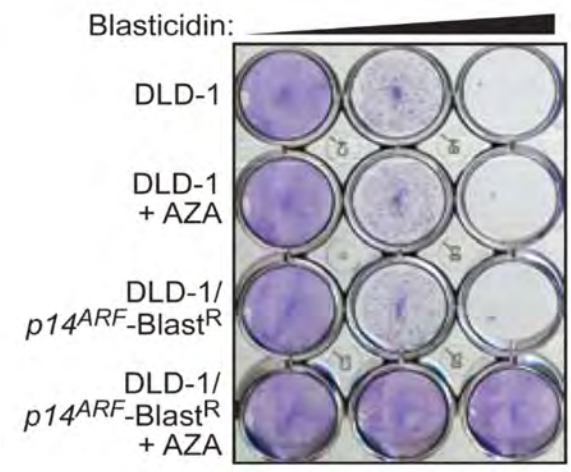

Figure 3-3. Validation of the DLD-1/*p14*^{ARF}-Blast^{R} reporter cell line.
0.5 x 10^4 DLD-1 or DLD-1/*p14*^{ARF}-Blast^{R} cells were treated with either DMSO or 5-AZA for three days and subsequently challenged with 0, 5 or 10 μM Blasticidin for 6 days. Plates were stained with crystal violet.

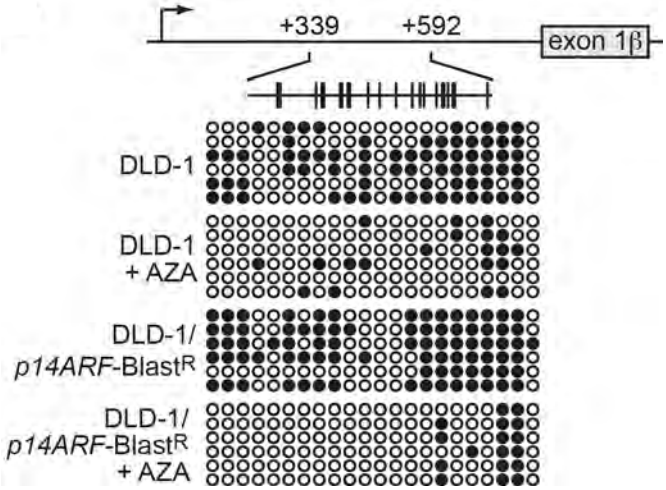

Figure 3-4. Bisulfite Sequencing of DLD-1/*p14*^{ARF}-Blast^{R} reporter cell line. DLD-1 or DLD-1/*p14*^{ARF}-Blast^{R} cells were treated with either DMSO or 5-AZA for three days and harvested for genomic DNA and subsequent bisulfite sequencing analysis. Each line represents and individual sequencing clone.

epigenetically silenced reporter gene, were selected and the shRNAs identified by sequence analysis [Figure 3-1].

Positive candidates identified in the primary screen were validated by stably transducing DLD-1 cells with an shRNA directed against each candidate gene, followed by analysis of endogenous $p14^{ARF}$ mRNA expression by qRT-PCR. Using this approach, I identified eight genes that, following shRNA-mediated knockdown, resulted in de-repression of the entire endogenous *INK4-ARF* locus, $p14^{ARF}$, $p15^{INK4B}$ *and* $p16^{INK4A}$, which are silenced in DLD-1 cells [Ishiguro, 2006, Zheng, 2000] [Figure 3-5, 3-6 and Table 3-1]. qRT-PCR analysis confirmed that each shRNA efficiently knocked down target gene expression [Figure 3-7]. For all genes, a second shRNA whose sequence was unrelated to that isolated from the primary screen also resulted in target gene knockdown and de-repression of endogenous $p14^{ARF}$ [Figure 3-7]. Therefore I believe the eight genes identified mediate silencing in of the entire *INK4-ARF* locus in DLD-1 cells.

My lab's previous studies show that epigenetic silencing of tumor suppressor genes [TSGs] is initiated by a sequence-specific DNA binding protein. Therefore, I elected to focus on ZNF304, a zinc finger DNA-binding protein that contains a Krüppel-associated box [KRAB] repressor domain [Sabater, 2002].

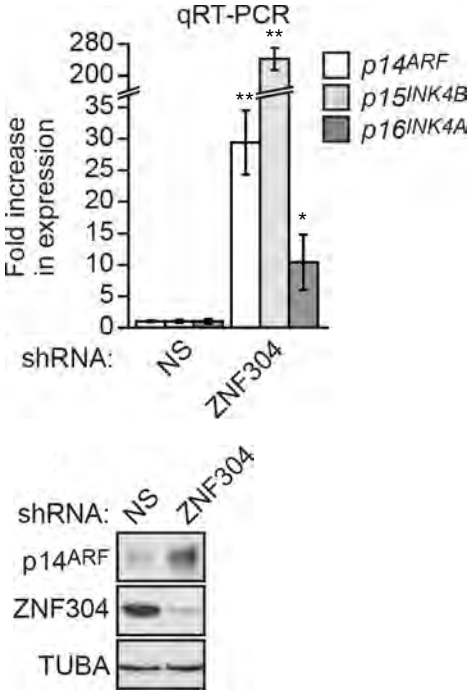

Figure 3-5. Validation of ZNF304 shRNA identified in RNAi screen.

[Top] qRT-PCR analysis of $p14^{ARF}$, $p15^{INK4B}$ and $p16^{INK4A}$ mRNA expression in DLD-1 cells stably infected with either a NS or a ZNF304 shRNA identified in the RNAi screen. Data was normalized to the NS control. Data were collected from experiments performed in at least triplicate, and expressed as mean ± standard deviation. Differences between groups were assayed using two-tailed student *t*-test using Excel [Microsoft]. Significant differences were considered when $P < 0.05$. n.s., not significant [$P > 0.05$]; *$P \leq 0.05$ and **$P \leq 0.01$ indicate statistical significance.

[Bottom] Immunoblot analysis of $p14^{ARF}$ and ZNF304 expression in DLD-1 cells stably infected with either a NS or a ZNF304 shRNA identified in the RNAi screen. Tubulin was used as a loading control.

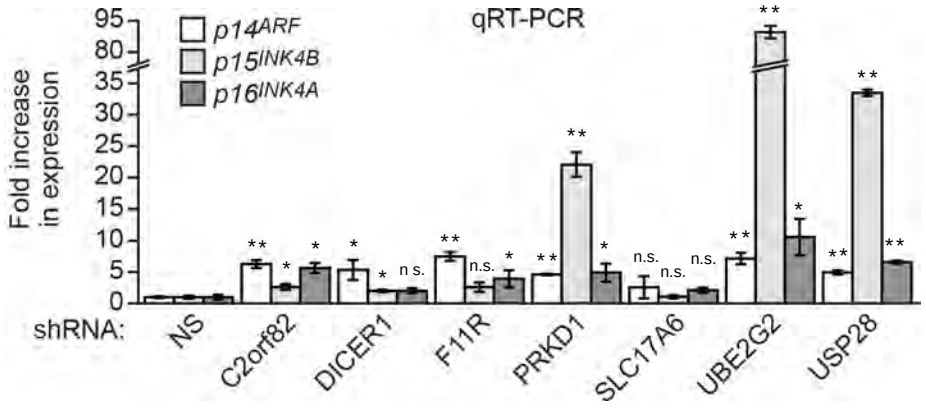

Figure 3-6. Validation of individual shRNAs identified in RNAi screen.
qRT-PCR analysis of $p14^{ARF}$, $p15^{INK4B}$ and $p16^{INK4A}$ mRNA expression in DLD-1 cells stably infected with either a NS or one of 7 shRNAs identified in the RNAi screen. Data was normalized to a NS control. Data were collected from experiments performed in at least triplicate, and expressed as mean ± standard deviation. Differences between groups were assayed using two-tailed student *t*-test using Excel [Microsoft]. Significant differences were considered when $P < 0.05$. n.s., not significant [$P > 0.05$]; *$P \leq 0.05$ and **$P \leq 0.01$ indicate statistical significance.

Biological Process	Accession number	Gene symbol	Gene name
Signal transduction	NM_002742	PRKD1	protein kinase D1
	NM_016946	F11R	F11 receptor
mRNA stability	NM_177438	DICER1	dicer1, ribonuclease type III
Protein stability	NM_003343	UBE2G2	ubiquitin-conjugating enzyme E2G 2
	NM_020886	USP28	ubiquitin specific peptidase 28
Transcription regulation	NM_020657	ZNF304	zinc finger protein 304
Transporter	NM_020346	SLC17A6	solute carrier family 17 (sodium-dependent inorganic phosphate
Unknown	NM_206895	C2orf82	chromosome 2 open reading frame 82

Table 3-1. Genes required for epigenetic silencing of $p14^{ARF}$.

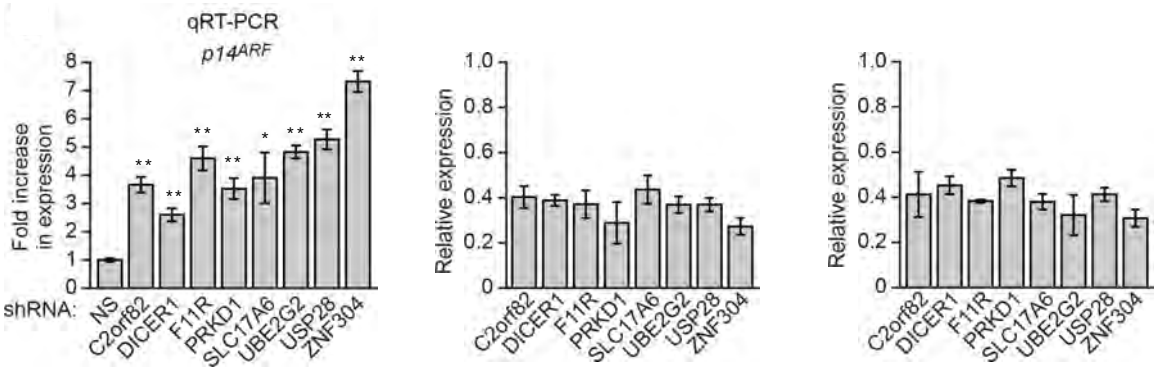

Figure 3-7. Candidate repressor knockdown efficiencies and validation using a second unrelated shRNA.

[Left] qRT-PCR analysis of $p14^{ARF}$ mRNA expression in DLD-1 cells stably infected with either a NS or one of eight unrelated shRNAs for candidates identified in the RNAi screen. Data was normalized to a NS control.

[Middle] Analysis of target gene expression in the primary DLD-1 KD cell lines. Quantitative real-time RT-PCR was used to analyze target gene expression in each of the KD cell lines used in Figures 3-5 and 3-6. All values are normalized to a NS control.

[Right] Analysis of target gene expression in the secondary DLD-1 KD cell lines. Quantitative real-time RT-PCR was used to analyze target gene expression in each of the KD cell lines used Figure 3-7 [Middle]. All values are normalized to a NS control. Data were collected from experiments performed in at least triplicate, and expressed as mean ± standard deviation. Differences between groups were assayed using two-tailed student *t*-test using Excel [Microsoft]. Significant differences were considered when $P < 0.05$. n.s., not significant [$P > 0.05$]; *$P \leq 0.05$ and **$P \leq 0.01$ indicate statistical significance.

KRAB domain proteins function by recruiting a co-repressor complex that includes the scaffolding protein KAP1 and histone methyltransferase SETDB1 [Bellefroid, 1991, Friedman, 1996, Margolin, 1994, Urrutia, 2003, Witzgall, 1994]. Knockdown of KAP1 or SETDB1 resulted in de-repression of $p14^{ARF}$ [Figure 3-8]. $p14^{ARF}$ was also significantly de-repressed following knockdown of DNMT1 but the effect was less in the knockdown of the other DNA methyltransferases, DNMT3A and DNMT3B [Figure 3-8]. The identification of KAP1, SETDB1 and DNMT1 as ZN304 cofactors indicates that my shRNA screen, like other large-scale shRNA screens [see, for example, Mullenders, 2009] was not saturating.

qRT-PCR analysis confirmed that each co-repressor shRNA efficiently knocked down target gene expression [Figure 3-9]. Furthermore, for all genes, a second shRNA whose sequence was unrelated to that used in Figure 3-8 also resulted in target gene knockdown and de-repression of endogenous $p14^{ARF}$, $p15^{INK4B}$ and $p16^{INK4A}$ [Figure 3-9]. Therefore I believe ZNF304, KAP1, SETDB1 and DNMT1 contribute to the silencing of the *INK4-ARF* locus in DLD-1 cells.

The chromatin immunoprecipitation [ChIP] assay of Figure 3-10 shows that ZNF304 as well as KAP1, SETDB1 and DNMT1 were bound to the promoters of the *INK4-ARF* locus in DLD-1 cells. Knockdown of ZNF304 resulted in decreased binding of KAP1, SETDB1 and DNMT1. Taken together I believe ZNF304 is the

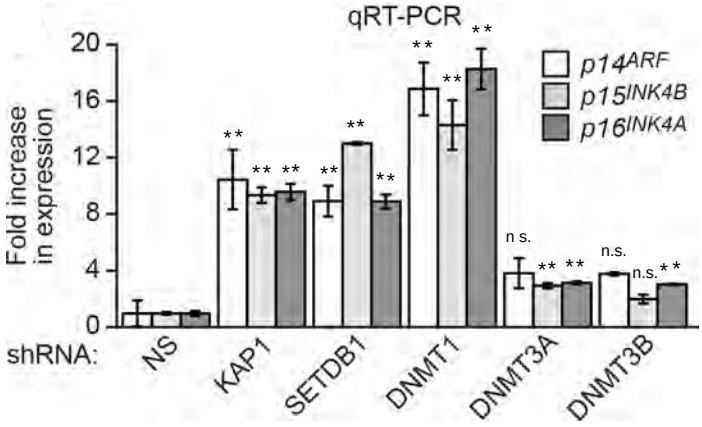

Figure 3-8. qRT-PCR analysis of *INK4-ARF* locus mRNA expression in DLD-1 cells stably infected with either a NS or candidate co-repressor shRNA. Data was normalized to a NS control. Data were collected from experiments performed in at least triplicate, and expressed as mean ± standard deviation. Differences between groups were assayed using two-tailed student *t*-test using Excel [Microsoft]. Significant differences were considered when $P < 0.05$. n.s., not significant [$P > 0.05$]; *$P \leq 0.05$ and **$P \leq 0.01$ indicate statistical significance.

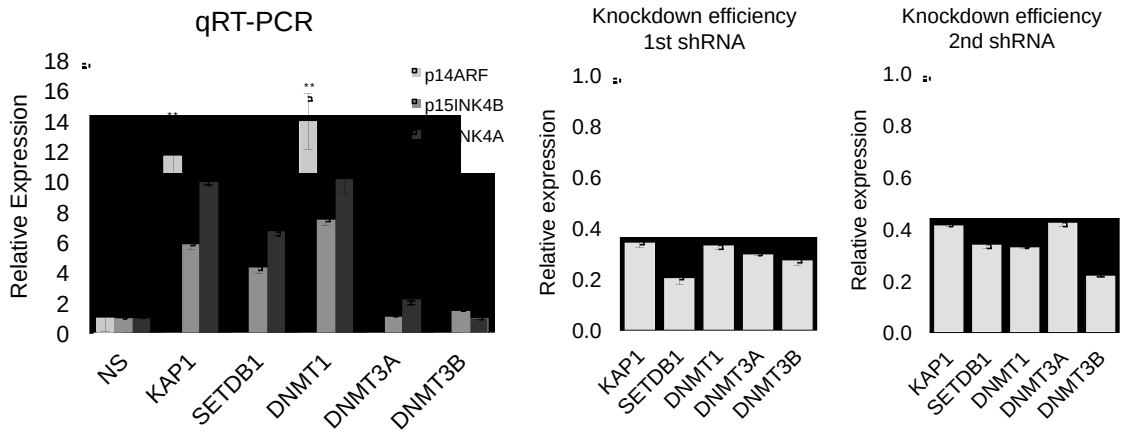

Figure 3-9. Co-repressor knockdown efficiencies and validation using a second unrelated shRNA.

[Left] qRT-PCR analysis of $p14^{ARF}$, $p15^{INK4B}$ and $p16^{INK4A}$ mRNA expression in DLD-1 cells stably infected with either a NS or one of five unrelated shRNAs for candidate co-repressors of ZNF304. Data was normalized to a NS control.

[Middle] Analysis of target gene expression in the primary DLD-1 KD cell lines. Quantitative real-time RT-PCR was used to analyze target gene expression in each of the KD cell lines used in Figures 3-8 and 3-11. All values are normalized to a NS control.

[Right] Analysis of target gene expression in the secondary DLD-1 KD cell lines. Quantitative real-time RT-PCR was used to analyze target gene expression in each of the KD cell lines used Figure 3-9 [Middle]. All values are normalized to a NS control.

Data were collected from experiments performed in at least triplicate, and expressed as mean ± standard deviation. Differences between groups were assayed using two-tailed student *t*-test using Excel [Microsoft]. Significant differences were considered when $P < 0.05$. n.s., not significant [$P > 0.05$]; *$P \leq 0.05$ and **$P \leq 0.01$ indicate statistical significance.

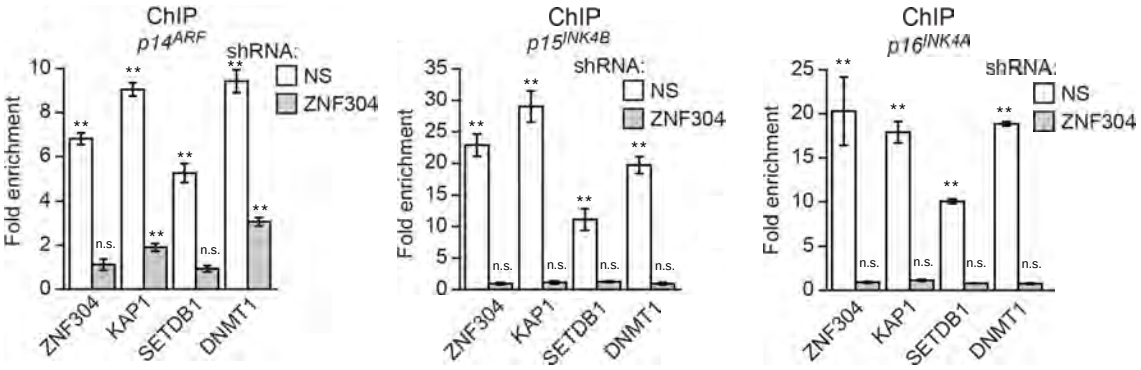

Figure 3-10. ChIP analysis of the *p14*^{ARF} [left], *p15*^{INK4B} [middle] and *p16*^{INK4A} [right] promoters was performed on chromatin extracts from DLD-1 cells stably infected with either a NS or ZNF304 shRNA. Data was normalized to a control IgG immunoprecipitation. Data were collected from experiments performed in at least triplicate, and expressed as mean ± standard deviation. Differences between groups were assayed using two-tailed student *t*-test using Excel [Microsoft]. Significant differences were considered when $P < 0.05$. n.s., not significant [$P > 0.05$]; *$P \leq 0.05$ and **$P \leq 0.01$ indicate statistical significance.

specificity determinant for the KRAB co-repressor complex and its subsequent epigenetic silencing function.

Bisulfite sequence analysis showed that shRNA-mediated knockdown of ZNF304, KAP1, SETDB1 or DNMT1 resulted in decreased *p14*^{ARF} DNA hypermethylation [Figure 3-11]. Collectively, these results indicate that following binding to the *p14*^{ARF} promoter ZNF304 recruits the KRAB co-repressor complex and DNMT1, which is responsible for DNA hypermethylation and epigenetic silencing of the *INK4-ARF* locus.

Our lab's previous findings revealed that epigenetic silencing of tumor suppressors is often initiated and maintained by oncogenic signaling. DLD-1 cells contain an activated KRAS allele and I next investigated the relationship between KRAS and silencing of the *INK4-ARF* locus. shRNA-mediated knockdown of KRAS in DLD-1 [Figure 3-13] cells resulted in depression of the *INK4-ARF* locus [Figure 3-12] and substantially reduced binding of ZNF304 and its co-repressors on the *INK4-ARF* promoters [Figure 3-14]. Binding of ZNF304 and its cofactors was comparably reduced following treatment with Manumycin A, a farnesyltransferase inhibitor that antagonizes RAS localization and function [Figure 3-14]. As expected treatment with Manumycin A also causes a robust loss of hypermethylation of the *p14*^{ARF} promoter region as determined by bisulfite

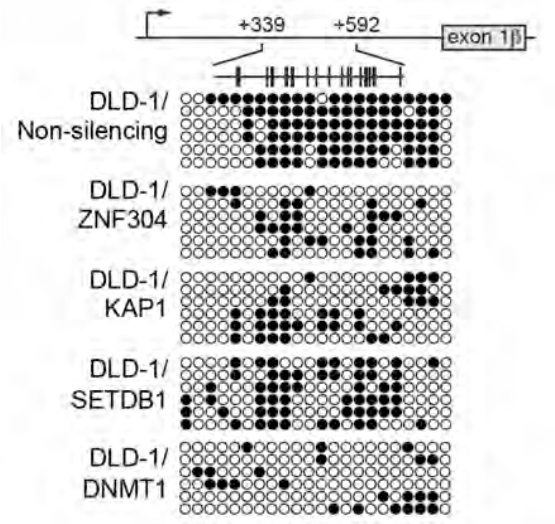

Figure 3-11. Bisulfite Sequencing of *p14*^{ARF} promoter region using bisulfite converted genomic DNA from DLD-1 cells stably infected with indicated shRNAs. Each line represents an independent sequencing clone.

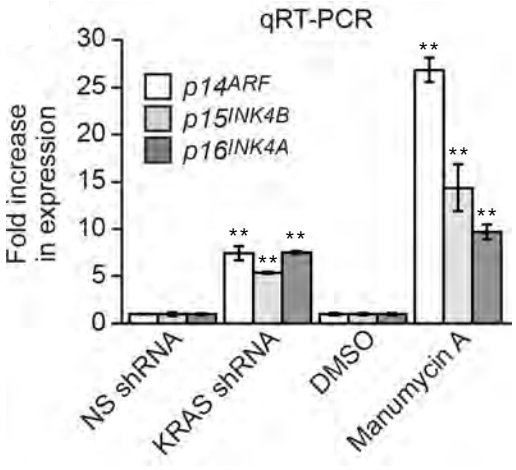

Figure 3-12. qRT-PCR analysis of $p14^{ARF}$, $p15^{INK4B}$ and $p16^{INK4A}$ mRNA expression using DLD-1 cells stably infected with NS or KRAS shRNAs or DLD-1 cells treated with DMSO or 10 μM Manumycin A for 24 hours. Data was normalized to NS and DMSO controls, respectively. Data were collected from experiments performed in at least triplicate, and expressed as mean ± standard deviation. Differences between groups were assayed using two-tailed student *t*-test using Excel [Microsoft]. Significant differences were considered when $P < 0.05$. NS, not significant [$P > 0.05$]; *$P \leq 0.05$ and **$P \leq 0.01$ indicate statistical significance.

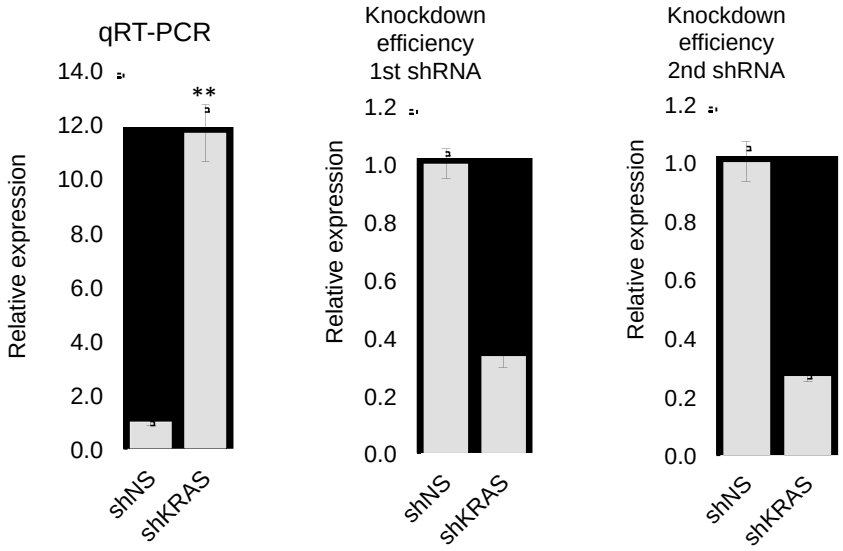

Figure 3-13. KRAS knockdown efficiency and validation using a second unrelated shRNA.

[Left] qRT-PCR analysis of $p14^{ARF}$ mRNA expression in DLD-1 cells stably infected with either an unrelated NS or KRAS from Figure 3-12. Data was normalized to a NS control.

[Middle] Analysis of KRAS gene expression in the primary DLD-1 KRAS KD cell line. Quantitative real-time RT-PCR was used to analyze KRAS gene expression in the KD cell lines used Figure 3-12. All values are normalized to a NS control.

[Right] Analysis of KRAS gene expression in the secondary DLD-1 KRAS KD cell line. Quantitative real-time RT-PCR was used to analyze KRAS gene expression in the KD cell lines used Figure 3-13 [right]. All values are normalized to a NS control.

Data were collected from experiments performed in at least triplicate, and expressed as mean ± standard deviation. Differences between groups were assayed using two-tailed student *t*-test using Excel [Microsoft]. Significant differences were considered when $P < 0.05$. n.s., not significant [$P > 0.05$]; *$P \leq 0.05$ and **$P \leq 0.01$ indicate statistical significance.

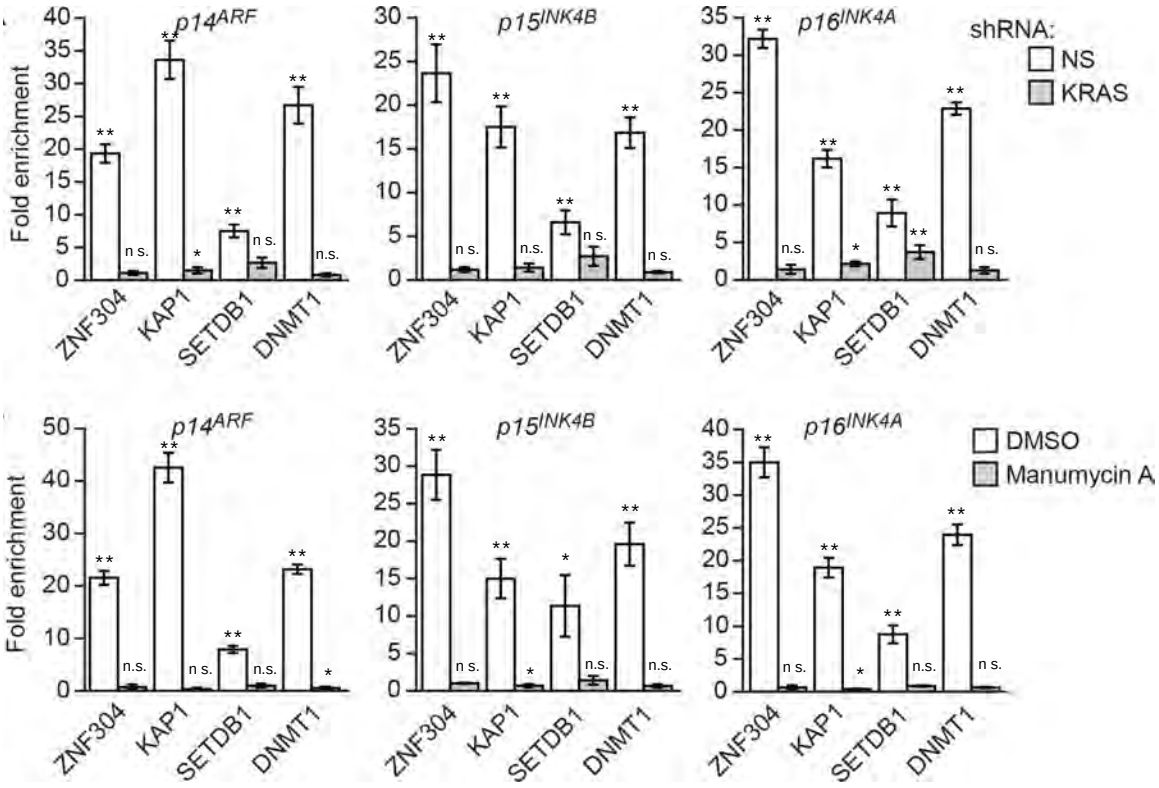

Figure 3-14. ChIP analysis of the *p14*^{ARF}, *p15*^{INK4B} and *p16*^{INK4A} promoters performed using chromatin extracts from DLD-1 cells stably infected with either NS or KRAS shRNA [Top] or DMSO or Manumycin A [Bottom]. Data was normalized to control IgG immunoprecipitation for each set of conditions. Data were collected from experiments performed in at least triplicate, and expressed as mean ± standard deviation. Differences between groups were assayed using two-tailed student *t*-test using Excel [Microsoft]. Significant differences were considered when $P < 0.05$. NS, not significant [$P > 0.05$]; *$P \leq 0.05$ and **$P \leq 0.01$ indicate statistical significance.

sequencing [Figure 3-15] and subsequent re-expression of the *INK4-ARF* locus [Figure 3-12].

To determine the generality and clinical relevance of these results I analyzed additional CRC cell lines and human patient-derived tumor samples that contained activated KRAS mutations. ChIP analysis shows that in HCT116 and HCT15 cells, two other KRAS-positive CRC cell lines in which the *INK4-ARF* locus is epigenetically silenced [Figure 3-16], ZNF304 was associated with the *INK4-ARF* promoters [Figure 3-17] and shRNA-mediated knockdown of ZNF304 or KRAS or Manumycin A treatment derepressed $p14^{ARF}$, $p15^{INK4B}$ and $p16^{INK4A}$ mRNA expression [Figure 3-18].

I next performed immunohistochemistry to measure ZNF304 levels in 68 KRAS-positive CRC human tumor samples. I found that in ~90% of these KRAS-positive CRCs, ZNF304 was over-expressed relative to normal colon [Figure 3-19 and Table 3-2]. I also used a pathology tissue ChIP [PAT-ChIP] assay to measure association of ZNF304 with the $p14^{ARF}$, $p15^{INK4B}$ and $p16^{INK4A}$ promoters in KRAS-positive CRC human tumor samples compared to adjacent normal colonic tissue. Figure 3-20 shows that ZNF304 was substantially enriched at the $p14^{ARF}$, $p15^{INK4B}$ and $p16^{INK4A}$ promoters in the KRAS-positive CRCs. I then sought to confirm hypermethylation of the $p14^{ARF}$ promoter in these patient

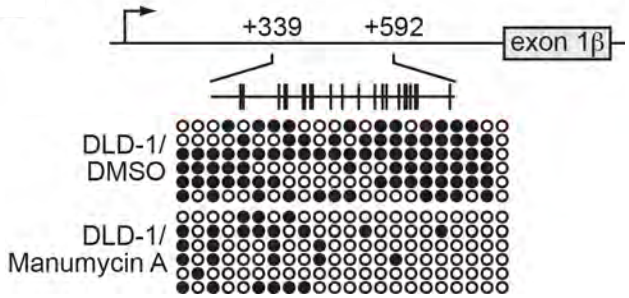

Figure 3-15. Bisulfite Sequencing of the *p14*^{ARF} promoter region using bisulfite converted genomic DNA from DLD-1 cells treated with DMSO or 10 μM Manumycin A for 24 hours. Each line represents and independent sequencing clone.

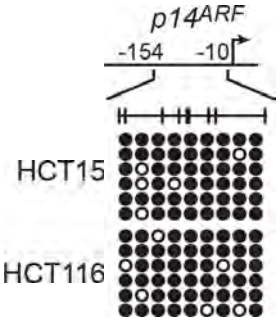

Figure 3-16. Bisulfite Sequencing of the *p14*^{ARF} promoter region using bisulfite converted genomic DNA from either HCT116 or HCT15 cells. Each line represents and independent sequencing clone.

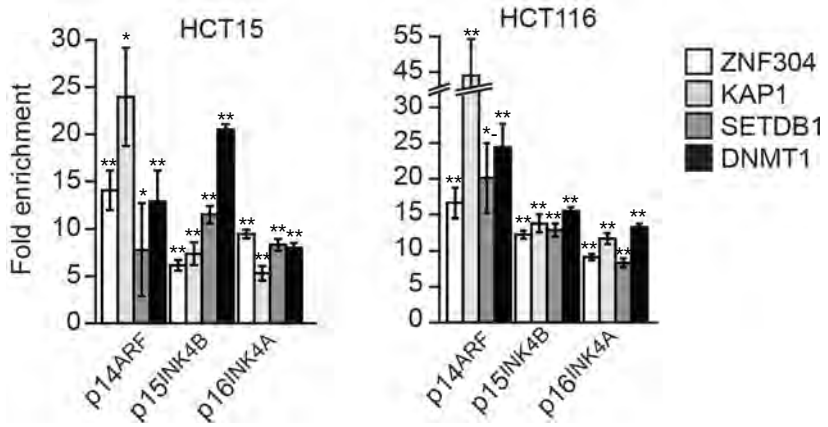

Figure 3-17. ChIP analysis of the *p14*^{ARF}, *p15*^{INK4B} and *p16*^{INK4A} promoter regions in HCT116 and HCT15 chromatin extracts. Data were collected from experiments performed in at least triplicate, and expressed as mean ± standard deviation. Differences between groups were assayed using two-tailed student *t*-test using Excel [Microsoft]. Significant differences were considered when $P < 0.05$. NS, not significant [$P > 0.05$]; *$P \leq 0.05$ and **$P \leq 0.01$ indicate statistical significance.

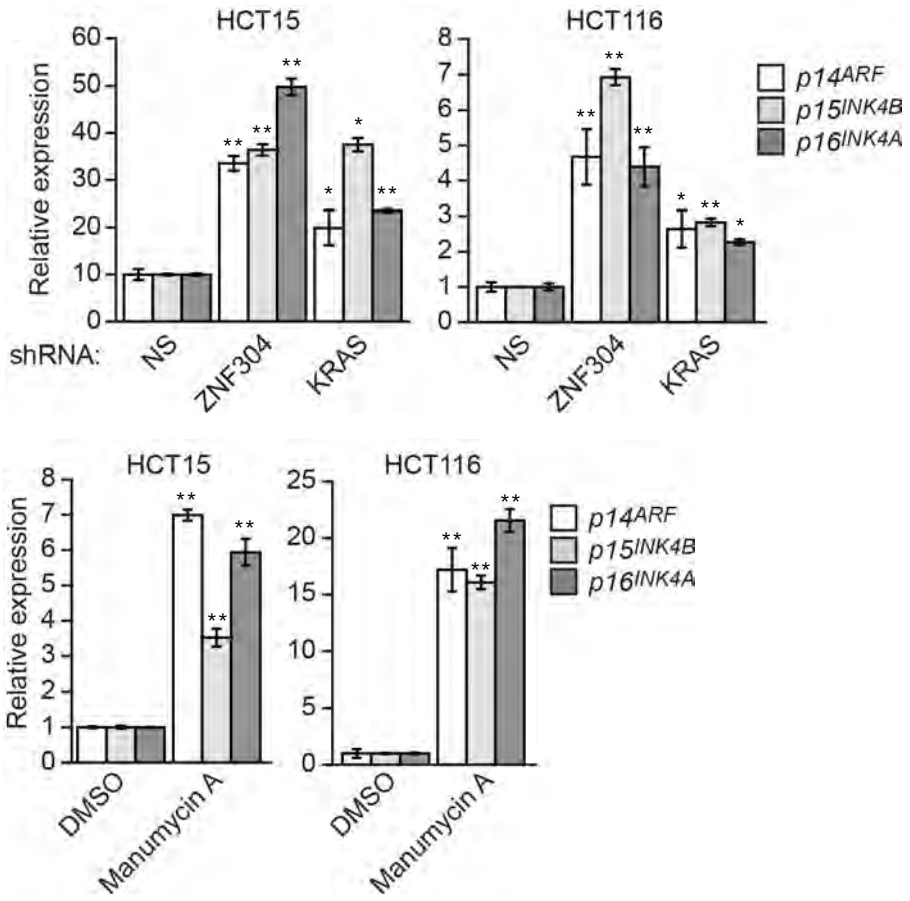

Figure 3-18. *INK4-ARF* mRNA Expression upon KRAS inhibition.
[Top] qRT-PCR analysis of $p14^{ARF}$, $p15^{INK4B}$ and $p16^{INK4A}$ mRNA expression in HCT116 and HCT15 cells that have been stably infected with NS, ZNF304 and KRAS shRNAs.

[Bottom] qRT-PCR analysis of $p14^{ARF}$, $p15^{INK4B}$ and $p16^{INK4A}$ mRNA expression in HCT116 and HCT15 cells that have been treated with either DMSO or 10 μM Manumycin A for 24 hours.

Data were collected from experiments performed in at least triplicate, and expressed as mean ± standard deviation. Differences between groups were assayed using two-tailed student *t*-test using Excel [Microsoft]. Significant differences were considered when $P < 0.05$. NS, not significant [$P > 0.05$]; *$P \leq 0.05$ and **$P \leq 0.01$ indicate statistical significance.

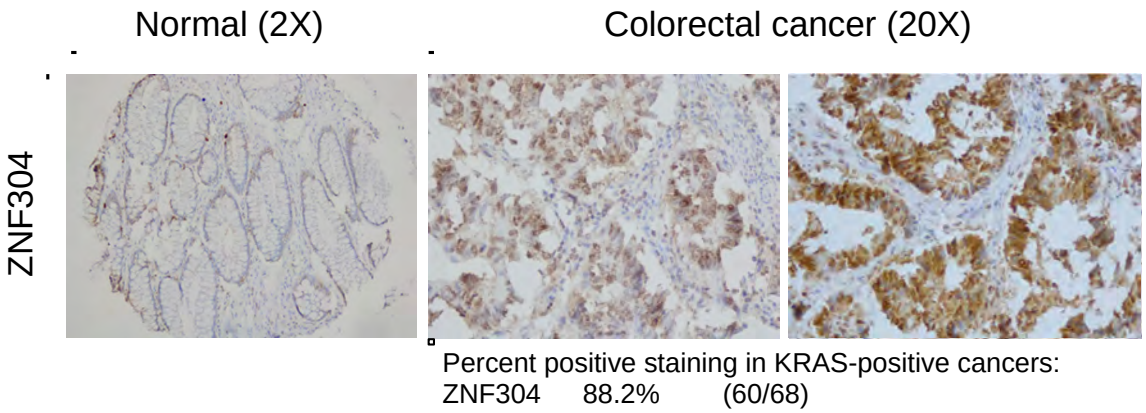

Figure 3-19. Immunohistochemistry staining for ZNF304 expression in normal tissue and KRAS-positive colorectal adenocarcinoma samples. Table below shows quantitation of KRAS-positive cohort.

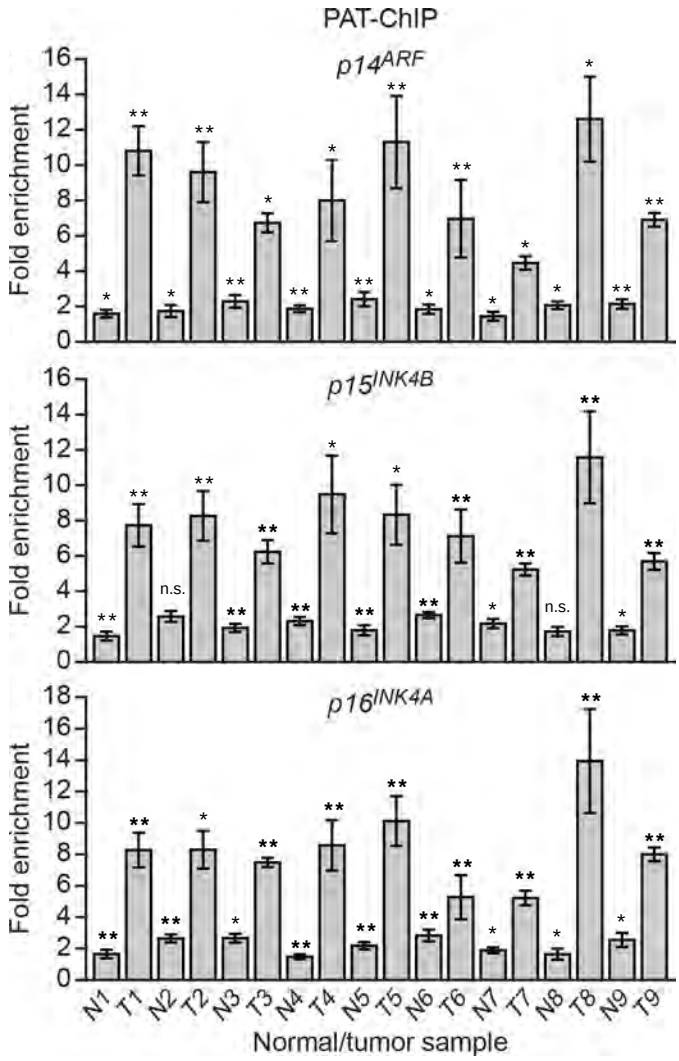

Figure 3-20. PAT-ChIP analysis of the *p14*^{ARF}, *p15*^{INK4B} and *p16*^{INK4A} promoters using ZNF304 in matched patient-derived normal adjacent and KRAS-positive colorectal adenocarcinoma tissue samples chromatin preps. Bars represent ZNF304 enrichment at the indicated target promoter after normalization to a IgG control immunoprecipitation. Data were collected from experiments performed in at least triplicate, and expressed as mean ± standard deviation. Differences between groups were assayed using two-tailed student *t*-test using Excel [Microsoft]. Significant differences were considered when $P < 0.05$. NS, not significant [$P > 0.05$]; *$P \leq 0.05$ and **$P \leq 0.01$ indicate statistical significance.

derived tissues. I confirmed that the *p14*^{ARF} promoter was in fact hypermethylated in the tumor tissue compared to the matched normal control tissue [Figure 3-21].

Notably, shRNA-mediated knockdown or pharmacological inhibition of KRAS markedly reduced ZNF304 protein levels [Figure 3-22], whereas ZNF304 mRNA was relatively unaffected [Figure 3-23]. Thus, activated KRAS post-transcriptionally upregulates ZNF304 expression. Consistent with this idea, the reduction of ZNF304 protein levels following KRAS inhibition can be counteracted by proteasome inhibitions [Figure 3-24].

USP28, a nuclear localized de-ubiquitinase, was another candidate isolated in the primary RNAi screen for *p14*^{ARF} repressors. I asked whether USP28 was responsible for KRAS-mediated stabilization of ZNF304. Similar to the results with KRAS, knockdown of USP28 substantially reduced ZNF304 protein [Figure 3-25] but not mRNA [Figure 3-26] levels. The co-immunoprecipitation experiments of Figure 3-27 shows that USP28 and ZNF304 physically interact. Moreover, co-transfection of wildtype USP28, but not a catalytically inactive USP28^{C171A} mutant, reduced ubiquitination of ZNF304 [Figures 3-28]. Therefore I believe USP28 antagonizes the ubiquitin-mediated degradation of ZNF304 and thus contributes to epigenetic silencing of the *INK4-ARF* locus.

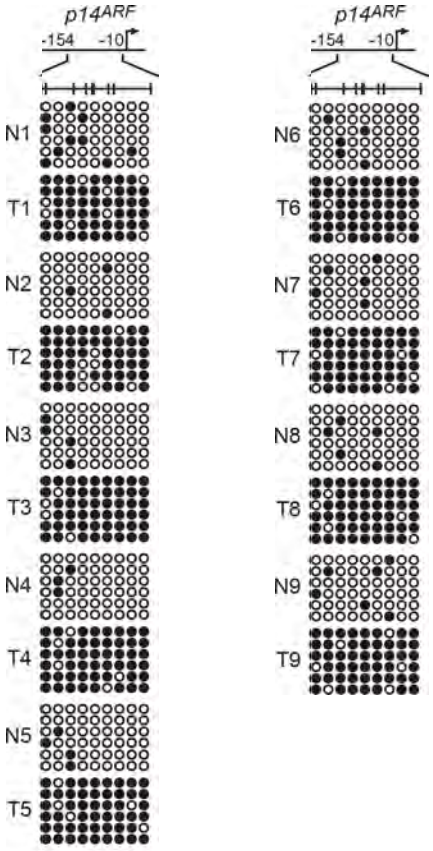

Figure 3-21. Bisulfite sequencing analysis of the *p14*^{ARF} promoter region. Genomic DNA derived from patient-derived matched adjacent normal colonic tissue and KRAS-positive colorectal cancer was analyzed by bisulfite sequencing analysis.

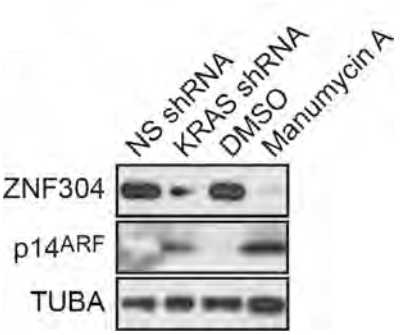

Figure 3-22. Immunoblot analysis of DLD-1 cells stably infected with either NS or KRAS shRNA or treated with DMSO or 10 μM Manumycin A for 24 hours. Tubulin was used as a loading control.

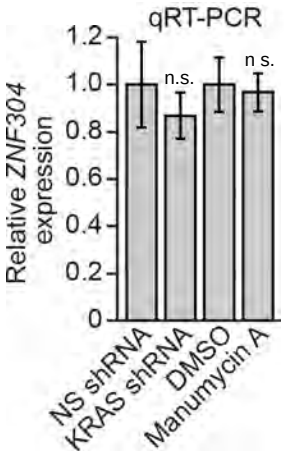

Figure 3-23. qRT-PCR analysis of $p14^{ARF}$ and ZNF304 mRNA expression in DLD-1 cells stably infected with either NS or KRAS shRNA or treated with DMSO or 10 μM Manumycin A for 24 hours. Data was normalized to a NS or DMSO control respectively. Data were collected from experiments performed in at least triplicate, and expressed as mean ± standard deviation. Differences between groups were assayed using two-tailed student *t*-test using Excel [Microsoft]. Significant differences were considered when $P < 0.05$. NS, not significant [$P > 0.05$]; *$P \leq 0.05$ and **$P \leq 0.01$ indicate statistical significance.

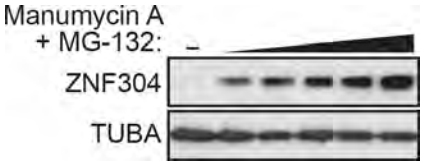

Figure 3-24. Immunoblot analysis of ZNF304 expression in DLD-1 cells that have been treated with 10 μM Manumycin A for 24 hours then subsequently treated with 0, 2, 4, 6, 8, 10 μM MG-132 for 4 hours. Tubulin was used as a loading control.

Figure 3-25. Immunoblot analysis of DLD-1 cells stably infected with NS or USP28 shRNA. Tubulin was used as a loading control.

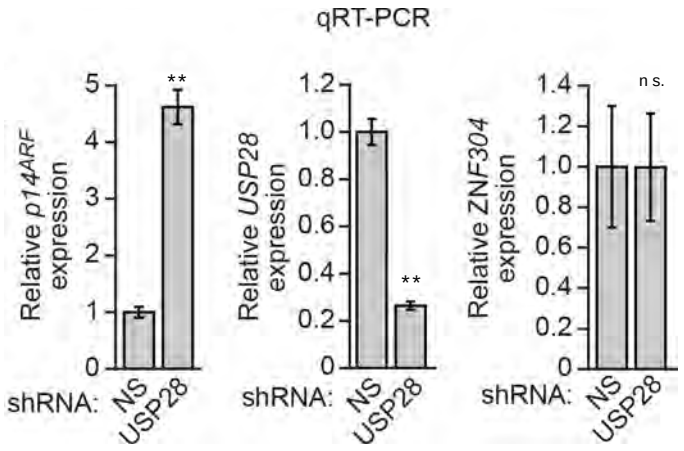

Figure 3-26. qRT-PCR analysis of $p14^{ARF}$, USP28 and ZNF304 mRNA expression in DLD-1 cells stably infected with NS or USP28 shRNA. Data was normalized to a NS control. Data were collected from experiments performed in at least triplicate, and expressed as mean ± standard deviation. Differences between groups were assayed using two-tailed student *t*-test using Excel [Microsoft]. Significant differences were considered when $P < 0.05$. NS, not significant [$P > 0.05$]; *$P \leq 0.05$ and **$P \leq 0.01$ indicate statistical significance.

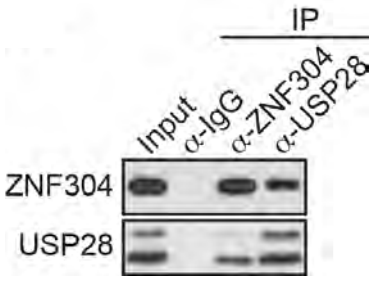

Figure 3-27. Co-immunoprecipitation analysis of ZNF304 and USP28 interactions performed using DLD-1 cell lysate.

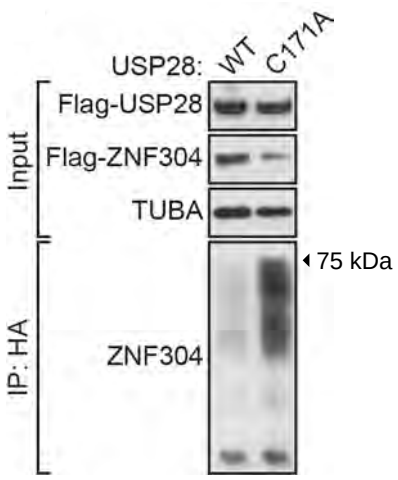

Figure 3-28. Ubiquitination of ZNF304 is antagonized by USP28. 293T were transfected with HA-Ubiquitin, Flag-ZNF304 and either Flag-USP28 or Flag-USP28^{C171A} for 48 hours and cell lysates were prepared. Ubiquitinated ZNF304 was pulled down using anti-HA beads. In the mutant USP28 lane, ubiquitinated ZNF304 is present and appears as a smear below full-length ZNF304 [<75 kDa]. Tubulin was used as a loading control.

Notably, knockdown or pharmacological inhibition of KRAS led to reduced levels of USP28 protein and mRNA [Figure 3-29 and Figure 3-30]. These results suggest that KRAS signaling up-regulates expression of USP28, which in turn stabilizes ZNF304. Analogous to my studies of ZNF304 expression in patient samples I performed IHC analysis on 256 KRAS-positive CRCs and found elevated USP28 expression in ~28% compared to normal tissue control [Figure 3-31]. Taken together, I believe KRAS antagonizes ZNF304 proteasomal degradation by up-regulating USP28 expression both in KRAS-positive cell lines and in patient samples.

Previous studies have shown that deubiquitinase-substrate interactions are regulated by phosphorylation [Kessler and Edelman, 2011]. PRKD1, another candidate isolated in the primary RNAi screen for $p14^{ARF}$ repressors, is a serine/threonine kinase that is deregulated in a variety of cancers [Eiseler et al. 2009]. I noticed that USP28 contains a putative PRKD1 phosphorylation site [LxxRxS/T] [Nishikawa et al., 1997] and analyzed the role of PRKD1 in RAS-mediated stabilization of ZNF304. Figure 3-32 shows that shRNA-mediated knockdown of PRKD1 resulted in decreased ZNF304 protein levels, whereas ZNF304 mRNA levels were relatively unaffected [Figure 3-33]. Furthermore, treatment of DLD-1 cells with a PRKD1 chemical inhibitor, CRT0066101, also resulted in decreased ZNF304 protein levels as well as derepression of $p14^{ARF}$, $p15^{INK4B}$ and $p16^{INK4A}$ [Figure 3-34].

Figure 3-29. Immunoblot analysis of USP28 expression in DLD-1 cells stably infected with NS or KRAS shRNA or treated with DMSO or 10 µM Manumycin A for 24 hours. Tubulin was used as a loading control.

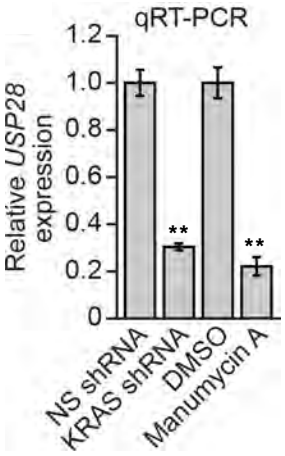

Figure 3-30. qRT-PCR analysis of USP28 mRNA expression in DLD-1 cells stably infected with NS or KRAS shRNA or treated with DMSO or 10 μM Manumycin A for 24 hours. Data was normalized to a NS or DMSO control, respectively. Data were collected from experiments performed in at least triplicate, and expressed as mean ± standard deviation. Differences between groups were assayed using two-tailed student *t*-test using Excel [Microsoft]. Significant differences were considered when $P < 0.05$. NS, not significant [$P > 0.05$]; *$P \leq 0.05$ and **$P \leq 0.01$ indicate statistical significance.

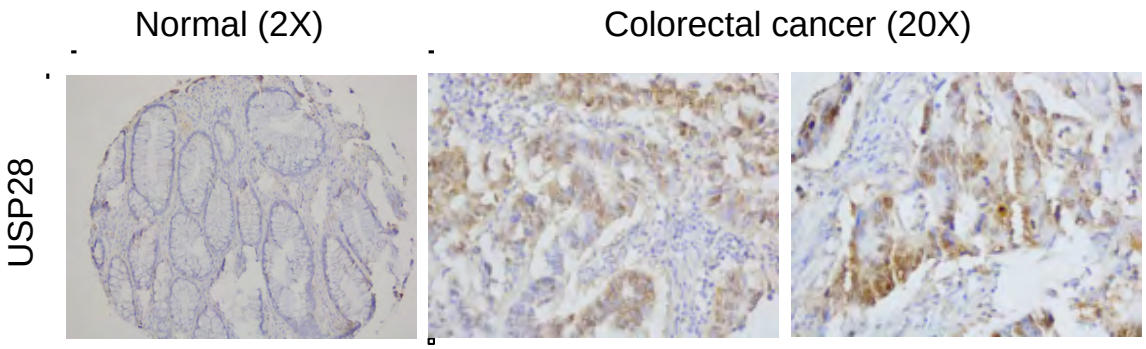

Percent positive staining in KRAS-positive cancers:

USP28	28.1%	(72/256)

Figure 3-31. Immunohistochemistry staining of USP28 was performed on normal adjacent colonic tissue and KRAS-positive colorectal adenocarcinoma. The table below quantitates the positive staining for the colorectal cancer samples.

Figure 3-32. Immunoblot analysis of DLD-1 cells stably infected with NS or PRKD1 shRNA. Tubulin was used as a loading control.

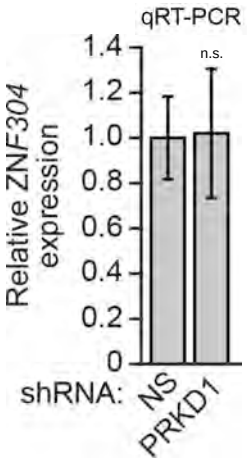

Figure 3-33. qRT-PCR analysis of ZNF304 mRNA expression in DLD-1 cells stably infected with either NS or PRKD1 shRNA. Data was normalized to a NS control. Data were collected from experiments performed in at least triplicate, and expressed as mean ± standard deviation. Differences between groups were assayed using two-tailed student *t*-test using Excel [Microsoft]. Significant differences were considered when $P < 0.05$. NS, not significant [$P > 0.05$]; *$P \leq 0.05$ and **$P \leq 0.01$ indicate statistical significance.

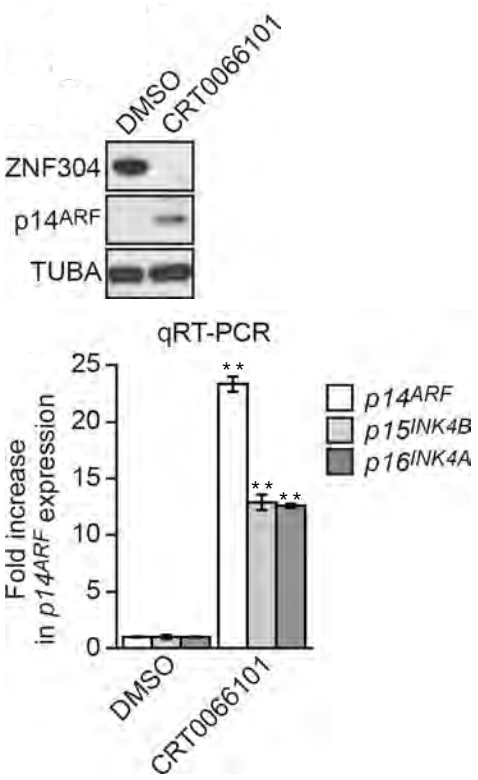

Figure 3-34. [Top] Immunoblot analysis of DLD-1 cells treated with DMSO or 10 µM CRT0066101 for 24 hours. Tubulin was used as a loading control.

[Bottom] qRT-PCR analysis of $p14^{ARF}$, $p15^{INK4B}$ and $p16^{INK4A}$ mRNA expression in DLD-1 cells treated with DMSO or 10 µM CRT0066101 for 24 hours. Data was normalized to a DMSO control. Data were collected from experiments performed in at least triplicate, and expressed as mean ± standard deviation. Differences between groups were assayed using two-tailed student *t*-test using Excel [Microsoft]. Significant differences were considered when $P < 0.05$. NS, not significant [$P > 0.05$]; *$P \leq 0.05$ and **$P \leq 0.01$ indicate statistical significance.

Due to dramatic re-expression of the *INK4-ARF* locus upon treatment with CRT0066101, we sought to determine whether the KRAB co-repressor complex was present at the *INK4-ARF* promoters under these conditions. Figure 3-35 displays a marked loss of co-repressor binding to the *INK4-ARF* promoters in DLD-1 cells treated with CRT0066101. Furthermore we obtained a similar result as USP28 following knockdown or pharmacological inhibition of KRAS [Figures 3-29 and 3-30]. Figures 3-36 and 3-37 show decreased PRKD1 protein and mRNA levels when RAS is inhibited suggesting that RAS signaling is responsible for PRKD1expression.

I next asked whether USP28 is a substrate of PRKD1, given the phenocopying we find with USP28 and PRKD1 KDs and the presence of two putative PRKD1 phosphorylation sites within the protein. Consistent with this hypothesis, I found that USP28 and PRKD1 were stably associated in a co-immunoprecipitation assay [Figure 3-38]. I next performed an *in vitro* kinase assay with purified PRKD1 capable of autophosphorylation at Serine 916, a hallmark of PRKD1 activity [Rybin et al 2009] [Figure 3-39]. Figure 3-40 shows that PRKD1 could phosphorylate a peptide containing the predicted USP28 phosphorylation site located at serine residue 899 but not other predicted sites in USP28. Notably, unlike wild type USP28, a USP28 derivative containing a mutation in the PRKD1 phosphorylation site, $USP28^{S899A}$, mutant was less capable at reducing ZNF304 ubiquitination [Figure 3-41]. Importantly, this effect is lower than what is seen

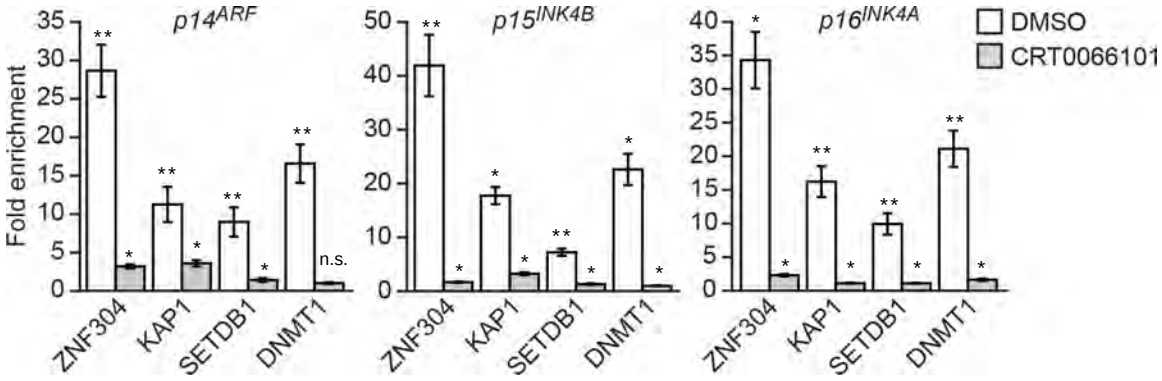

Figure 3-35. ChIP analysis of the *p14*^{ARF}, *p15*^{INK4B} and *p16*^{INK4A} promoters performed using chromatin extracts from DLD-1 cells treated with DMSO or CRT0066101. Data was normalized to a control IgG immunoprecipitation under each set of conditions. Data were collected from experiments performed in at least triplicate, and expressed as mean ± standard deviation. Differences between groups were assayed using two-tailed student *t*-test using Excel [Microsoft]. Significant differences were considered when $P < 0.05$. NS, not significant [$P > 0.05$]; *$P \leq 0.05$ and **$P \leq 0.01$ indicate statistical significance.

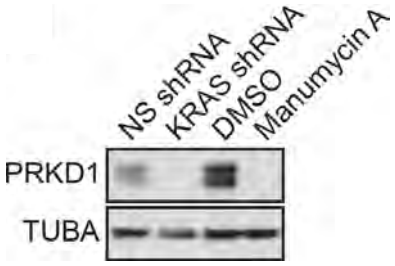

Figure 3-36. Immunoblot analysis PRKD1 expression in DLD-1 cells stably infected with either NS or KRAS shRNA or treated with DMSO or 10 μM Manumycin A for 24 hours. Tubulin was used as a loading control.

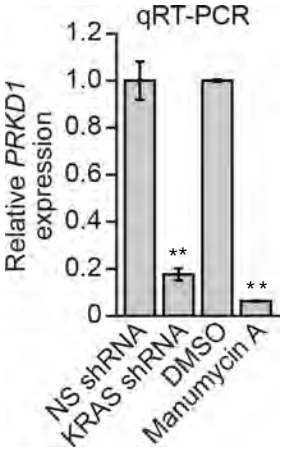

Figure 3-37. qRT-PCR analysis of PRKD1 mRNA expression in DLD-1 cells stably infected with either NS or KRAS shRNA or treated with DMSO or 10 μM Manumycin A for 24 hours. Data was normalized to a NS or DMSO control, respectively. Data were collected from experiments performed in at least triplicate, and expressed as mean ± standard deviation. Differences between groups were assayed using two-tailed student *t*-test using Excel [Microsoft]. Significant differences were considered when $P < 0.05$. NS, not significant [$P > 0.05$]; *$P \leq 0.05$ and **$P \leq 0.01$ indicate statistical significance.

Figure 3-38. Co-Immunoprecipitation analysis of USP28 and PRKD1 interaction performed on DLD-1 cell lysate.

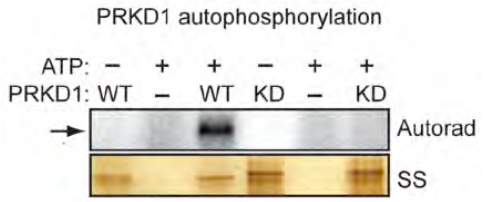

Figure 3-39. Purified wildtype and kinase dead versions of PRKD1 were incubated with radioactive ATP. Only the wildtype version was capable of auto-phosphorylation, indicative of kinase activity in PRKD1. The bottom image is silver stained to show the abundance of each protein.

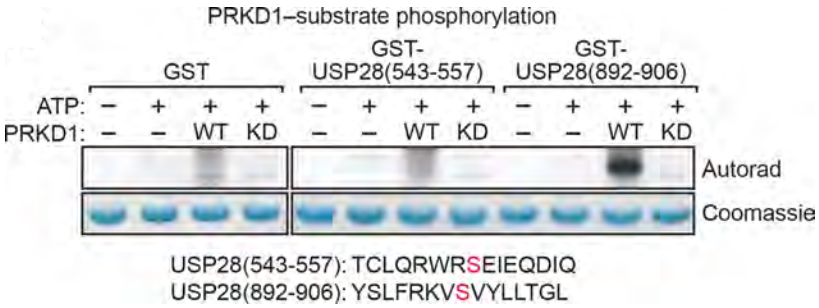

Figure 3-40. Peptides corresponding to the indicated potential PRKD1 phosphorylation residues were incubated with purified wildtype and kinase dead versions of PRKD1. Only the serine residue at position 899 in USP28 was actively phosphorylated by PRKD1 indicated by the signal present in the second to last lane. The bottom row is coomassie stained to show the relative abundance of the peptide.

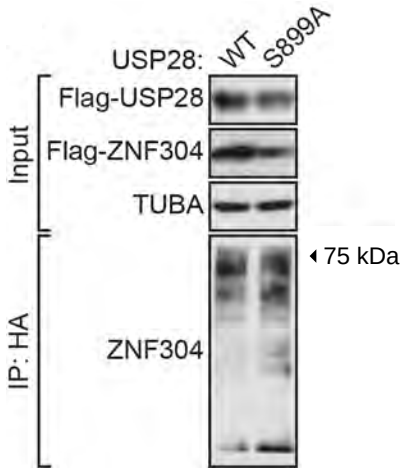

Figure 3-41. Ubiquitination of ZNF304 is antagonized by USP28 and PRKD1-mediated phosphorylation modulates this activity. 293T were transfected with HA-Ubiquitin, Flag-ZNF304 and either Flag-USP28 or Flag-USP28^{S899A} for 48 hours and cell lysates were prepared. Ubiquitinated ZNF304 was pulled down using anti-HA beads. In the mutant USP28 lane, ubiquitinated ZNF304 is present and appears as a smear below full-length ZNF304 [<75 kDa]. Tubulin was used as a loading control.

with the catalytic-inactive form of USP28 [Figure 3-28]. Therefore PRKD1-mediated phosphorylation of USP28 Ser899 may contribute to USP28-mediated stabilization of ZNF304 but may not be the only contributing regulator of this event.

Kinases present a potentially druggable target and I sought to investigate PRKD1 inhibition as a viable therapeutic avenue for reversing *INK4-ARF* hypermethylation and causing a loss of cell viability. I used a small molecule inhibitor of the protein kinase D family, CRT0066101, in DLD-1 and other cell lines. In DLD-1 cells treated with increasing amounts of CRT0066101 for 4 hours, I see a marked reduction in DNMT1, SETDB1, KAP1, USP28, ZNF304, PRKD1 protein levels and a coordinate increase in $p14^{ARF}$ [Figure 3-42]. Importantly there is significant decrease in $PRKD1^{Ser916}$ auto-phosphorylation at 1uM CRT0066101 indicating there is effective inhibition of PRKD1 enzymatic activity. Furthermore there is an abundance of lower molecular weight bands for the USP28, ZNF304 and PRKD1, which I believe to be degradation products. Therefore, I believe CRT0066101 to effectively inhibit PRKD1 and cause a subsequent down-regulation of the entire KRAB co-repressor complex.

I next treated a panel of cell lines with 8 μM CRT0066101 for 48 hours, then performed the cell viability Alamar Blue assay. Cell lines that harbored both a KRAS and PI_3K mutation were significantly more sensitive compared to PFF cells

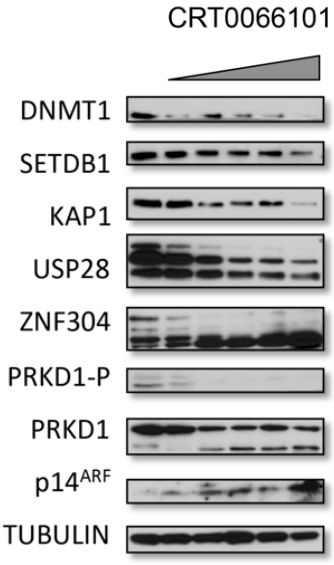

Figure 3-42. Immunoblot analysis of the co-repressor complex expression in DLD-1 cells following treatment with DMSO or 1, 2, 4, 6, and 8 μM CRT0066101 for 24 hours. Tubulin was used as a loading control.

or singly mutated counterparts [Figure 3-43]. Despite its moderate toxicity in PFF cells, CRT0066101 represents a potential therapy for KRAS and PI_3K positive colorectal cancers. Perhaps future improvements in the chemistry of the molecule will yield a version that is less toxic to normal cells while retaining its potent growth inhibitory effect on tumor cells.

As stated previously, aberrant silencing of the *INK4-ARF* locus occurs frequently in cancers. In fact, in colon cancer there exists well-described epigenotypes termed CpG Island Methylator Phenotypes, CIMPs [Yagi et al. 2009]. These CIMP profiles termed CIMP-High and CIMP-low are distinguished from one another based on the hypermethylation and epigenetic silencing of characteristic marker genes that include $p14^{ARF}$ and $p16^{INK4A}$ hypermethylation. Many of the CIMP marker genes are known tumor suppressors. In CIMP-High there is essentially hypermethylation of all the marker genes [approximately 60 genes] and in CIMP-Low, the majority of the marker genes [approximately 50 of the 60] are hypermethylated save a select few. The genes methylated in CIMP- Low are termed Group 2 marker genes and the genes methylated only in CIMP-High are termed Group 1 marker genes. These CIMP epigenotypes are also associated with distinct oncogeneotypes. CIMP-High is associated with BRAF mutation and CIMP-Low with KRAS mutation [Yagi et al. 2010]. The molecular basis of the CIMP subtypes and how they are related to specific oncogenes remains to be determined.

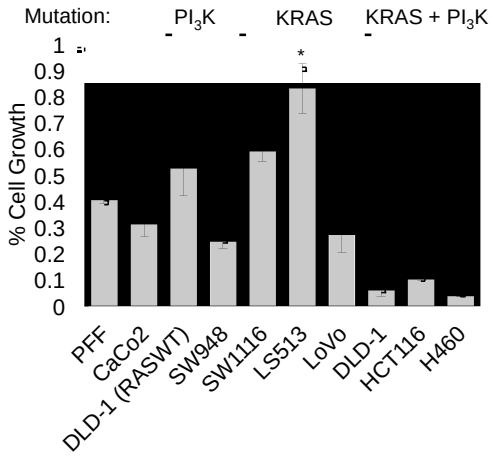

Figure 3-43. Proliferation was measured using the Alamar blue assay for the indicated cell lines following two days of treatment with 8 μM of CRT0066101. Data was normalized to a DMSO control for each cell line. Data were collected from experiments performed in at least triplicate, and expressed as mean ± standard deviation. Differences between groups were assayed using two-tailed student *t*-test using Excel [Microsoft]. Significant differences were considered when $P < 0.05$. NS, not significant [$P > 0.05$]; *$P \leq 0.05$ and **$P \leq 0.01$ indicate statistical significance.

I hypothesized that my ZNF304-KRAB corepressor complex may be responsible for silencing Group 2 CIMP marker genes in KRAS-positive colorectal cancers since $p14^{ARF}$ and $p16^{INK4A}$ are part of this group. I performed KRAS and ZNF304 knockdown experiments in DLD-1 cells then analyzed mRNA expression of the 50 Group 2 CIMP marker genes [See Table 3-2 for gene list]. Strikingly, in every case, knockdown of either KRAS or ZNF304 resulted in a significant increase in gene expression [Figure 3-44]. In addition to Group 2 CIMP marker genes, I find that KD of either ZNF304 or KRAS in DLD-1 cells results in the re-expression of two genes that are used clinically as biomarkers in CRC. Figure 3-45 shows re-expression of vimentin, VIM, and septin 9, SEPT9, when ZNF304 or KRAS is knocked down. Furthermore I tested a representative subset of Group 2 CIMP marker genes for re-expression upon KD of either ZNF304 or KRAS in HCT15 and HCT116 cells. Figure 3-46 shows a significant increase in expression of the tested genes upon KD of either ZNF304 or KRAS. These results are consistent with my hypothesis that KRAS promotes an epigenetic silencing pathway that uses ZNF304 to target the Group 2 CIMP marker genes.

I next tested whether the ZNF304-KRAB corepressor complex directly bound the promoters of Group 2 CIMP marker genes. Figure 3-46 shows ChIP experiment results where I find significant enrichment of ZNF304, KAP1, SETDB1 and DNMT1 at the promoters of several Group 2 CIMP marker genes that we tested in DLD-1 cells. This representative subset of Group 2 CIMP marker genes will

Group 2 CIMP Marker Genes

Gene Symbol	Gene Name	Accession number	Biological Process
p16INK4A	CDKN2A - cyclin-dependent kinase inhibitor 2A	NM_000077	cell cycle regulation
p14ARF	CDKN2A - isoform p14ARF	NM_058195	cell cycle regulation
NEUROG1	neurogenin 1	NM_006161	transcription
CACNA1G	calcium channel, voltage-dependent, T type, alpha 1G subunit	NM_001256324	transporter
RUNX3	runt-related transcription factor 3	NM_001031680	transcription
SOCS1	suppressor of cytokine signaling 1	NM_003745	signal transduction
CRABP1	cellular retinoic acid binding protein 1	NM_004378	signal transduction
ABTB2	ankyrin repeat and BTB (POZ) domain containing 2	NM_145804	cell cyle regulation?
NDNF	neuron-dreived neurotrophic factor	NM_024574	cell cycle regulation
CHFR	checkpoint with forkhead and ring finger domains, E3 ubiquitin protein ligase	NM_001161344	protein stability
COL4A2	collagen, type IV, alpha 2	NM_001846	structural component
EFEMP1	EGF containing fubulin-like extracellular matrix protein 1	NM_001039348	structural component
IGFBP3	insulin-like growth factor binding protein 3	NM_001013398	signal transduction
IGFBP7	insulin-like growth factor binding protein 7	NM_001553	signal transduction
IRF8	interferon regulatory factor 8	NM_002163	signal transduction
LOX	lysyl oxidase	NM_002317	enzyme
PPP1R3C	protein phosphatase 1, regulatory subunit 3C	NM_005398	signal transduction
SFRP1	secreted frizzled-related protein 1	NM_003012	signal transduction
TMEFF2	transmembrane protein with EGF-like and two follistatin-like domains 2	NM_016192	structural component
UCHL1	ubiquitin carboxyl-terminal esterase L1 (ubiquitin thiolesterase)	NM_004181	protein stability
ADAMTS1	ADAM metallopeptidase with thrombospondin type 1 motif, 1	NM_006988	protein stability
AOX1	aldehyde oxidase 1	NM_001159	enzyme
CDO1	cysteine dioxygenase, type I	NM_001801	enzyme
CLDN23	claudin 23	NM_194284	structural component
EDIL3	EGF-like repeats and discoidin I-like domains 3	NM_005711	signal transduction
EFHD1	EF-hand domain family, member D1	NM_025202	unknown
ELMO1	engulfment and cell motility 1	NM_014800	signal transduction
EPHB1	EPH receptor B1	NM_004441	signal transduction
FBN2	fibrillin 2	NM_001999	structural component
HAND1	heart and neural crest derivatives expressed 1	NM_004821	transcription
ID4	inhibitor of DNA binding 4, dominant negative helix-loop-helix protein	NM_001546	transcription
TP73-AS1	TP73 antisense RNA 1	NR_033711	unknown
PENK	proenkephalin	NM_001135690	signal transduction
SFRP2	secreted frizzled-related protein 2	NM_003013	signal transduction
SLC30A10	solute carrier family 30, member 10	NM_018713	transporter
SPON1	spondin 1, extracellular matrix protein	NM_006108	structural component
THBD	thrombomodulin	NM_000361	signal transduction
TSPYL5	testis-specific Y-encoded-like protein 5	NM_033512	cell cycle regulation
ZSCAN18	zinc finger and SCAN domain containing 18	NM_001145542	transcription
BNIP3	BCL2/adenovirus E1B 19kDa interacting protein 3	NM_004052	apoptosis
CIDEB	cell death-inducing DFFA-like effector b	NM_014430	apoptosis
DFNA5	deafness, autosomal dominant 5	NM_004403	unknown
OVOL1	ovo-like 1(Drosophila)	NM_004561	transcription
RASSF2	Ras association (RalGDS/AF-6) domain family member 2	NM_014737	signal transduction
TOLLIP	toll interacting protein	NM_019009	signal transduction
ALX4	ALX homeobox 4	NM_021926	transcription
RASSF5	Ras association (RalGDS/AF-6) domain family member 5	NM_182663	signal transduction
STOX2	storkhead box 2	NM_020225	unknown
PPP1R14A	protein phosphatase 1, regulatory (inhibitor) subunit 14A	NM_033256	signal transduction
LRP2	low density lipoprotein receptor-related protein 2	NM_004525	signal transduction

Table 3-2. Group 2 CIMP Marker genes

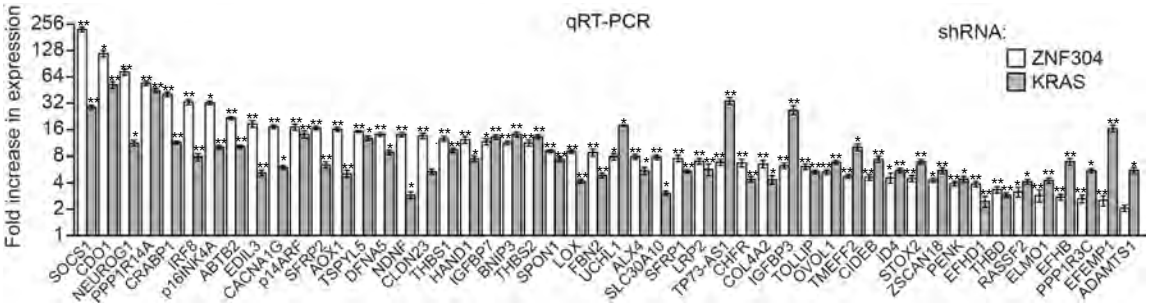

Figure 3-44. qRT-PCR of a panel of CIMP marker gene expression in DLD-1 cells stably infected with either a NS, ZNF304 or KRAS shRNA. Data was normalized to a NS control. Data were collected from experiments performed in at least triplicate, and expressed as mean ± standard deviation. Differences between groups were assayed using two-tailed student *t*-test using Excel [Microsoft]. Significant differences were considered when $P < 0.05$. NS, not significant [$P > 0.05$]; *$P \leq 0.05$ and **$P \leq 0.01$ indicate statistical significance.

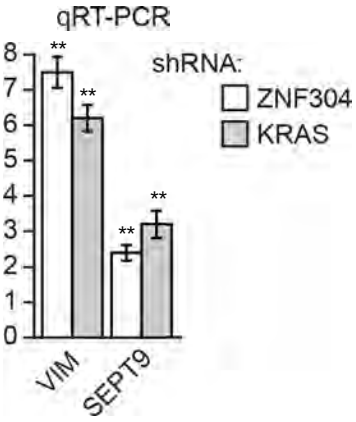

Figure 3-45. qRT-PCR of VIMENTIN and SEPT9 gene expression in DLD-1 cells stably infected with either a NS, ZNF304 or KRAS shRNA. Data was normalized to a NS control. Data were collected from experiments performed in at least triplicate, and expressed as mean ± standard deviation. Differences between groups were assayed using two-tailed student *t*-test using Excel [Microsoft]. Significant differences were considered when $P < 0.05$. NS, not significant [$P > 0.05$]; *$P \leq 0.05$ and **$P \leq 0.01$ indicate statistical significance.

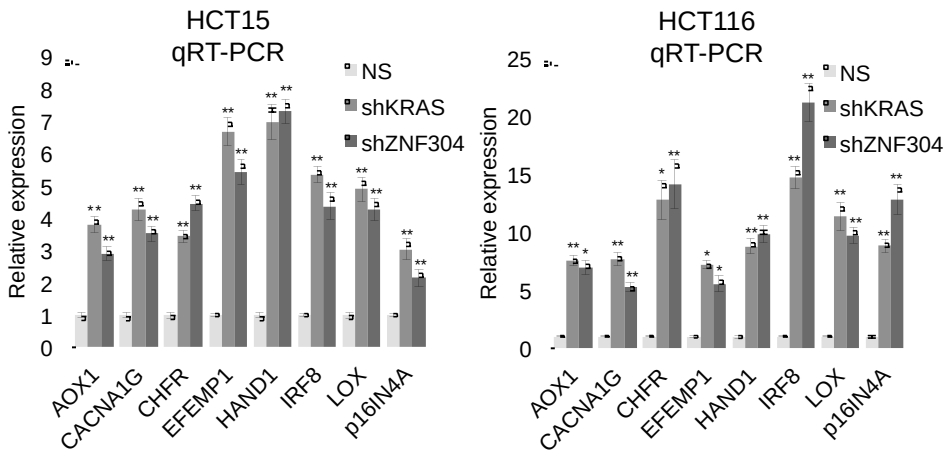

Figure 3-46. qRT-PCR of a panel of CIMP marker gene expression in HCT116 and HCT15 cells stably infected with either a NS, ZNF304 or KRAS shRNA. Data was normalized to a NS control. Data were collected from experiments performed in at least triplicate, and expressed as mean ± standard deviation. Differences between groups were assayed using two-tailed student *t*-test using Excel [Microsoft]. Significant differences were considered when $P < 0.05$. NS, not significant [$P > 0.05$]; *$P \leq 0.05$ and **$P \leq 0.01$ indicate statistical significance.

be used throughout several of the subsequent experiments. Again, we sought to confirm our results in the two KRAS-positive CRC cell lines, HCT116 and HCT15. Figure 3-47 shows ChIP experiment results where we find enrichment of the KRAB co-repressor complex at the promoters of a subset of Group 2 CIMP marker genes.

Finally, I find that shRNA-mediated knockdown of KRAS and ZNF304 results in a loss of Group 2 CIMP marker gene promoter hypermethylation as shown by bisulfite sequencing [Figure 3-48]. I also confirmed hypermethylation of *AOX1*, *CACNA1G* and *CHFR* in the HCT15 and HCT116 cells using bisulfite sequencing [Figure 3-49]. Taken together my results suggest that KRAS initiates a pathway that uses the ZNF304-containing KRAB co-repressor complex to silence Group 2 CIMP marker genes.

I then returned to the PAT-ChIP analysis I had undertaken for ZNF304 recruitment to the *INK4-ARF* promoters to investigate the relevance of the ZNF304 KRAB co-repressor complex's role in silencing Group 2 CIMP marker genes *in vivo*. When a subset of Group 2 CIMP marker gene promoters were analyzed I found more enrichment of ZNF304 at nearly all promoters in CRC samples versus their matched normal controls [Figure 3-50] when normalized to the control IgG immunoprecipitation in the normal tissue. Furthermore, I confirmed that the promoters of *AOX1, CACNA1G, IRF8* and $p14^{ARF}$ were

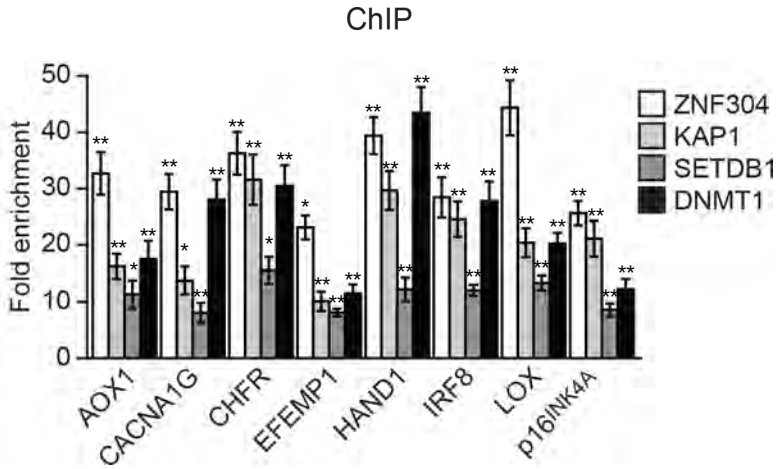

Figure 3-47. ChIP analysis on a panel of CIMP marker gene promoters performed on DLD-1 cell chromatin extracts. Data was normalized to a control IgG immunoprecipitation. Data were collected from experiments performed in at least triplicate, and expressed as mean ± standard deviation. Differences between groups were assayed using two-tailed student *t*-test using Excel [Microsoft]. Significant differences were considered when $P < 0.05$. NS, not significant [$P > 0.05$]; *$P \leq 0.05$ and **$P \leq 0.01$ indicate statistical significance.

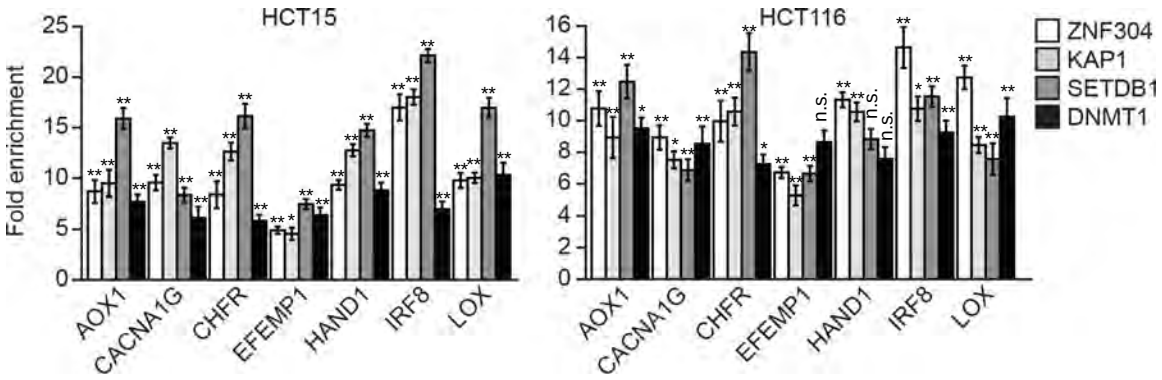

Figure 3-48. ChIP analysis on a panel of CIMP marker gene promoters performed on HCT15 [left] and HCT116 [right] cell chromatin extracts. Data was normalized to a control IgG immunoprecipitation. Data were collected from experiments performed in at least triplicate, and expressed as mean ± standard deviation. Differences between groups were assayed using two-tailed student *t*-test using Excel [Microsoft]. Significant differences were considered when $P < 0.05$. NS, not significant [$P > 0.05$]; *$P \leq 0.05$ and **$P \leq 0.01$ indicate statistical significance.

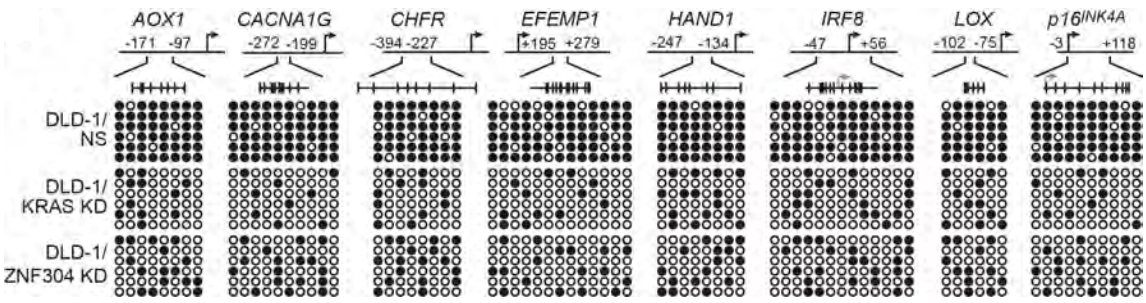

Figure 3-49. Bisulfite sequencing performed on the promoter regions of a panel of CIMP marker genes in bisulfite converted genomic DNA from DLD-1 cells stably infected with NS, ZNF304 or KRAS shRNAs.

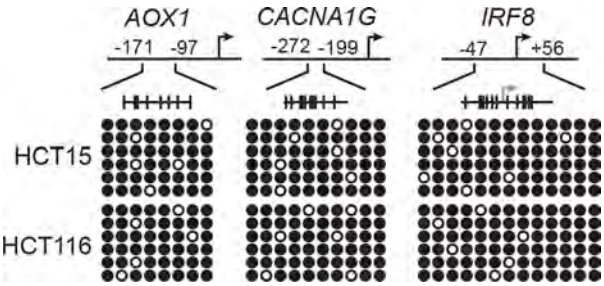

Figure 3-50. Bisulfite sequencing performed on the promoter regions of a panel of CIMP marker genes in bisulfite converted genomic DNA from HCT15 [top] and HCT116 cells [bottom].

hypermethylated in the CRC but not the normal tissue in the same set of matched samples as determined by bisulfite sequencing [Figure 3-51]. Taken together, my results show that KRAS up-regulates ZNF304, which then specifies Group 2 CIMP marker gene hypermethylation and epigenetic silencing in human KRAS-positive CRCs.

As stated earlier, $p14^{ARF}$ is a well-established tumor suppressor and cell cycle regulator [Sherr, 1998, Sherr, 2006]. Mouse knockout models of the murine $p14^{ARF}$ homolog, $p19^{ARF}$, display increased frequency of lymphomas and sarcomas with early onset [Kamijo, 1997] and, conversely, over-expression of $p14^{ARF}$ results in cell cycle arrest or apoptosis [Asker et al, 1999].

Based upon these considerations I predicted that loss of ZNF304 [or DNMT1], which results in increased expression of $p14^{ARF}$, would reduce tumorigenicity of the DLD-1 cell line. To test this prediction, I performed double-knockdown experiments in a mouse xenograft system in which DLD-1 cells stably express two different shRNAs. DLD-1 cells were transduced with pSM2 retroviral shRNAs directed against a non-silencing control or ZNF304. Subsequently infected cells were selected using puromycin resistance. Then, the puromycin-resistant cells were infected with GFP-expressing pGIPZ shRNAs directed against a non-silencing control or $p14^{ARF}$. pGIPZ containing cells were FACS sorted using the GFP marker. The four double-knockdown cell lines were

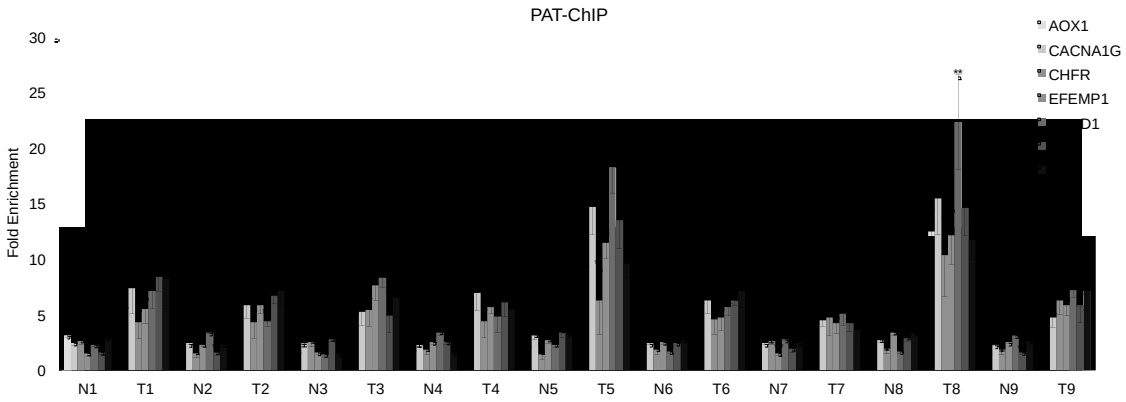

Figure 3-51. PAT-ChIP analysis of ZNF304 enrichment on the promoters of a panel of CIMP marker genes in matched patient derived normal colonic tissue and KRAS-positive colorectal adenocarcinoma. ZNF304 enrichment in both normal and tumor tissue was normalized to the control IgG immunoprecipitation in normal tissue. Data were collected from experiments performed in at least triplicate, and expressed as mean ± standard deviation. Differences between groups were assayed using two-tailed student *t*-test using Excel [Microsoft]. Significant differences were considered when $P < 0.05$. NS, not significant [$P > 0.05$]; *$P \leq 0.05$ and **$P \leq 0.01$ indicate statistical significance.

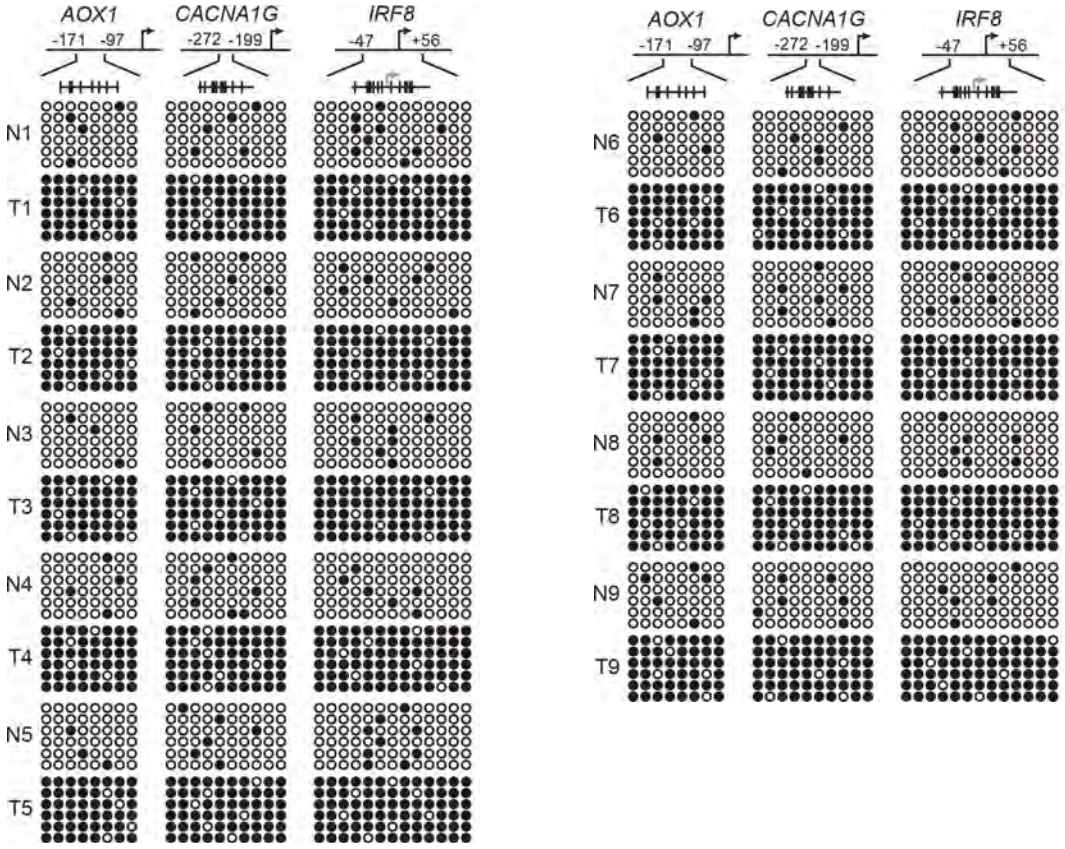

Figure 3-52. Bisulfite sequencing performed on the promoter regions of a panel of CIMP marker genes in bisulfite converted genomic DNA from patient derived matched adjacent normal colonic tissue and KRAS-positive colorectal cancer.

injected subcutaneously into the flanks of BALB/c nu/nu mice [n=3 for each treatment group]. Figure 3-53 shows that knockdown of ZNF304 in DLD-1 cells significantly inhibited tumor growth compared to control DLD-1 cells expressing a non-silencing shRNA.

Importantly, the double-knockdown of $p14^{ARF}$ and ZNF304 resulted in an incomplete rescue of DLD-1 tumor forming ability. Presumably knocking down ZNF304 causes re-expression of additional tumor suppressors in group 2 CIMP marker genes besides $p14^{ARF}$ [Figure 3-44]. Therefore the $p14^{ARF}$/ZNF304 double knockdown still expresses these other tumor suppressing genes and maintains a deficient tumor forming ability compared to the control. Similarly, Figure 3-54 shows that DNMT1 knockdown DLD-1 cells formed a smaller tumor than DLD-1 cells containing a non-silencing shRNA. Significantly, knockdown of $p14^{ARF}$ as well as DNMT1 also results in a partial rescue of tumor forming ability. Taken together these results indicate that loss of ZNF304 or DNMT1 and subsequent re-expression of $p14^{ARF}$ hinders the tumorigenicity of DLD-1 cells. These results also support the hypothesis that the KRAB co-repressor complex repress many TSGs besides $p14^{ARF}$.

Throughout this work I have been curious as to what the normal function of ZNF304 is. There is a significant body of work suggesting that $p14^{ARF}$ and the

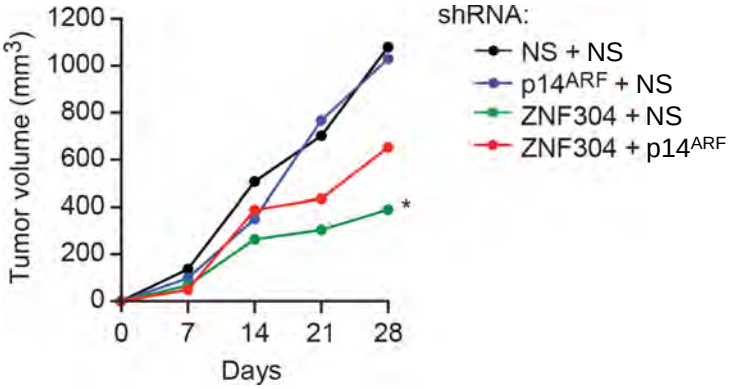

Figure 3-53. 2 x 10^6 DLD-1 cells stably infected with either NS/NS, NS/$p14^{ARF}$, NS/ZNF304 or ZNF304/$p14^{ARF}$ double knockdowns were injected into the flanks of Balb/C nu/nu mice and monitored for tumor growth at indicated times. Data were collected from experiments performed in at least triplicate, and expressed as mean ± standard deviation. Differences between groups were assayed using two-tailed student *t*-test using Excel [Microsoft]. Significant differences were considered when $P < 0.05$. NS, not significant [$P > 0.05$]; *$P \leq 0.05$ and **$P \leq 0.01$ indicate statistical significance.

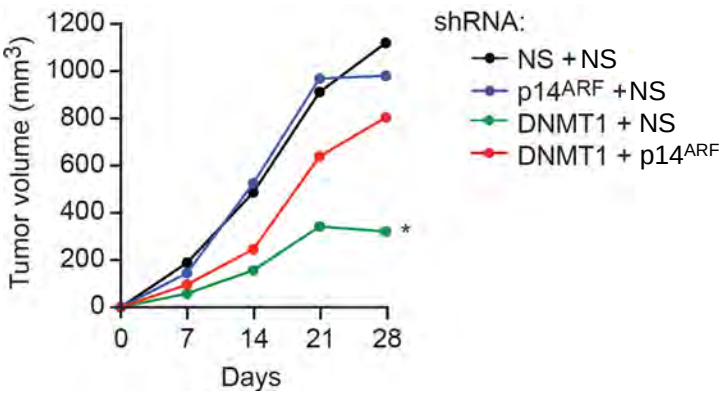

Figure 3-54. 2 x 10^6 DLD-1 cells stably infected with either NS/NS, NS/$p14^{ARF}$, NS/DNMT1 or DNMT1/$p14^{ARF}$ double knockdowns were injected into the flanks of Balb/C nu/nu mice and monitored for tumor growth at indicated times. Data were collected from experiments performed in at least triplicate, and expressed as mean ± standard deviation. Differences between groups were assayed using two-tailed student *t*-test using Excel [Microsoft]. Significant differences were considered when $P < 0.05$. NS, not significant [$P > 0.05$]; *$P \leq 0.05$ and **$P \leq 0.01$ indicate statistical significance.

mouse homolog, $p19^{ARF}$, must be maintained at very low levels in stem cell lines [Pardal et al 2005 and Kim and Sharpless 2006]. Defects in the epigenetic machinery responsible for *$p19^{ARF}$* silencing results in developmental defects [ie BMI1 KO mice] [Jacobs et al 1999]. Analagous to PRC1-mediated silencing of *$p19^{ARF}$* in the mouse, I postulate that ZNF304 KRAB co-repressor complex to function in ES cells for repressing $p14^{ARF}$ levels. In the human ES cell line, H9, I find that shRNA-mediated knockdown of ZNF304 causes a significant increase in the mRNA expression of $p14^{ARF}$, $p15^{INK4B}$ and $p16^{INK4A}$ [Figure 3-55]. Therefore I can conclude that the ZNF304 KRAB co-repressor complex contributes to the down regulation of the *INK4-ARF* locus in undifferentiated H9 cells.

I next sought to determine whether the ZNF304 KRAB co-repressor complex was involved in undifferentiated or differentiated H9 cells. The immunoblot in Figure 3-56 reveals a marked reduction in ZNF304 levels upon retinoic acid-induced differentiation of H9 cells. Furthermore the ChIP experiment in Figure 3-57 supports the role of ZNF304, KAP1, SETDB1 and DNMT1 on the *INK4-ARF* locus in undifferentiated H9 cells. I find there to be a significant reduction in enrichment at the *INK4-ARF* locus for these four factors upon retinoic acid treatment [Figure 3-57].

Taken together these results support the hypothesis that ZNF304 normally functions in proliferating stem cells to repress INK4-ARF transcription. Upon

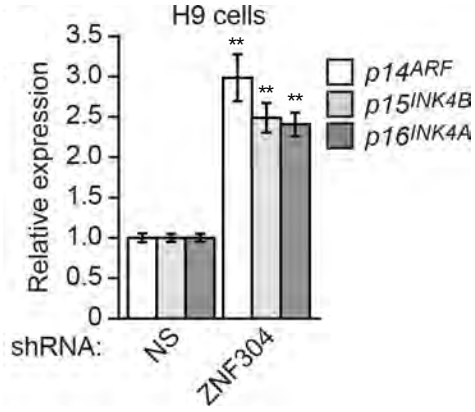

Figure 3-55. qRT-PCR of $p14^{ARF}$, $p15^{INK4B}$ and $p16^{INK4A}$ mRNA expression in H9 cells that are stably infected with either NS or ZNF304 shRNA. Data was normalized to a NS control. Data were collected from experiments performed in at least triplicate, and expressed as mean ± standard deviation. Differences between groups were assayed using two-tailed student *t*-test using Excel [Microsoft]. Significant differences were considered when $P < 0.05$. NS, not significant [$P > 0.05$]; *$P \leq 0.05$ and **$P \leq 0.01$ indicate statistical significance.

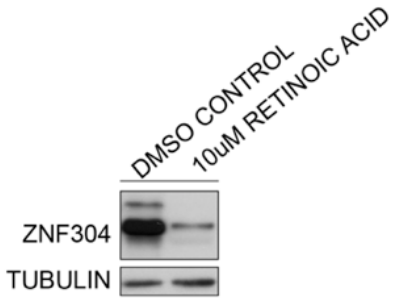

Figure 3-56. Immunoblot analysis of ZNF304 expression in H9 cells that have been treated with DMSO or 10 μM retinoic acid for three days. Tubulin was used as a loading control.

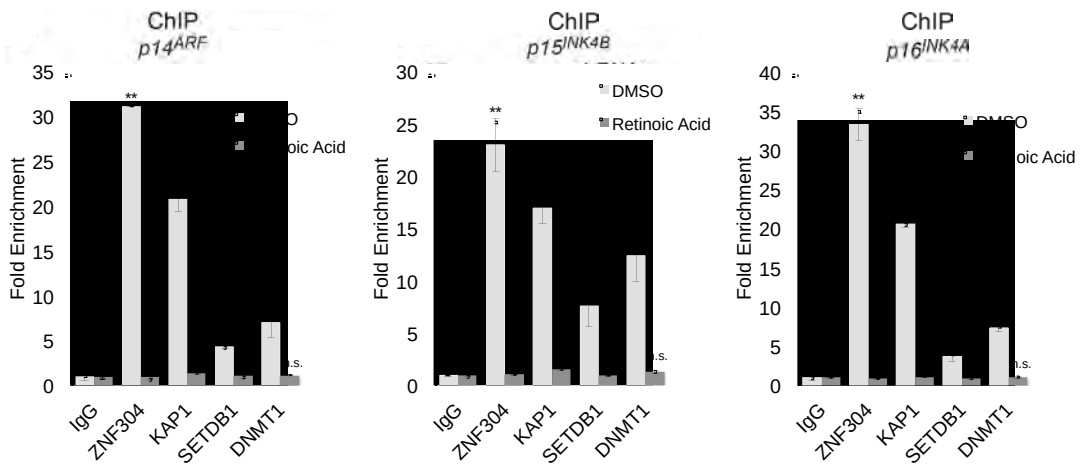

Figure 3-57. ChIP analysis of the *p14*^{ARF}, *p15*^{INK4B} *and p16*^{INK4A} promoters performed on chromatin extracts from H9 cells that have been treated with DMSO or 10 µM retinoic acid for four days. Data was normalized to a control IgG immunoprecipitation in each treatment group. Data were collected from experiments performed in at least triplicate, and expressed as mean ± standard deviation. Differences between groups were assayed using two-tailed student *t*-test using Excel [Microsoft]. Significant differences were considered when $P < 0.05$. NS, not significant [$P > 0.05$]; *$P \leq 0.05$ and **$P \leq 0.01$ indicate statistical significance.

differentiation, ZNF304 levels decrease and the replicative potential of the cells drops as a result. Cells that have undergone differentiation now contain an *INK4-ARF* locus that is poised for activation upon oncogene activation.

Conclusions

Here I have described a genome-wide RNAi screening method to identify factors required for epigenetic silencing of the tumor suppressor *p14^{ARF}*. Using this approach, I have identified eight genes whose knockdown leads to de-repression of the epigenetically silenced *INK4-ARF* locus. I find that one of these factors, ZNF304, binds and recruits a KRAB co-repressor complex, comprising KAP1 and SETDB1, and DNMT1 directly to the promoters of p14^{ARF}, p15^{INK4B} and p16^{INK4A} as well as the promoters of Group 2 CIMP marker genes. Upon binding, DNMT1 hypermethylates the promoter region near the transcriptional start site and silences gene transcription.

RAS signaling is responsible for directing this silencing because USP28 is promoted by RAS signalling and in turn antagonizes ZNF304 ubiquitin-mediated degradation. USP28's interaction with ZNF304 is directed by a phosphorylation at Serine 899 by PRKD1, the absence of which prevents ZNF304 deubiquitination. Inhibition of the RAS signaling cascade results in re-expression of the *INK4-ARF* locus and Group 2 marker genes due to a loss of ZNF304-mediated specificity [Figure 3-58].

I find there to be an overexpression of ZNF304 in the majority of colorectal adenocarcinomas tested [~88%], suggesting that this protein is a proto-oncogene. Furthermore my investigations PAT-ChIP and bisulfite sequencing on

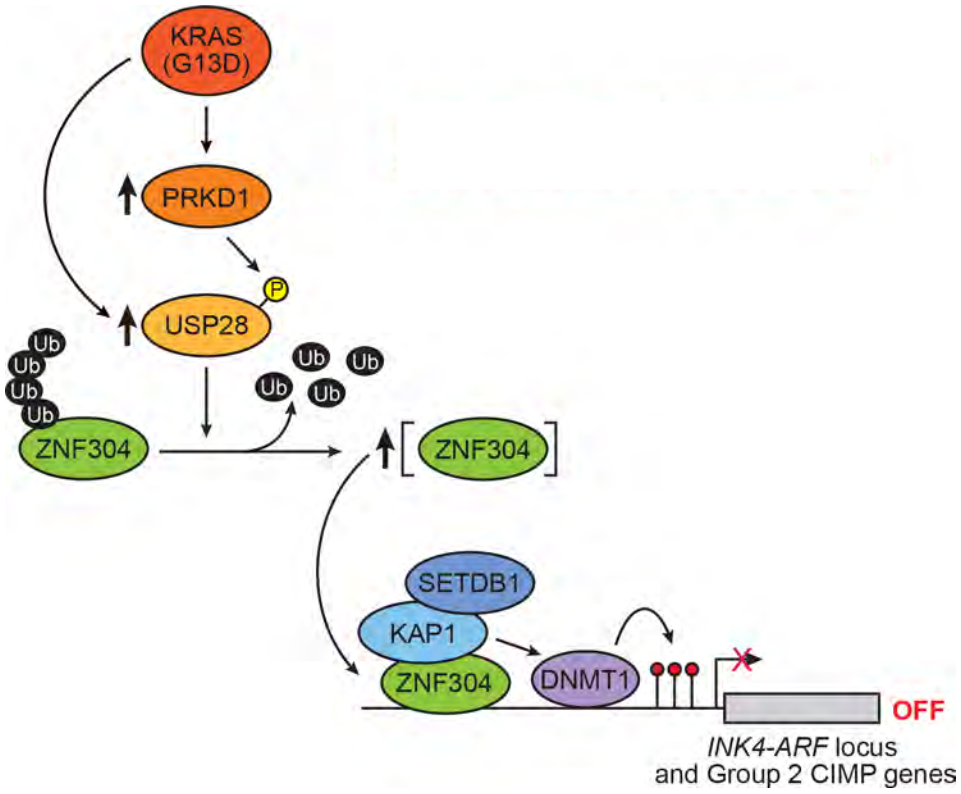

Figure 3-58. Schematic model of KRAS-induced epigenetic silencing of Group 2 CIMP marker genes.

RAS activation results in increased RAF-MEK-ERK pathway signaling. In turn there is increased mRNA expression of USP28 and PRKD1. PRKD1 phosphorylates and activates USP28 that then deubiquitinates ZNF304. ZNF304 then forms a co-repressor complex with KAP1, SETDB1 and DNMT1. This co-repressor complex is directed by ZNF304 to the promoters of Group 2 CIMP marker genes and initiates epigenetic silencing.

patient derived colorectal cancer tissues have revealed that this mechanism is indeed present in patients and found quite frequently.

My preliminary investigations into ZNF304's normal function have revealed a use in proliferating stem cell populations who must maintain low INK4-ARF levels. Presumably a premalignant population of cells has reinitiated this function of ZNF304 and allowed them to obtain increased proliferative potential and develop into carcinoma. Our results are consistent with a variety of previous studies showing similarities between cancer cells and stem cells [for example see Ohm, et al. 2007 and Riggs, et al. 2013].

Collectively, our results indicate that ZNF304 directs epigenetic silencing of $p14^{ARF}$, $p15^{INK4B}$ and $p16^{INK4A}$ and other TSGs thereby facilitating RAS-directed tumorigenicity. Thus, in addition to its well-established role in promoting cellular proliferation and preventing apoptosis through downstream signaling pathways, RAS induces "secondary" oncogenic events by inactivating TSGs through epigenetic silencing. This additional activity may explain, at least in part, why RAS is such a potent onco-protein and why activating RAS mutations are found at high frequency in human tumors.

Methods

Cell Lines and Culture

DLD-1, HCT116, HCT15, H460, 293T, SW48, PFF, CaCo2, SW948, SW1116, H9, LS513 and LoVo cells were obtained from ATCC and grown as recommended by the supplier. For 5-AZA [Calbiochem] treatment, cells were treated with 10 µM 5-AZA [Calbiochem] and the drug was exchanged every 24 hrs for 72 hours. 10 µM Manumycin A [Calbiochem], 10 µM PI-103 [Cayman Chemical] and 20 µM U0126 [Cell Signaling] was added for the indicated amount of time. 0-10 µM MG-132 [Cayman Chemical], 10 µM Retinoic Acid [Sigma-Aldrich] , 0-10µM CRT0066101 [Cancer Research Technologies] was added at the concentration and length of time indicated.

Reporter Construct Cloning and Validation

The 3.98 kb $p14^{ARF}$ promoter was PCR amplified using primers with *BglII* and *SalI* restriction sites engineered in and cloned into a TK^r/$Blast^r$/RFP fusion reporter. This was then linearized using *NheI* and stably transfected into DLD-1 cells using Amaxa. Briefly, nucleofection was performed with the aid of a Nucleofector device [Amaxa Biosystems, Cologne, Germany] and nucleofection buffer V. 1x 10^6 DLD-1 cells were transfected with 5 ug linearized $p14^{ARF}$-$Blast^R$ reporter vector. The nucleofection procedure was performed using program X-12. Immediately after nucleofection, the cells were placed in complete growth medium and allowed to recover for 72 hours. Viable cells were allowed to grow

colonies and then subjected to 500 ug/mL G418 [Calbiochem] selection. Surviving colonies were then individually isolated and expanded for characterization. Clones were treated with 10 µM 5-aza-2'-deoxycytodine [5-AZA] for 72 hours. After 24 hours treatment, blasticidin [Sigma-Aldrich] was added at indicated concentrations and continued for a total of seven days at which point cells were fixed and stained with 0.1% crystal violet to assess viability.

shRNA Screen

The human shRNA^{mir} library [release 1.20; Open Biosystems] was obtained through the UMass Medical School shRNA library core facility. Retroviral pools were generated and used to transduce DLD-1/*p14*^{ARF}*-Blast*^{R} cells as described [Gazin et al., 2007]. Cells were then selected with puromycin for 3 days at 4 µg per mL. Subsequently, the puromycin-resistant population was challenged with blasticidin for 14 days at a concentration of 10 µg per mL. Cells that bypassed the blasticidin challenge formed colonies that were picked individually and expanded. The shRNAs were identified by sequence analysis as previously described [Gazin et al., 2007]. Individual knockdown cell lines were generated by stable transduction of 1 x 10^5 cells with a single shRNA followed by puromycin selection. Individual shRNAs were obtained from the Open Biosystems library [Table 3-3].

Validation: Briefly, shRNAs were packaged into infectious retrovirus particles and DLD-1, HCT15 and HCT116 cells were infected and subsequently selected with 4, 5, and 2 µg per mL puromycin for 3 days, respectively. At which point they were harvested for RNA and analyzed for target gene expression using qRT-PCR.

Quantitative Real-Time RT-PCR

Total RNA was isolated and reverse transcription was performed as described [Gazin et al., 2007], followed by quantitative real-time PCR using Power SYBR Green PCR Master Mix [Applied Biosystems]. GAPDH was used as an internal reference gene for normalization. Primer sequences are provided in Table 3-4.

Antibodies and Immunoblot Analysis

21st Century generated the ZNF304 antibody against a peptide corresponding to amino acids [GFWCEAEHEAPSEQSV] of the ZNF304 coding region. Cell extracts were prepared by lysis in Laemmli buffer in the presence of protease inhibitor cocktail [Roche]. The following antibodies were also used: α-KAP1 [Bethyl], α-SETDB1 [Millipore], α-DNMT1 [Imgenex], α-DNMT3A [Imgenex], α-DNMT3B [Imgenex], USP28 [Bethyl], p14^{ARF} [Millipore], ACTB [in house], TUBULIN [in house], FLAG-M2 [Sigma-Aldrich], HA [Cell Signaling], PRKD1 [Cell Signaling], PRKD1-Ser916 [Cell Signaling], PRKD1-Ser744/748 [Cell Signaling], and KRAS [Abcam].

ChIP Assays

ChIP Assays were performed using the following antibodies: α-ZNF304 [21st Century-see above], α-KAP1 [Bethyl], α-SETDB1 [Millipore], α-DNMT1 [Imgenex], α-DNMT3A [Imgenex], α-DNMT3B [Imgenex]. ChIP primers can be found in Table 3-5. ChIP products were analyzed by quantitative real-time PCR using Power SYBR Green PCR Master Mix [Applied Biosystems]. Calculation of fold-differences was done as follows. Samples were quantitated as percentage of input, and then normalized to an unrelated region in the genome [~-3.2 kb upstream from the TSS of GCLC]. Fold enrichment was calculated by setting the IgG control immunoprecipitation sample to a value of one and comparing the experimental values.

Tumor Formation Assays

2 x 10^6 DLD-1 cells infected with either non-silencing/non-silencing, non-silencing/ZNF304, $p14^{ARF}$/non-silencing or $p14^{ARF}$/ZNF304 [as described below] were suspended in 100 µl of serum-free RPMI and injected subcutaneously into the right flank of athymic Balb/c [nu/nu] mice [Taconic]. Briefly, DLD-1 cells were initially infected with pSM2 retrovirus containg either $p14^{ARF}$ or non-silencing shRNA. Cells were puromycin selected to ensure a pure population of infected cells. Then this population was infected with pGIPZ shRNA virus containing either ZNF304 or non-silencing shRNAs. Subsequently the cells were FACS sorted for GFP^+ cells to ensure a pure population of pGIPZ infected cells.

Tumor dimensions were measured every seven days for four weeks and tumor volume was calculated using the formula $\pi/6$ x [length] x $[width]^2$. Animal experiments were performed in accordance with the Institutional Animal Care and Use Committee [IACUC] guidelines.

Bisulfite Sequencing

Bisulfite modification was carried using the QIAGEN Epitect Bisulfite Conversion kit according to the manufacturer's instructions. Multiple clones were sequenced from each nested PCR product within each cell line [see Table 3-6 for primer sequences] of which 6 representative clones are displayed. Assay kits from EpigenDX were also used according to manufacturer's instructions and similarly sequenced and represented. [see Table 3-6 for a list of assay kits used].

Immunohistochemistry

Tissue microarrays were constructed as previously described [Chn et al. 2007]. For ZNF304 and USP28 immunohistochemistry, antigen retrieval was performed using deparaffinized tissue sections in citrate buffer [BioGenex, San Ramon, CA] that were treated in a microwave for 15 min. Tissue sections were incubated for 10 min with 3% H_2O_2 [to block endogenous peroxidase], with 10% normal goat serum [Vector Laboratories, Burlingame, CA] in phosphate-buffered saline for 10 min. The primary antibodies against ZNF304 [21^{st} Century, 1:250 dilution], USP28 [Bethyl, 1:100 dilution] was applied for 30 min at room temperature.

Later, the secondary antibody [BioGenex] was applied for 20 min and then streptavidin peroxidase conjugate [BioGenex] was applied for 20 min. Sections were visualized with diaminobenzidine for 5 min and by methyl green counterstain. Appropriate positive and negative controls were included in each run of immunohistochemistry such as cell lines that overexpressed the target protein or cell lines that harbor an shRNA against the target protein.

ZNF304 and USP28 positivity was defined as 50% or more of tumor cells with unequivocal moderate/strong nuclear staining, as recommended for improved specificity. All immunohistochemically stained slides were interpreted by a pathologist [Shuji Ogino] blinded to any other clinical or laboratory data. A random sample of tumors was reexamined by a second pathologist [Xiaoyun Liao] who was unaware of other data. The concordance between the two observers was 0.89 [$\kappa = 0.78$; $p < 0.0001$], indicating substantial agreement.

HA-Ubiquitin Pulldown

2 x10^6 293T cells were plated on 10 cm dishs and transfected with 0.5 µg eGFP [for transfection efficiency monitoring], 1.0 µg p3XFLAG-ZNF304, 1.0 µg p3XFLAG-USP28 [wildtype and C171A or S899A mutants] and 1.0 µg HA-Ubiquitin plasmids using the Effectene reagent [QIAGEN]. eGFP expression was monitored 48 hours later to ensure equvalent transfection efficiency. Cells were

harvested in NETN-150 buffer [20 mM Tris-HCL, pH 8.0, 150 mM NaCl, 1 mM EDTA and 0.05% NP-40] plus 1X protease inhibitor cocktail [Roche]. Pulldown were performed using anti-rabbit Trublot beads [eBioscience] and HA-tag antibody [Cell Signaling]. Beads were incubated with lysate for 4-24 hours and washed three times using NETN-150 buffer and eluted in 2X sample buffer.

***in vitro* kinase assay**

HIS tagged-PRKD1 was cloned from pcDNA3.1-PRKD1 and pcDNA3.1-PRKD1-KW constructs by digestion with BamHI and XhoI and ligation into pRSET using the same enzyme sites. HIS-PRKD1 was purified and 60 nM was incubated with 10 µM radiolabeled ATP. Autophosphorylation of the wildtype plasmid was confirmed to ensure activity by immunoblotting for PRKD1 Ser916 phosphorylation. Subsequently, HIS-PRKD1 and radiolabeled ATP were incubated with peptides corresponding to amino acids [TCLQRWRSEIEQDIQ] and [YSLFRKVSVYLLTGL] in USP28 and monitored for radiolabel phosphorylation of the peptide. A 20 µL reaction was set up with the following components: 1 µL of 32P-gamma-ATP [10mCi], 1 µL of 10 µM ATP, 0.2 mM Microcystin, 4 µL of 5X kinase buffer [see composition below], 5 µL [60 nM final] kinase diluted in 1X kinase buffer, 5 µL of substrate [10 µM final] diluted in 1X kinase buffer, 3.8 µL ddH_2O. 5X Kinase buffer: 23 mM MOPS, 11.5 mM β-glycerphosphate, 23 mM $MgCl_2$, 4.6 mM EGTA, 1.8 mM EDTA, 0.25 mM DTT

[pH 7.0]. Reactions were incubated for 30 minutes and stopped using 2X Laemmli Sample Buffer.

Alamar Blue assay

Between 0.05 $x10^6$ and 0.3 $x10^6$ cells were seeded per well of a 12-well plate and allowed to adhere for 24 hours. Either DMSO or 8 uM CRT0066101 was then added for 48 hours. 111 uL of 10X Alamar Blue Dye [Invitrogen] was added for between 2 and 4 hours. Readings were taken with a Spectramax M5 [Molecular Devices] with an excitation wavelength of 530 nm and emission of 590 nm. Percent survival was calculated using the DMSO control well as 100%.

PAT-ChIP assay

Four formalin-fixed paraffin embedded tissue sections were collected and de-paraffinized in Histolemon-Erba RS solution [Carlo Erba Reagents] for ten minutes at room temperature. Spin down tissue and repeat de-paraffinization four times. Resuspend tissue in 100% ethanol and incubate for ten minutes at room temperature. Spin down tissue and repeat resuspension in 95% ethanol. Repeat washing/resuspension gradually increasing the percentage of water [70%, 50%, 20%, 0%] to rehydrate the tissue. Material can now be processed as normal ChIP material with lysis buffer and sonication.

Statistics

All quantitative data were collected from experiments performed in at least triplicate, and expressed as mean ± s.d. Differences between groups were assayed using two-tailed student *t*-test using Excel [Microsoft]. Significant differences were considered when $P < 0.05$. NS, not significant [$P > 0.05$]; *$P \leq 0.05$ and **$P \leq 0.01$ indicate statistical significance.

Open Biosystems shRNAs

Gene	Source ID	Location
C2orf82	V2HS_41608	SH2372-A9
	V2HS_245198	SH2590-E1
DICER1	V2HS_233045	SH2412-E5
	V2HS_239140	SH2487-B1
F11R	V2HS_16017	SH2124-F8
	V2HS_16012	SH2252-H6
PRKD1	V2HS_170465	SH2480-A2
	V2HS_170464	SH2328-G1
SLC17A6	V2HS_39419	SH2360-G12
	V2HS_39421	SH2037-A7
UBE2G2	V2HS_254940	SH2624-D8
	V2HS_171768	SH2761-B1
USP28	V2HS_14019	SH2625-E8
	V2HS_6063	SH2559-D5
ZNF304	V2HS_58488	SH2305-A9
	V2HS_58485	SH2515-D6
	V2HS_58488	172_0266-D7
KAP1	V2HS_2091	SH2337-A9
	V2HS_201585	172_0577-G3
SETDB1	V2HS_43632	172_0650-B2
	V3LHS_388251	172_1525-B10
DNMT1	V2HS_113503	172_0491-D7
	V2HS_113505	172_0616-G1
DNMT3A	V2LHS_74666	172_0060-F1
	V3LHS_391163	172_1400-E9
DNMT3B	V2HS_11913	172_0514-H3
	V2HS_77233	172_0103-F2
KRAS	V2HS_203252	172_0410-B8
	V2HS_169384	172_0236-C8
CDKN2A ($p14^{ARF}$)	V2HS_195839	SH2517-C6

Table 3-3. shRNA information

qRT-PCR

Gene	Sequence (5'->3')
$p14^{ARF}$	CCCTCGTGCTGATGCTACTG
	ACCTGGTCTTCTAGGAAGCGG
$p15^{INK4B}$	GGCGCGGGGACTAGTGGAGA
	GCCCATCATCATGACCTGGATCGC
$p16^{INK4A}$	GAAGGTCCCTCAGACATCCCC
	CCCTGTAGGACCTTCGGTGAC
$BLAST^{R}$	GTCGCCAGCGCAGCTCTCTC
	AGTCAGGTTGCCAGCTGCCG
ZNF304	AAGAGCTGTACAGTCCACATG
	TCTCACCTCAGCATGAGTC
USP28	AGGGGCCATGGTGGAGGGTG
	TCTGGCTGCCCAAGGGACTGA
PRKD1	GGGGCTTTTCAGGCAGGGCT
	ACTCTGCCCCAGGGCTAAGCA
C2orf82	GGGCTCCTGTGGAACATC
	TTAACCAGCGCAGTCCTCC
DICER1	GTACGACTACCACAAGTACTTC
	ATAGTACACCTGCCAGACTGT
F11R	CTATAGCCGAGGCCACTTTG
	ACACCAGGAATGACGAGGTC
SLC17A6	TCGGCCAGATCTACAGGGTGCT
	CACAGCGGCGCCTTCCTCTC
UBE2G2	CAGCTGTTGCGGGGCCATGG
	GGGCCTGCTACAATTCCTTCCGGA
KAP1	AATGATGCCCAGAAGGTGAC
	TTGAGGTCCCACTGAAACTT
SETDB1	ACATCCTCAGCCTCTGCAT
	TTCCAGTACCGGTCAGATCC
DNMT1	TCCACAGCAAAGTGAAAGTCATCT
	CTCGCGTAGTCTTGATCATACCA
DNMT3A	CACACCTGAGCGCGACTGCA
	ACGATCCACGCGCCCATTCC
DNMT3B	CCCCGGAGATCAGAGGCCGAA
	CCCGCCGTCTCAGGGACTGT
KRAS	TAGACACAAAACAGGCTCAGG
	TAATTACACACTTTGTCTTTGA
SOCS1	CTCCTTCCCCTTCCAGATTT
	CACATGGTTCCAGGCAAGTA
CDO1	GTACGCCAAGTTCGACCAGT
	GTCCTTCACCCCAACAGAGA
NEUROG1	GTTACTTTCCCCCTCCCCTA
	CTTTAAAGCTCCCGCTTCCT
PPP1R14A	CTGGACGTGGAGAAGTGGAT
	AGCAGCTCCTGGATGAAGTC
CRABP1	GCAAGTGCAGGAGTTTAGCC
	CACGGGTCCAGTAGGTTTTG

Gene	Sequence (5'->3')
IRF8	AGTGGCTGATCGAGCAGATT
	AGTGGCTGGTTCAGCTTTGT
ABTB2	GCTGGTCAGTTTGTTGCTGA
	TGGCTGAAGCAGTTCATGTC
EDIL3	TTGGCTGATGGTTCCTTTTC
	ATGGCATGGATTAGGAGTGC
CACNA1G	AAGCAGACAGTGGAGCCTGT
	TCTGAGTCAGGCATTTCACG
SFRP2	GGGTCTGGTTGGTTGTTGTT
	GGGCCACAGAGAAAATTGAA
AOX1	TCACTCACGGTGGAATTGAA
	CAGGTGGACATTCGACATTG
TSPYL5	TCCCACTTTCAGCAGTCCTT
	CCCAGGAGAAGCTTGAGATG
DFNA5	GAATGAGGTCCTGTGCGTTT
	GATGCCACCACACTTCTCCT
NDNF	CGCTCCCTGCAGTTTAAAAG
	AAGTTGCTGCGAAGTGGAGT
CLDN23	TTGCCATGCAAACTCTCAAG
	CCATTAAGCTGCTGGCATTT
THBS1	ACCAAAGCCTGCAAGAAAGA
	TCTGTACCCCTCCTCCACAG
HAND1	GTCCGCAGAAGGGTTAAACA
	GGCAAGGCTGAAAATGAGAC
IGFBP7	GGCATGGAGTGCGTGAAGAG
	CTTGCTGACCTGGGTGATGG
BNIP3	TTCCTTCCATCTCTGCTGCT
	ATCAAAAGGTGCTGGTGGAG
THBS2	AAGTGTGTGAGCCCGAAAAC
	GTACATGGGGTCGCTGAAGT
SPON1	CACATTTGATGGGGTGACTG
	TGTCTTCTCGGACCAATTCC
LOX	ATATTCCTGGGAATGGCACA
	CCAGGACTCAATCCCTGTGT
FBN2	TCCTGGATATCAGGCTACGC
	TGAATTTGTGCACTGGGTGT
UCHL1	AGCGTGAGCAAGGAGAAGTC
	TTGAAGGGAAGAGGGGAAAT
ALX4	AGAGAGCAACAAGGGCAAGA
	CACGTCTGGGTAGTGGGTCT
SLC30A10	ATCCACAATGTGACCATCCA
	CTTGGAGATGCAGGGTGAGT
SFRP1	AAGGGAGGCTCTCTGTAGGC
	AATGACCAGGCCAATCAGTC
LRP2	AAACAATGGTGGGTGCTCTC
	TTCTTGCCATCACTTTGCAG

Gene	Sequence (5'->3')
TP73-AS1	GGGTAACTCCCCACTGTTGA
	GGCTGAGCTGGACAAAAGAC
CHFR	CCTCTGTGGCAAGTGATGAA
	TCCAAATCCTCCTGATCCTG
COL4A2	AAGGAATCATGGGCTTTCCT
	CTCTGGCACCTTTTGCTAGG
IGFBP3	AGGGCACTCTGGGAACCTAT
	TGCAGTCATCCGAAGAATTG
TOLLIP	CGGTGGTACAGAGAGCCTTC
	ACCACTTGTCCTCCACCTTG
OVOL1	CAGGGCTTCTAATGCTCAGG
	AGTGCACACACACAAGCACA
TMEFF2	CAATGGGGAGAGCTACCAGA
	TCTGTGGCACATGATCCTTC
CIDEB	GGAACTGCAGTGGACAGTGA
	CACTCCTTGTAGGGCTCCAG
D4	GGGTGGGCTACTTTTCTTCC
	GTCGCTCTGGGTTTTACGAG
STOX2	GGCGAACTCAACTCTTGTCC
	TTCTTTCCCAGAGGTGATGG
ZSCAN18	GCTTTCCTGCAGCCATTTAG
	TTGAAGAAAGCACTGGCAGA
PENK	AAGCCAAAGAGCTGCAGAAG
	TTCAGGAAACCTCCATACCG
EFHD1	GATGGCTTCATCGACCTGAT
	GTCCTCATCCACCTCCTTGA
THBD1	CGGGTTGTGTGTCTGTTCAC
	CCTCCATGCATCTCATAGCA
RASSF2	GGTCTTCCTGCACTTGAAGC
	GCATCTCCACACACAAGGTG
ELMO1	CTGCTCAGCATGGAAATCAA
	TCATAGTTGCTGGGCTCCTT
EFHB1	CCTCCCTAATGTCCCAGGAT
	CCTCAGACCAGAAGGCTGAC
PPP1R3C	TTGCAAGAGCGAACAGTGAC
	TGCTCAGTTGGAATGACAGG
EFEMP1	CAGGGACGCACAACTGTAGA
	ATTGAAACCCAGGACTGCAC
ADAMTS1	GGATGGCTGATGTTGGAACT
	TAATTCATGGGCTGTGGTGA
VIM	GGCCCAGCTGTAAGTTGGTA
	CCTAGCGGTTTAGGGGAAAC
SEPT9	CATCACGCACGATATTGAGG
	CCAGCAGTTCTCGTTGTTGA

Table 3-4. RT-PCR primer information

ChIP

Gene	Sequence (5'->3')
$p14^{ARF}$	GTGGGTCCCAGTCTGCAGTTA
	CCTTTGGCACCAGAGGTGAG
$p15^{INK4B}$	GGAACCTAGATCGCCGATGTAG
	TGTTTTACGCGTGGAATGCAC
$p16^{INK4A}$	ACCCCGATTCAATTTGGCAG
	AAAAAGAAATCCGCCCCCG
AOX1	ATCCTGGCTGTGGGTAACTG
	TATCGCTAGCGCATTCTCCT
CACNA1G	GTCTGGGCAGCAGTCTGATT
	GGAGAGAACCACAGCTGGAA
CHFR	TGTGCAACTGTACCCGAAAG
	ATTCTGAGAGCCCCGCTAAT
EFEMP1	TCCACCAACAGCATACAAGC
	TGTGAGGTGGGGTTTGTTTT
HAND1	GATAGCCACTCCCCCTTTTC
	CGGCTTTGATGTCAACCTCT
IRF8	AATATCCAGCGCTCGTGAAG
	GGCCCATTAATCAGAATCCA
LOX	GCCAGAATAAGACCGTGAGC
	AGAACCCCAATCCCAGAGTT
GCLC	ACCGCCTCCCCGTGACTCAG
	CAGCAGCAGCAGCCCAGAGG

Table 3-5. ChIP primer information

Bisulfite Sequencing

Gene	Sequence (5'->3')
$p14^{ARF}$	TGATGTGGAAGAAAAGGGG
	CCAAACCTCCAAAATCTCAAAA
$p14^{ARF}$ #2	AAGGGGAGGAGGGGATA*TGG*
	ACCACCATCTTCCCACCCTC
AOX1	ADS2444*
CACNA1G	ADS2300*
IRF8	ADS1254*
CHFR	ADS1462*
EFEMP1	ADS043*
HAND1	ADS1690*
LOX	ADS852*
$p16^{INK4A}$	ADS1067*
$p14^{ARF}$	ADS2130*

*Commercially available assay kit from EpigenDX

Table 3-6. Sodium Bisulfite Sequencing primer information

CHAPTER IV: FINAL SUMMARY AND CONCLUSIONS

Through my series of investigations, I have uncovered the mechanism of action of a novel TSG, IGFBP7, and the mechanism of epigenetic silencing for a panel of TSGs through the action of ZNF304. Unexpectedly, I found these two research endeavors were linked in that IGFBP7 is a member of this panel of TSGs silenced by ZNF304.

This body of work has provided novel insights into the relationship between oncogenes and TSGs. For instance, I uncovered the complex tumor-suppressing secretory response initiated in melanocytes upon introduction of an oncogene such as $BRAF^{V600E}$. Furthermore I identified some of the key players involved in the process whereby an oncogene such as RAS promotes the epigenetic silencing of a network of TSGs. These interrelationships illuminate the interconnectedness of the cellular response to pro-growth signaling and the checks and balances in place to constrain growth. Ultimately cancer subverts these checks and balances on its path to causing disease.

Novel cancer therapeutics may make use of this knowledge about oncogene-TSG signaling. For instance, as demonstrated with BRAF and IGFBP7, in the disease state IGFBP7 is silenced. However, ectopic reintroduction of this natural TSG causes robust cell death and tumor regression in a melanoma model that harbors $BRAF^{V600E}$. In a sense, rIGFBP7 administration restores the natural

defenses that cells use to prevent cancer. In this way, therapeutics may cause fewer side effects due to the natural role this protein plays in the body already.

It is somewhat surprising that the ectopic reintroduction of IGFBP7 in melanoma and primary cell lines does not cause any cell death [Figures, 2-21, 2-22 and 2-23]. While this is a very good attribute that argues it is specific to BRAF-positive melanoma, it remains to be determined why these cells are resistant. It would be interesting and beneficial to study the cause for this phenomenon. If the molecular determinants were characterized, perhaps this information could be used in allowing IGFBP7 to target melanomas that do not harbor an activated BRAF allele.

Future directions for the IGFBP7 project have revolved around its adaptation as an anti-cancer therapeutic. Post-doctoral fellows in my lab have generated adeno-associated virus vectors for expressing IGFBP7 *in vivo* in a mouse model of BRAF-induced melanoma and well as xenograft models. Thus far this work has proven promising but not without it's own set of technical difficulties. Furthermore, Narendra, my co-author of this study, continues to work on IFGBP7 and has initiated an shRNA screen to identify the factors required for IFGBP7-mediated cell death. It will be interesting to see where the study of this protein goes in the future and whether or not it yields any clinical benefit.

Similar to my results with IGFBP7, RAS signaling promotes a set of regulated interactions between the proteins PRKD1, USP28 and ZNF304. While USP28 and ZNF304 are not particularly druggable, PRKD1, being a kinase, represents a drug target with its well-conserved ATP pocket. Hence the use of the PRKD inhibitor, CRT0066101 represents a potent antagonist to this set of RAS promoted interactions. While unproven, I hypothesize that normal cells that do not harbor elevated RAS activity or PRKD1, USP28 or ZNF304 expression will be relatively unaffected by PRKD1 inhibition. Therefore I believe this small molecule that targets an oncogene-induced epigenetic silencing pathway will bear fewer side effects than broader treatment modalities such as radiation.

I think the study of ZNF304 requires a great deal more attention and resource development. In the future, I believe we would benefit greatly from a ChIP-SEQ analysis of its binding sites within the genomes of DLD-1, HCT116 and HCT15 cells. Furthermore, a PAT-ChIP-SEQ analysis in actual patient samples would be a tremendous resource. From these datasets, hopefully, we can derive some idea of what the ZNF304 binding sequence constitutes. A superficial look at the zinc fingers of the protein reveals that it most likely binds to cytosines and guanines, which fits with our model that it binds within CpG islands [Scot Wolfe, personal communication].

An additional benefit from having the genome-wide binding site analysis is it would provide an additional rationale for delineating whether a gene belongs within the CIMP gene signature. Currently, the concept of CIMP in CRC is well accepted. However, like any new field, there are many conflicting nomenclatures and definitions. There is yet to be a definitive CIMP marker panel and there are several papers that use related yet different methodologies for defining this panel. Perhaps the presence of ZNF304 at the promoter will constitute one hallmark for group 2 CIMP marker genes.

Another aspect of KRAS-mediated epigenetic silencing that deserves more attention is the role of PRKD1 in stabilizing ZNF304. We have clear results that PRKD1 is required for ZNF304 stabilization, yet the *in vitro* ubiquitination assay in Figure 3-41 does not yield a robust result that supports this hypothesis. Perhaps this experiment bears further biological replicates. However, an alternate explanation is that this phosphorylation stabilizes USP28 itself from degradation. It is interesting to note in this figure that it does appear that there is slightly less USP28 in the mutant lane. Perhaps the overexpression via transfection somewhat masks this result. An ongoing experiment that I am performing is looking at USP28 protein levels upon PRKD1 knockdown in DLD-1 cells. In support of this hypothesis is the result of Figure 3-42 where DLD-1 cells are treated with increasing amounts of the PRKD1 inhibitor, CRT0066101. We

see that levels of USP28 begin to drop off upon PRKD1 inhibition and it appears that a lower molecular weight degradation product begins to accumulate.

Another important and understudied aspect of this work is the upregulation of USP28 and PRKD1 via RAS signaling. It remains to be determined how these two proteins are activated transcriptionally by RAS signaling as shown in Figures 3-30 and 3-37. Analysis of the two promoters of these genes may yield a common transcription factor binding site that may coordinately regulate their gene expression in the presence of activated RAS.

Yet another aspect of this work that could use significant insight is the role of ZNF304 in undifferentiated stem cells. The experiments using H9 cells are preliminary at best. H9 cells are an acceptable model of human stem cells yet they display many properties of transformed cells such as unlimited replicative potential [if maintained in an undifferentiated state]. Therefore, at the very least, I believe additional models of human stem cells should be used to validate the results of Figure 3-55, 3-56 and 3-57. Unfortunately, ZNF304 is specific to humans and does not have a mouse homolog. This is very common with the zinc finger transcription factor family since it has expanded rapidly during evolution. Therefore, it is impossible to explore the biology of ZNF304 in a mouse model or examine its role in mouse stem cell systems. I believe only

through studies in a wide variety of human stem cell lines will we achieve any true understanding of what ZNF304 does normally.

Finally, this body of work represents a paradigm for investigating the biology of cancer. shRNA screens are a robust and high throughput method for interrogating virtually any biological process where a response can be stratified and isolated. In my cases I used cell survival as the stratification method since it was one of the easiest methods available at the time. In this way I identified many novel molecular players and ultimately novel regulatory nodes and networks that would have been unobtainable using previously available methods. Future work carried out using shRNA screens will yield innumerable insights into the biological paradigms we currently hold.

Above all else, these types of approaches, especially in the context of cancer, humble anyone with a respect for the natural world. I can only sit back and admire the complexity of living systems once I experience the interrelatedness of the gene expression and regulation. Biological processes are unbelievably complex and it seems that once I think I understand one aspect I am led to question many others.

In reality it is extremely difficult to isolate the effects of a single gene and study it. shRNA screens assist us in identifying some of these single genes that are able

to be studied thankfully. However, for anyone who has done one or more of these screens know, the list of primary candidates can be exhilarating yet daunting. At times you may have a list with hundreds of genes and no clue how to validate effectively, prioritize or follow up the mechanism of any particular gene. Ultimately you hope to elucidate at least a portion of the problem you are studying.

This is where science meets art and it is up to the researcher to divine a solution. Every researcher has a different background and approach to these types of problems. For me, this is the greatest aspect of academic science where you exercise the freewill to be curious and clever and potentially discover something that no other person could possibly know. shRNA screens are a treasure trove of opportunities and one can literally spend the rest of their life studying that initial list of genes you get at the conclusion of a screen. Furthermore, working with others who perform the screens exposes you to wildly different assays and concepts. From all this you become a much more rounded scholar than if you were to be highly specialized in a single area of research.

shRNA screens have allowed us to strike out and pioneer the understanding of two poorly studied aspects of cancer biology, OIS and epigenetic silencing of TSGs. Hopefully this body of work will be the foundation for other researchers to follow in their investigations of these processes and someday yield human

therapies. Furthermore, I hope this approach and use of screening methods to be framework for others who wish to investigate novel processes in biology.

BIBLIOGRAPHY

The History of Cancer. American Cancer Society, 2012. [pages 1 and 4] Print.

Adams, J.M., Harris, A.W., Pinkert, C.A., Corcoran, L.M., Alexander, W.S., Cory, S., Palmiter, R.D., and Brinster, R.L. The c-Myc oncogene driven by immunoglobulin enhancers induces lymphoid malignancy in transgenic mice. Nature. 1985 Dec 12-18;318[6046]:533-8.

Agata, Y., Matsuda, E., and Shimizu, A. Two novel Kruppel-associated box-containing zinc-finger proteins, KRAZ1 and KRAZ2, repress transcription through functional interaction with the corepressor KAP-1 [TIF1beta/KRIP-1]. J Biol Chem. 1999 Jun 4;274[23]:16412-22.

Asker, C., Wiman, K.G., and Selivanova, G. p53-induced apoptosis as a safegurad against cancer. Biochem Biophys Res Commun. 1999 Nov; 265[1]:1-6

Baker, S.J., Markowitz, S., Fearon, E.R., Willson, J.K., and Vogelstein, B. Suppression of human colorectal carcinoma cell growth by wild-type p53. Science. 1990 Aug 24;249[4971]:912-5.

Beausejour, C.M., Krtolica, A., Galimi, F., Narita, M., Lowe, S.W., Yaswen, P., and Campisi, J. [2003]. Reversal of human cellular senescence: roles of the p53 and p16 pathways. EMBO J. 22, 4212–4222.

Bellefroid, E.J., Poncelet, D.A., Lecocq, P.J., Revelant, O., and Martial, J.A. The evolutionary conserved Kruppel-associated box domain defines a subfamily of eukaryotic multifingered proteins. Proc Natl Acad Sci U.S.A. 1991 May 1;88[9]:3608-12.

Ben-Porath, I., and Weinberg, R.A. [2005]. The signals and pathways activating cellular senescence. Int. J. Biochem. Cell Biol. 37, 961–976.

Bennett, D.C. [2003]. Human melanocyte senescence and melanoma susceptibility genes. Oncogene 22, 3063–3069.

Bultman, S., Gebuhr, T., Yee, D., La Mantia, C., Nicholson, J., Gilliam, A., Randazzo, F., Metzger, D., Chambon, P., Crabtree, G., and Magnuson, T. [2000]. A Brg1 null mutation in the mouse reveals functional differences among mammalian SWI/SNF complexes. Mol. Cell 6, 1287–1295.

Burri, N., Shaw, P., Bouzourene, H., Sordat, I., Sordat, B., Gillet, M., Schorderet, D., Bosman, F.T., and Chaubert, P. Methylation silencing and mutation of the p14ARF and p16INK4a genes in colon cancer. Lab Invest. 2001 Feb;81[2]:217-29

Campisi, J. [2005]. Suppressing cancer: the importance of being senescent. Science 309, 886–887.

Chan AT, Ogino S, Fuchs CS. Aspirin and the risk of colorectal cancer in relation to the expression of COX-2. N Engl J Med 2007; 356:2131–2142.

Chang, L.L., Yeh, W.T., Yang, S.Y., Wu, W.J., and Huang, C.H. Genetic alterations of p16INK4a and p14ARF genes in human bladder cancer. J Urol. 2003 Aug;170[2 Pt 1]:595-600.

Chin, L., Merlino, G., and DePinho, R.A. [1998]. Malignant melanoma: modern black plague and genetic black box. Genes Dev. 12, 3467–3481.

Crawford, L.V., Pim, D.C. and Bulbrook, R.D. Detection of antibodies against the cellular protein p53 in sera from patients with breast cancer. 1982 Int. J. Cancer 30: 403-408.

Davies, H., Bignell, G.R., Cox, C., Stephens, P., Edkins, S., Clegg, S., Teague, J., Woffendin, H., Garnett, M.J., Bottomley, W., et al. [2002]. Mutations of the BRAF gene in human cancer. Nature 417, 949–954.

De Leo, A.B., Jay, G., Appella, E., Dubois, G.C., Law, L.W. and Old, L.J. Detection of a transformation-related antigen in chemically induced sarcomas and other transformed cells of the mouse. 1979. Proc Natl Acad Sci USA 76: 2420-2424.

Dhomen, N., and Marais, R. [2007]. New insight into BRAF mutations in cancer. Curr. Opin. Genet. Dev. 17, 31–39.

Dimri, G.P., Lee, X., Basile, G., Acosta, M., Scott, G., Roskelley, C., Medrano, E.E., Linskens, M., Rubelj, I., Pereira-Smith, O., et al. [1995]. A biomarker that identifies senescent human cells in culture and in aging skin in vivo. Proc. Natl. Acad. Sci. USA 92, 9363–9367.

Dominguez, G., Carballido, J., Silva, J., Silva, J.M., Garcia, J.M., Menendez, J., Provencio, M., Espana, P., and Bonilla, F. p14ARF promoter hypermethylation in plasma DNA as an indicator of disease recurrence in bladder cancer patients. Clin Cancer Res. 2002 Apr;8[4]:980-5.

Dominguez, G., Silva, J., Garcia, J.M., Silva, J.M., Rodriguez, R., Munoz, C., Chacon, I., Sanchez, R., Carballido, J., Colas, A., Espana, P., and Bonilla, F. Prevalence of aberrant methylation p14ARF over p16INK4a in some human primary tumors. Mutat Res. 2003 Sep 29;530[1-2]:9-17

Donehower, L.A., Harvey, M., Slagle, B.L., McArthur, M.J., Montgomery, C.A. Jr., Butel, J.S., Bradley, A. Mice deficient for p53 are developmentally normal but susceptible to spontaneous tumours. Nature. 1992 Mar 19;356[6366]:215-21.

Eiseler, T., Doppler, H., Yan, I.K., Kitatani, K., Mizuno, K., and Storz, P. Protein kinase D1 regulates cofilin-mediated F-actin reorganziationand cell motilitiy through slingshot. Nat Cell Biol. 2009 May; 11[5]: 545-56.

El-Deiry, W.S., Kern, S.E., Pietenpol, J.A., Kinzler, K.W. and Vogelstein, B. Definition of a consensus binding site for p53. Nat Genet. 1992 Apr;1[1]:45-9.

Emrick, M.A., Lee, T., Starkey, P.J., Mumby, M.C., Resing, K.A., and Ahn, N.G. [2006]. The gatekeeper residue controls autoactivation of ERK2 via a pathway of intramolecular connectivity. Proc. Natl. Acad. Sci. USA 103, 18101–18106.

Esteller, M. CpG island hypermethylation and tumor suppressor genes: a booming present, a brighter future. Oncogene. 2002 Aug 12;21[35]:5427-40.

Fearon, E.R., and Vogelstein, B. A genetic model for colorectal tumorigenesis. Cell. 1990 Jun 1;61[5]:759-67.

Formstecher, E., Ramos, J.W., Fauquet, M., Calderwood, D.A., Hsieh, J.C., Canton, B., Nguyen, X.T., Barnier, J.V., Camonis, J., Ginsberg, M.H., and Chneiweiss, H. [2001]. PEA-15 mediates cytoplasmic sequestration of ERK-MAP kinase. Dev. Cell 1, 239–250.

Friedman, J.R., Fredericks, W.J., Jensen, D.E., Speicher, D.W., Huang, X.P., Neilson, E.G., and Rauscher, F.J. 3rd. KAP-1, a novel corepressor for the highly conserved KRAB repression domain. Genes Dev. 1996 Aug 15;10[16]:2067-78.

Frommer, M., McDonald, L.E., Millar, D.S., Collis, C.M., Watt, F., Grigg, G.W., Molloy, P.L., and Paul, C.L. [1992]. A genomic sequencing protocol that yields a positive display of 5-methylcytosine residues in individual DNA strands. Proc. Natl. Acad. Sci. USA 89, 1827–1831.

Gansuage, S., Gansuage, F., Gause, H., Poch, B., Schoenberg, M.H., and Beger, H.G. The induction of apoptosis in proliferating human fibroblasts by oxygen radicals is associated with a p53- and p21WAF1CIP1 induction. FEBS Lett. 1997 Mar 3;404[1]:6-10

Gazin, C., Wajapeyee, N., Gobeil, S., Virbasius, C.M., and Green, M.R. An elaborate pathway required for RAS-mediated epigenetic silencing. Nature. 2007 Oct25;449[7165]:1073-7.

Goll, M.G. and Bestor, T.H. Eukaryotic cytosine methyltransfeRASes. Annu Rev Biochem. 2005;74:481-514. Review.

Gray-Schopfer, V., Wellbrock, C., and Marais, R. [2007]. Melanoma biology and new targeted therapy. Nature 445, 851–857.

Hannahan, D., and Weinberg, R.A. Hallmarks of cancer: the next generation. Cell, 2011 Mar 4;144[5];646-74.

Hall, P.A., McKee, P.H., Menage, H.D., Dover, R., and Lane, D.P. High levels of p53 protein in UV-irradiated normal human skin. Oncogene 1993 Jan;8[1]:203-7

Harris, S.L., and Levine, A.J. The p53 pathway: positive and negative feedback loops. Oncogene. 2005 Apr 18;24[17]:2899-908

Hartman, S.E., Bertone, P., Nath, A.K., Royce, T.E., Gerstein, M., Weissman, S., and Snyder, M. [2005]. Global changes in STAT target selection and transcription regulation upon interferon treatments. Genes Dev. 19, 2953–2968.

Hingorani, S.R., Jacobetz, M.A., Robertson, G.P., Herlyn, M., and Tuveson, D.A. [2003]. Suppression of BRAF[V599E] in human melanoma abrogates transformation. Cancer Res. 63, 5198–5202.

Hinoue, T., Weisenberger, D.J., Pan, F., Campan, M., Kim, M., Young, J., Whitehall, V.L., Leggett, B.A., and Laird, P.W. [2009]. PLoS ONE **4**, e8357.

Hoeflich, K.P., Gray, D.C., Eby, M.T., Tien, J.Y., Wong, L., Bower, J., Gogineni, A., Zha, J., Cole, M.J., Stern, H.M., et al. [2006]. Oncogenic BRAF is required for tumor growth and maintenance in melanoma models. Cancer Res. 66, 999–1006.

Honda, R., Tanaka, H., and Yasuda, H. Oncoprotein MDM2 is a ubiquitin ligase E3 for tumor suppressor p53. FEBS Lett. 1997 Dec 22;420[1]:25-7

Honda, R. and Yasuda, H. Association of p19[ARF] with Mdm2 inhibits ubiquitin ligase activity of Mdm2 for tumor suppressor p53. EMBO. 1999 Jan 4;18[1]:22-7

Jacobs, J.J., Kieboom, K., Marino, S., DePinho, R.A., and van Lohuizen, M. The oncogene and Polycomb-group gene bmi-1 regulates cell proliferation and senescence through the ink4a locus. Nature, 1999 Jan 14;397[6715]:164-8.

Kamijo, T., Bodner, S., van de Kamp, E., Randle, D.H., and Sherr, C.J. Tumor spectrum in ARF-deficient mice. Cancer Res. 1999 May 1;59[9]:2217-22.

Kamijo, T., Weber, J.D., Zambetti, G., Zindy, F., Roussel, M.F. and Sherr, C.J. Functional and physical interactions of the ARF tumor suppressor with p53 and Mdm2. Proc Natl Acad Sci USA 1998 Jul 7;95[14]:8292-7

Kamijo, T., Zindy, F., Roussel, M.F., Quelle, D.E., Downing, J.R., Ashmun, R.A., Grosveld, G., and Sherr, C.J. Tumor suppression at the mouse INK4a locus mediated by the alternative reading frame product p19ARF. Cell. 1997 Nov 28;91[5]:649-59

Karnoub, A.E. and Weinberg, R.A. Ras oncogenes: split personalities. Nat Rev Mol Cell Biol. 2008 Jul;9[7]:517-31.

Kawamoto, K., Enokida, H., Gotanda, T., Kubo, H., Nishiyama, K., Kawahara, M., and Nagagawa, M. p16INK4a and p14ARF methylation as a potential biomarker for human bladder cancer. Biochem Biophys Res Commun. 2006 Jan 20;339[3]:790-6.

Kessler, B.M. and Edelmann, M.J. PTMs in Conversation: Activity and Function of Deubiquitinating Enzymes Regulated via Post-Translational Modifications. Cell Biochem Biophys. 2011 April 12; 60:21-38.

Kim, S.S., Chen, Y.M. O'Leary, E., Witzgall, R., Vidal, M., and Bonventre, J.V. A novel member of the RING finger family, KRIP-1, associates with the KRAB-A transcriptional repressor domain of zinc finger proteins. Proc Natl Acad Sci U.S.A. 1996 Dec 24;93[26]:15299-304.

Kim, W.Y. and Sharpless, N.E. The Regulation of INK4/ARF in Cancer and Aging. Cell 2006 Oct 20; 127[2]: 265-75. Review

Kubbutat, M.H., Jones, S.N., and Vousden, K.H. Regulation of p53 stability by Mdm2. Nature. 1997 May 15;387[6630]:299-303

Laird, P.W. and Jaenisch, R. DNA methylation and cancer. Hum Mol Genet 1994;2 Spec No:1487-95.

Lane, D.P. and Crawford, L.V. T antigen is bound to a host protein in SV40-transformed cells. 1979. Nature 278: 261-263.

Leppa, S., Saffrich, R., Ansorge, W., and Bohmann, D. [1998]. Differential regulation of c-Jun by ERK and JNK during PC12 cell differentiation. EMBO J. 17, 4404–4413.

Li, W.Q., Kawakami, K., Ruszkiewicz, A., Bennett, G., Moore, J., and Iacopetta, B. BRAF mutations are associated with distinctive clinical, pathological and molecular features of colorectal cancer independently of microsatellite instability status. Mol Cancer. 2006 Jan 10;5:2

Lind, G.E., Thorstensen, L., Lovig, T., Meling, G.I., Hamelin, R., Rognum, T.O., Esteller, M., and Lothe, R.A. A CpG island hypermethylation profile of primary colorectal carcinomas and colon cancer cell lines. Mol Cancer. 2004 Oct 11;3:28.

Linzer, D.I.H. and Levine, A.J. Characterization of a 54 K dalton cellular SV40 tumor antigen resent in SV40-transformed cells and in infected embryonal carcinoma cells. 1979. Cell 1: 43-52.

Lowe, S.W., Cepero, E., and Evan, G. Intrinsic tumour suppression. Nature. 2004 Nov 18;432[7015]:307-15

Maltzman, W., and Czyzyk, L. UV irradiation stimulates levels of p53 cellular tumor antigen in nontransformed mouse cells. Mol Cell Biol. 1984 Sep;4[9]:1689-94

Margolin, J.F., Friedman, J.R., Meyer, W.K., Vissing, H., Thiesen, H.J., and Rauscher, F.J. 3rd. Kruppel-associated boxes are potent transcriptional repression domains. Proc Natl Acad Sci U.S.A. 1994 May 10;91[10]:4509-13.

Mello, C.C. and Conte, D. Jr. Revealing the world of RNA interference. Nature. 2004 Sep 16;431[7006]:338-42.

Meyer, N. and Penn, L.Z. Reflecting on 25 years with MYC. Nat Rev Cancer. 2008 Dec;8[12]:976-90.

Michaloglou, C., Vredeveld, L.C., Soengas, M.S., Denoyelle, C., Kuilman, T., van der Horst, C.M., Majoor, D.M., Shay, J.W., Mooi, W.J., and Peeper, D.S. [2005]. BRAFE600-associated senescence-like cell cycle arrest of human naevi. Nature 436, 720–724.

Mooi, W.J., and Peeper, D.S. [2006]. Oncogene-induced cell senescence–halting on the road to cancer. N. Engl. J. Med. 355, 1037–1046.

Moosman, P., Georgiev, O., Le Douarin, B., Bourquin, J.P., and Schaffner, W. Transcriptional repression by RING finger protein TIF1 beta that interacts with the KRAB repressor domain of KOX1. Nucleic Acids Res. 1996 Dec 15;24[24]:4859-67.

Mullenders, J., Fabius, A.W., Madiredjo, M., Bernards, R., and Beijersbergen, R.L. A large scale shRNA barcode screen identifies the circadian clock component ARNTL as a putative regulator of the p53 tumor suppressor pathway. PLoS One. 2009 Mar 11; 4[3]:e4798

Mutaguchi, K., Yasumoto, H., Mita, K., Matsubara, A., Shiina, H., Igawa, M., Dahiya, R., and Usui, T. [2003]. Restoration of insulin-like growth factor binding protein-related protein 1 has a tumor-suppressive activity through induction of apoptosis in human prostate cancer. Cancer Res. 63, 7717–7723.

Nagy, E., Beck, Z., Kiss, A., Csoma, E., Telek, B., Konya, J., Olah, E., Rak, K., and Toth, F.D. Frequent methylation of p16INK4A and p14ARF genes implicated in the evolution of chronic myeloid leukaemia from its chronic to accelerated phase. Eur J Cancer. 2003 Nov;39[16]:2298-305.

Nakamura, M., Sakaki, T., Hashimoto, H., Nakase, H., Ishida, E., Shimada, K., and Konishi, N. Frequent alterations of the p14[ARF] and p16[INK4a] genes in primary central nervous system lymphomas. Cancer Res. 2001 Sep 1;61[17]:6335-9.

Narita, M., Krizhanovsky, V., Nunez, S., Chicas, A., Hearn, S.A., Myers, M.P., and Lowe, S.W. [2006]. A novel role for high-mobility group a proteins in cellular senescence and heterochromatin formation. Cell 126, 503–514.

Nishikawa, K., Toker, A., Johannes, F.J., Songyang, Z., and Cantley, L.C. Determination of the Specific Substrate Sequences Motifs of Protein Kinase C Isozymes. Journal of Biological Chem, 1997 Jan 10; 272:952-960.

Oh, Y., Nagalla, S.R., Yamanaka, Y., Kim, H.S., Wilson, E., and Rosenfeld, R.G. [1996]. Synthesis and characterization of insulin-like growth factor-binding protein [IGFBP]-7. Recombinant human mac25 protein specifically binds IGF-I and -II. J. Biol. Chem. 271, 30322–30325.

Ohm, J.E., McGarvey, K.M., Yu, X., Cheng, L., Schuebel, K.E., Cope, L., Mohammad, H.P., Chen, W., Daniel, V.C., Yu, W., Berman, D.M., Jenuwein, T., Pruitt, K., Sharkis, S.J., Watkins, D.N., Herman, J.G., and Baylin, S.B. A stem cell-like chromatin pattern may predispose tumor suppressor genes to DNA hypermethylation and heritable gene silencing. Nat Genet. 2007 Feb;39[2]:237-42.

Olive, K.P., Tuveson, D.A., Ruhe, Z.C., Yin, B., Willis, N.A., Bronson, R.T., Crowley, D. and Jacks, T. Mutant p53 gain of function in two mouse models of Li-Fraumeni syndrome. Cell. 2004 Dec 17;119[6]:847-60.

Pao, W. and Miller, V.A. Epidermal growth factor receptor mutations, small-molecule inhibitors, and non-small-cell lung cancer: current knowledge and future directions. J Clin Oncol. 2005 Apr 10;23[11]:2556-68.

Pardal R., Molofsky, A.V., He, S., and Morrison, S.J. Stem Cell Self-Renewal and Cancer Cell Proliferation Are Regulated by Common Networks That Balance the Activation of Proto-Oncogenes and Tumor Suppressors. Cold Spring Harb Symp Quant Biol 2005; 70:177-185.

Park, S., Yeung, M.L., Beach, S., Shields, J.M., and Yeung, K.C. [2005]. RKIP downregulates B-Raf kinase activity in melanoma cancer cells. Oncogene 24, 3535–3540.

Peeper, D.S., and Mooi, W.J. [2002]. Pathogenesis of melanocytic naevi: growth arrest linked with cellular senescence? Histopathology 41, S139–S143.

Peng, H., Begg, G.E., Schultz, D.C., Friendman, J.R., Jensen, D.E., Speicher, D.W., and Rauscher, F.J. 3rd. Reconstitution of the KRAB-KAP1 repressor complex: a model system for defining the molecular anatomy of RING-B box-coiled-coil domain-mediated protein-protein interactions. J Mol Biol. 2000 Feb 4;295[5]:1139-62.

Perucho, M., Goldfarb, M., Shimizu, K., Lama, C., Fogh, J., and Wigler, M. Human-tumor-derived cell lines contain common and different transforming genes. Cell 1981 Dec; 27[3 Pt 2]:467-76.

Pfaffl, M.W. [2001]. A new mathematical model for relative quantification in real-time RT-PCR. Nucleic Acids Res. 29, e45.

Pollock, P.M., Harper, U.L., Hansen, K.S., Yudt, L.M., Stark, M., Robbins, C.M., Moses, T.Y., Hostetter, G., Wagner, U., Kakareka, J., et al. [2003]. High frequency of BRAF mutations in nevi. Nat. Genet. 33, 19–20.

Pomerantz, J., Schreiber-Agus, N., Liegeois, N.J., Silverman, A., Alland, L., Chin, L., Potes, J., Chen, K., Orlow, I., Lee, H.W., Cordon-Cardo, C., and DePinho, R.A. The Ink4a tumor suppressor gene product, p19Arf, interacts with MDM2 and neutralizes MDM2's inhibition of p53. Cell. 1998 Mar 20;92[6]:713-23

Renzing, J., Hansen, S., and Lane, D.P. Oxidative stress is involved in the UV activation of p53. J Cell Sci. 1996 May;109 [Pt 5]:1105-12

Riggs, J.W., Barrilleaux, B.L., Varlakhanove, N., Bush, K.M., Chan, V., and Knoepfler, P.S. Induced pluripotency and oncogenic trasnformation are related processes. Stem Cells Dev. 2013 Jan 1;22[1]:37-50.

Ruan, W.J., Lin, J., Xu, E.P., Xu, F.Y., Ma, Y., Deng, H., Huang, Q., Lv, B.J., Hu, H., Cui, J., et al. [2006]. IGFBP7 plays a potential tumor suppressor role against colorectal carcinogenesis with its expression associated with DNA hypomethylation of exon 1. J. Zhejiang Univ. Sci. B 7, 929–932.

Ruas, M. and Peters, G. The p16INK4a/CDKN2A tumor suppressor and its relatives. Biochim Biophys Acta 1998 Oct 14;1378[2]:F115-77

Ryan, R.F., Schultz, D.C., Ayyanathan, K., Singh, P.B., Friedman, J.R., Fredericks, W.J., and Rauscher, F.J. 3rd. KAP-1 corepressor protein interacts and colocalizes with heterochromatic and euchromatic HP1 proteins: a potential role for Kruppel-associated box-zinc finger proteins in heterochromatin-mediated gene silencing. Mol Cell Biol. 1999 Jun;19[6]:4366-78.

Rybin, V.O., Guo, J., and Steinberg, S.F. Protein kinase D1 autophosphorylation via distinct mechanisms at Ser744/Ser748 and Ser916. J Biol Chem, 2009 Jan 23; 284[4]:2332-43.

Sabater, L., Ashhab, Y., Caro, P., Kolkowski, E.C., Pujol-Borrell, R., and Dominguez, O. Identification of a KRAB-containing zinc finger protein, ZNF304, by AU-motif-directed display method and intial characterazation in lymphocyte activation. Biochem Biophys Res Commun. 2002 May 10;293[3]:1066-72.

Satyamoorthy, K., Li, G., Gerrero, M.R., Brose, M.S., Volpe, P., Weber, B.L., Van Belle, P., Elder, D.E., and Herlyn, M. [2003]. Constitutive mitogen activated protein kinase activation in melanoma is mediated by both BRAF mutations and autocrine growth factor stimulation. Cancer Res. 63, 756–759.

Schultz, D.C., Ayyanathan, K., Negorev, D., Maul, G.G., and Rauscher, F.J. 3rd. SETDB1: a novel KAP-1-associated histone H3, lysine 9-specific methyltransfeRASe that contributes to HP1-mediated silencing of euchromatic genes by KRAB zinc-finger proteins. Genes Dev. 2002 Apr 15;16[8]:919-32.

Schultz, D.C., Friedman, J.R., and Rauscher, F.J. 3rd. Targeting histone deacetylase complexes via KRAB-zinc finger proteins: the PHD and bromodomains of KAP-1 form a cooperative unit that recruits a novel isoforms of the Mi-2alpha subunit of NuRD. Genes Dev. 2001 Feb 15;15[4]:428-43.

Scurr, L.L., Pupo, G.M., Becker, T.M., Lai, K., Schrama, D., Haferkamp, S., Irvine, M., Scolyer, R.A., Mann, G.J., Becker, J.C., et al. [2010]. Cell **141**, 717–727.

Sharma, A., Trivedi, N.R., Zimmerman, M.A., Tuveson, D.A., Smith, C.D., and Robertson, G.P. [2005]. Mutant V599EB-Raf regulates growth and vascular development of malignant melanoma tumors. Cancer Res. 65, 2412–2421.

Shen, L., Kondo, Y., Hamilton, S.R., RAShid, A., and Issa, J.P. P14 methylation in human colon cancer is associated with microsatellite instability and wild-type p53. Gastroenterology. 2003 Mar;124[3]:626-33.

Sherr, C.J. Divorcing ARF and p53: and unsettled case. Nat Rev Cancer. 2006 Sep;6[9]:663-73.

Sherr, C.J. Tumor surveillance via the ARF-p53 pathway. Genes Dev. 1998 Oct 1;12[19]:2984-91. Review.

Solit, D.B., Garraway, L.A., Pratilas, C.A., Sawai, A., Getz, G., Basso, A., Ye, Q., Lobo, J.M., She, Y., Osman, I., et al. [2006]. BRAF mutation predicts sensitivity to MEK inhibition. Nature 439, 358–362.

Sparrow, L.E., Eldon, M.J., English, D.R., and Heenan, P.J. [1998]. p16 and p21WAF1 protein expression in melanocytic tumors by immunohistochemistry. Am. J. Dermatopathol. 20, 255–261.

Suzuki, H., Igarashi, S., Nojima, M., Maruyama, R., Yamamoto, E., Kai, M., Akashi, H., Watanabe, Y., Yamamoto, H., Sasaki, Y., et al. [2010]. Carcinogenesis **31**, 342–349.

Swisshelm, K., Ryan, K., Tsuchiya, K., and Sager, R. [1995]. Enhanced expression of an insulin growth factor-like binding protein [mac25] in senescent human mammary epithelial cells and induced expression with retinoic acid. Proc. Natl. Acad. Sci. USA 92, 4472–4476.

Tao, W. and Levine, A.J. p19[ARF] stablizes p53 by blocking nucleo-cytoplasmic shuttling of Mdm2. Proc Natl Acad Sci USA. 1999 Jun 8;96[12]:6937-41

Tao, W. and Levine, A.J. Nucleocytoplasmic shuttling of oncoprotein Hdm2 is required for Hdm2-mediated degradation of p53. Proc Natl Acad Sci USA. 1999 Mar 16;96[6]:3077-80

Tournier, C., Whitmarsh, A.J., Cavanagh, J., Barrett, T., and Davis, R.J. [1999]. The MKK7 gene encodes a group of c-Jun NH2-terminal kinase kinases. Mol. Cell. Biol. 19, 1569–1581.

Urritia, R. KRAB-containing zinc-finger repressor proteins. Genome Biol. 2003;4[10]:231.

Wajapeyee, N., Kapoor, V., Mahalingam, M., and Green, M.R. [2009]. Efficacy of IGFBP7 for treatement of metastatic melanoma and other cancers in mouse models and human cell lines. Mol. Cancer Ther. **8**, 3009–3014.

Wajapeyee, N., Serra, R.W., Zhu, X., Mahalingam, M., and Green, M.R. [2008]. Oncogenic BRAF induces senescence and apoptosis through pathways mediated by the secreted protein IGFBP7. Cell **132**, 363–374.

Wajapeyee, N., and Somasundaram, K. [2003]. Cell cycle arrest and apoptosis induction by activator protein 2alpha [AP-2alpha] and the role of p53 and p21WAF1/CIP1 in AP-2alpha-mediated growth inhibition. J. Biol. Chem. 278, 52093–52101.

Wang, Y.L., Uhara, H., Yamazaki, Y., Nikaido, T., and Saida, T. [1996]. Immunohistochemical detection of CDK4 and p16INK4 proteins in cutaneous malignant melanoma. Br. J. Dermatol. 134, 269–275.

Watson, J.D. and Crick, F.H. Molecular structure of nucleic acids; a structure for deoxyribose nucleic acid. Nature. 1953 Apr 25; 171[4356]:737-8.

Weinberg, Robert A. *The Biology of Cancer*. New York: Garland Science, Taylor & Francis Group, LLC, 2007, pgs.. 11-13, 26-28, 57-61, 75-82, 99, 103-115, 129-140, 150-153, 166-184, 209-223, 277-284, 310-314, 318-323, 333, 358-262, 368-372, 376-380, 400-402, 423-424, 427-429, 559-563 and 594-597. Print.

Wilson, E.M., Oh, Y., and Rosenfeld, R.G. [1997]. Generation and characterization of an IGFBP-7 antibody: identification of 31kD IGFBP-7 in human biological fluids and Hs578T human breast cancer conditioned media. J. Clin. Endocrinol. Metab. 82, 1301–1303.

Wilson, H.M., Birnbaum, R.S., Poot, M., Quinn, L.S., and Swisshelm, K. [2002]. Insulin-like growth factor binding protein-related protein 1 inhibits proliferation of MCF-7 breast cancer cells via a senescence-like mechanism. Cell Growth Differ. 13, 205–213.

Witzgall, R., O'Leary, E., Leaf, A., Onaldi, D. and Bonventre, J.V. The Kruppel-associated box-A [KRAB-A] domain of zinc finger proteins mediates transcriptional repression. Proc Natl Acad Sci U.S.A. 1994 May 10;991[10]:4514-8.

Yagi, K., Akagi, K., Hayashi, H., Nagae, G., Tsuji, S., Isagawa, T., Midorikawa, Y., Nishimura, Y., Sakamoto, H., Seto, Y., Aburatani, H., and Kaneda, A. Three DNA Methylation Epigenotypes in Human Colorectal Cancer. Clin Cancer Res, 2010; 16:21-33

Yu, H., McDaid, R., Lee, J., Possik, P., Li, L., Kumar, S.M., Elder, D.E., Van Belle, P., Gimotty, P., Guerra, M., et al. [2009]. Am. J. Pathol. **174**, 2367–2377.

Zhang, S.J., Endo, S., Saito, T., Kouno, M., Kuroiwa, T., Washiyama, K., and Kumanishi, T. Primary malignant lymphoma of the brain: frequent abnormalities and inactivation of p14 tumor suppressor gene. Cancer Sci. 2005 Jan;96[1]:38-41.

Zheng, S., Chen, P., McMillan, A., Lafuente, A., Lafuente, M.J., Ballesta, A., Trias, M., and Wiencke, J.K. Correlations of partial and extensive methylation at the p14[ARF] locus with reduced mRNA expression in colorectal cancer cell lines and clinicopathological features in primary tumors. Carcinogenesis. 2000 Nov;21[11]:2057-64.

Zhu, J., Woods, D., McMahon, M., and Bishop, J.M. [1998]. Senescence of human fibroblasts induced by oncogenic Raf. Genes Dev. 12, 2997–3007.

Zilfou, J.T. and Lowe, S.W. Tumor suppressive functions of p53. Cold Spring Harb Perspect Biol. 2009 Nov;1[5]